Modeling 2012 in Massachusetts Bay using the unstructured grid Bays Eutrophication Model

Massachusetts Water Resources Authority
Environmental Quality Department
Report 2015-02

Modeling 2012 in Massachusetts Bay
Using the Unstructured-Grid Bays Eutrophication Model

Submitted to

Massachusetts Water Resources Authority
Environmental Quality Department
100 First Avenue
Charlestown Navy Yard
Boston, MA 02129
(617) 242-6000

Prepared by

Liuzhi Zhao and Changsheng Chen

School for Marine Science and Technology

University of Massachusetts-Dartmouth

New Bedford, MA 02744

Robert C. Beardsley

Woods Hole Oceanographic Institution

Woods Hole, MA 02543

Daniel L. Codiga, Wendy S. Leo, and Michael J. Mickelson

Massachusetts Water Resources Authority

Boston, MA 02129

March 2015

Citation:

Zhao L, Chen C, Beardsley RC, Codiga DL, Leo WS, Mickelson MJ. 2015. **Modeling 2012 in Massachusetts Bay Using the Unstructured-Grid Bays Eutrophication Model.** Boston: Massachusetts Water Resources Authority. Report 2015-02. 102p.

Acronyms

BEM	Massachusetts Bays Eutrophication Model: a coupled water quality and hydrodynamics model system
BH	Boston Harbor
CCB	Cape Cod Bay
DOC, DON, DOP	Dissolved Organic Carbon, Nitrogen, and Phosphorous
DIN	Dissolved Inorganic Nitrogen
ECOM-si	Estuarine and Coastal Ocean Model-semi-implicit: A structured-grid hydrodynamic model
FVCOM	Finite-Volume Community Ocean Model: An unstructured-grid hydrodynamic model
GoM/GB-FVCOM	FVCOM applied to the Gulf of Maine/Georges Bank[1]
MB	Massachusetts Bay
MB-FVCOM	FVCOM applied to Massachusetts Bay[2]
NERACOOS	Northeast Regional Association for Coastal Ocean Observing Systems
OA	Objective Analysis, method used to create input/forcing fields on boundary of model domain from observations located on or off boundary
OBC	Open Boundary Conditions, input/forcing along the offshore boundary of model domain
POC, PON, POP	Particular Organic Carbon, Nitrogen, and Phosphorous
RCA	Row Column Advanced (RCA) ecological systems operating program: a water quality model
UG-RCA	Unstructured-grid version of RCA
WRF	Weather Research and Forecast Model[3]
WMCC	Western Maine Coastal Current

[1] http://fvcom.smast.umassd.edu/research_projects/GB/index.html
[2] http://fvcom.smast.umassd.edu/research_projects/MassBay/index.html
[3] http://fvcom.smast.umassd.edu/research_projects/GB/WRF/index.html

EXECUTIVE SUMMARY

The Massachusetts Water Resources Authority (MWRA) contracted the Marine Ecosystem Dynamics Modeling laboratory at University of Massachusetts at Dartmouth to simulate hydrodynamic fields (including currents, temperature, and salinity) and water quality parameters (including nutrients, chlorophyll, and dissolved oxygen, DO) in the Massachusetts Bay (MB) system for calendar year 2012. This report presents the simulation results, with comparisons to observations, and uses them to describe and interpret 2012 water quality conditions. It also discusses (a) a scenario simulation that omits the MWRA outfall, to examine the potential impact of the effluent on system-wide ecosystem function such as algal production and DO levels, and (b) a sensitivity study investigating the effect on DO simulation results of different methods for using observations to specify conditions near the northeast boundary of the water quality model domain.

The hydrodynamic model (MB-FVCOM, Finite Volume Community Ocean Model) was driven at the sea surface by a mesoscale meteorological model, at the open boundary to its east by nesting in the regional Gulf of Maine (GoM) FVCOM simulation, by freshwater discharges from all local rivers, and by the MWRA outfall. The methods were the same as in the 2011 simulation but with an upgrade to the latest code version of FVCOM and improvements to the data assimilation that reduced artificially abrupt temperature and salinity changes. MB-FVCOM successfully reproduced temperature and salinity observations including the seasonal cycle of stratification, which in 2012 was more temperature-driven than in other years due to the lower than average runoff and hence relatively weak salinity variability. It also reproduced well the three-dimensional fields of tidal and non-tidal/residual currents, and indicated that movement of GoM water in to northern MB during spring was more pronounced in 2012 than in 2011.

The water quality model (UG-RCA, Unstructured Grid Row Column Advanced) was driven by the MB-FVCOM water circulation. Modeled growth of phytoplankton depends on solar input and nutrient availability, and is subject to a temperature-based zooplankton grazing parameterization. Cycling of nutrients and labile and refractory forms of dissolved and particulate organic carbon, nitrogen, and phosphorous is included. DO is determined by the surface reaeration flux, sediment oxygen demand at the bottom, water column mixing, and phytoplankton production and respiration. Open boundary forcing is based on MWRA monitoring program observations. Nutrient and carbon loadings include the MWRA effluent outfall, non-MWRA point sources, non-point sources, river discharge and atmospheric sources.

The water quality simulation captured general patterns in seasonal variations and vertical structure of many observed fields. This included the spring/summer reduction in shallow dissolved inorganic nitrogen, due to phytoplankton uptake, and its replenishment in fall when stratification breaks down. However, modeled chlorophyll did not show prominent blooms at any point during the year, in contrast to typical spring and fall blooms observed. This could be associated with nutrient concentrations assigned to model GoM water, which moved in to MB more strongly than in a typical year, that are based on sparse field sampling and may underestimate actual concentrations. The model exhibited the seasonal cycle of DO, with peak shallow values in spring due to phytoplankton growth, continuous decreases through summer and early fall at all depths, and replenishment during the winter mixed period. However, the observed high spring DO in MB was not captured well by the model. The sensitivity experiment demonstrated this is likely associated with limitations in using measurements to specify DO at the northeastern boundary of the model domain, where water advected in to the system originates. Model dissolved and particulate organic nitrogen showed modest agreement with observations, while model particulate organic carbon did not capture well the seasonal variations or the vertical structure of observations. In general for most water quality parameters the model showed a smaller range of values, and smaller surface-bottom differences during the stratified season, when compared to observations.

The scenario experiment removed MWRA effluent from the simulation and confirmed that except within 10-20 km of the outfall, effluent nutrients comprise a small percentage of natural background levels. The outfall plume was trapped nearer to the bottom during the stratified summer season. As seen in earlier studies, increased winds and vertical mixing in winter can cause the plume to reach the surface layer and disperse over longer distances. However, in winter, darkness slows phytoplankton growth such that effluent nutrients are not efficiently converted into biomass by phytoplankton. These results support conclusions from the MWRA long-term monitoring program that although nitrogen levels, mainly ammonium, are higher within 10-20 km of the outfall, no perceptible effect is seen in bay-wide chlorophyll or DO so the system-wide ecological function of MB in not influenced appreciably by the outfall.

The sensitivity experiment confirmed that DO simulation results are strongly influenced by the observations and method used to construct the model forcing at the boundary in the northeast portion of the domain, off Cape Ann. Therefore better field measurements in that vicinity, and improved methods for applying them, could be one way to improve performance of DO simulations.

Table of Contents

Table of Figures

Table of Tables

1. Introduction

1.1 *Project overview*

The Massachusetts Water Resources Authority (MWRA) has established a long-term monitoring program to evaluate the impact of MWRA sewage treatment plant effluent on the ecosystem function and water quality in the Massachusetts Bay system (MBS) including Boston Harbor (BH), Massachusetts Bay (MB) and Cape Cod Bay (CCB). The monitoring program primarily consists of an array of field observations, but is complemented by water quality modeling as required by the MWRA permit for effluent discharge into MB. This report presents the results of the Bays Eutrophication Model (BEM), which utilizes the FVCOM (Finite Volume Community Ocean Model) hydrodynamic model and the UG-RCA (Unstructured Grid Row Column Advanced) water quality model, for the 2012 calendar year simulation period including details of forcing treatment, model setup, model-data comparisons, and interpretation of findings.

1.2 *Background*

Readers unfamiliar with the geography of the MBS (Figure 1.1) and the current understanding of physical and biological oceanographic processes in it are referred to, for example, the introductory summaries given in sections 1.2 and 1.3 of Zhao et al. (2012), the annual MWRA outfall monitoring report (e.g., for calendar year 2012, Libby et al., 2013), and references therein.

The present-day BEM is the result of an extensive development process begun in the early 1990s. Section 1.4 of Zhao et al. (2012) reviews key improvements incorporated over the years. Complete background information on BEM is in MWRA Technical Reports, where the model development and updating process has been fully documented. Table 1.1 shows a comprehensive listing of MWRA Technical Reports about the BEM; for each, a summary of the specific topic, highlighted aspects of its content, the full citation, and a hyperlink to the downloadable PDF file in the online repository is included. Modeling activities have occurred in three main phases. The initial phase was original development of the hydrodynamic and water quality models by Hydroqual and the U.S. Geological Survey. It included simulations of the years 1989-1994, which were assessed by an independent Model Evaluation Group (Beardsley et al., 1995), and 1998-1999. The second phase consisted of adaptations and improvements by University of Massachusetts Boston researchers, with simulations and interpretations of 2000-2005. The third and current phase,

treating years from 2006 onward, is being implemented by UMass Dartmouth. Simulations of years from 2008 onward use FVCOM for hydrodynamics and UG-RCA for water quality.

2. Methods

2.1 *Summary of methods*

The methods used in the simulations of 2012 reported here are explained in detail in Zhao et al. (2012), which includes a complete listing of parameter values, and in other documents listed in Table 1.1. A brief summary is as follows.

The hydrodynamic model MB-FVCOM (FVCOM on grid spanning MB; Figure 2.1) was driven at the surface with calibrated wind stress, heat flux/shortwave irradiance, and precipitation/evaporation from the mesoscale meteorological model WRF (Weather Research and Forecast). Forcing at the open boundary, including tides, is by nesting in the regional Gulf of Maine / Georges Bank FVCOM (GoM/GB-FVCOM; Figure 2.1). Freshwater discharges enter at the coast from all local rivers. Effluent from the MWRA outfall enters at the seafloor. MB-FVCOM also assimilated available observations, including sea surface temperature and timeseries of water column temperature and salinity from moorings.

The water quality model UG-RCA is driven by transport and eddy diffusivity from the hydrodynamic model output. The grids for MB-FVCOM and UG-RCA are the same, except that UG-RCA does not extend as far eastward (Figure 2.1). Horizontal resolution ranges from about 0.29 km near the coast to 0.7-2.5 km at the eastern boundary of UG-RCA and 5–10 km near the MB-FVCOM nested boundary. In the vertical a hybrid fixed/terrain-following coordinate is used with 30 grid levels.

UG-RCA is based on RCA-v3.0 (Hydroqual, 2004) and has 26 state variables and 23 sediment variables (Figure 2.2). Growth of three phytoplankton groups (spring, summer, and fall) is based on solar radiation and nutrient availability, and subject to zooplankton grazing parameterized as a first-order temperature-dependent transformation to particulate and dissolved organic matter. Nutrients (including ammonium NH_4^+, nitrate NO_3^- and nitrite NO_2^-, phosphate PO_4^{3-} and dissolved silica SiO_3^{2-}) are formed through mineralization of organic substances in the water column and at the sediment-water interface. Cycling of labile and refractory forms of dissolved and particulate organic carbon, nitrogen, and phosphorous is treated. DO is computed by the reaeration flux at the sea surface, sediment oxygen demand (SOD) at the bottom and biological and biogeochemical

dynamics in the water column including phytoplankton photosynthetic production, consumption by respiration, biogeochemical oxygen demand through the mineralization of particulate and dissolved organic matter, and nitrification. Open boundary condition (OBC) fields are specified using objective analysis (OA) of MWRA monitoring program observations. Nutrient and carbon loadings are specified with recent observations when available, or historic observations and estimates, and include the MWRA effluent outfall from the Deer Island Treatment Plant, non-MWRA point sources, non-point sources, river discharge and atmospheric sources.

2.2 *Model improvements*

Compared to the description in Zhao et al. (2012), the simulations reported here incorporated three improvements. First, the code version of FVCOM used in MB-FVCOM was upgraded to 3.1.6 (the most recent User's Manual, Chen et al. (2013), gives detailed descriptions), and a corresponding update was made to the code modules that interface UG-RCA with FVCOM.

Second, the data assimilation methods used by the hydrodynamic model were improved. On reviewing an initial draft of this report, MWRA noted artificially abrupt changes to the temperature and salinity fields (Figure 2.3 shows examples; salinity values are on the Practical Salinity Scale, PSS). A test to see if the abrupt changes were associated with the data assimilation scheme indicated that they were. Consequently the Optimal Interpolation assimilation method was modified. The major changes were in the duration of the time window and size of the vertical correlation scale. The simulations were re-run and a substantial reduction of the abrupt temperature changes was among the benefits. The nature of the improvements is seen on comparing Figure 2.3, from before the modification was made, to outputs after the modification, shown in Figure 3.7 below. All results in this report are from simulations incorporating this improvement.

Third, a lower background eddy viscosity value was implemented. During the troubleshooting just noted, inaccurate mixing by a too-high background eddy viscosity level was investigated as a possible explanation. Initial FVCOM simulations of 2012 used a background eddy viscosity of 10^{-4} m^2 s^{-1}, as was appropriate in previous ECOM-si (Estuarine and Coastal Ocean Model, semi-implicit) model experiments for GoM and MB. Because the current simulations are on grids with much higher resolution than the ECOM-si experiments, a lower level of 10^{-5} m^2 s^{-1} is more appropriate. Simulations using 10^{-5} m^2 s^{-1} were completed and changes were found to be minimal, so runs described throughout this report use the lower value of 10^{-5} m^2 s^{-1}.

3. Results

3.1 *Forcing conditions*

3.1.1 Wind, heat flux, and Merrimack River

Monthly-mean wind, monthly-mean heat flux, and daily-mean Merrimack River discharges in 2012 are plotted in Figure 3.1 and compared with the climatological mean values averaged over the prior 18 years (1995–2012). Northwest wind (from the northwest) prevailed in January, February, and March in both 2012 and the 18-year average. January wind was slightly more westerly (eastward) in 2012 than in the 18-year average. April and May winds were stronger than the 18-year average, while June 2012 was calm (average wind speed < 1 m/s) as in the 18-year average. From May through September 2012 winds were mostly southerly, and north-northwesterly wind prevailed from October through December 2012, also as in the 18-year averages. Compared to the 18-year averages, the 2012 November wind was twice as strong and the 2012 December wind was weaker.

Surface heat flux in 2012 followed a seasonal cycle mostly comparable to the 18-year average, with high values in summer and low values in winter and late fall. However, 2012 heat flux was visibly lower than the 18-year average except in January and April, and particularly low in May.

River discharge was lower in mid-March and April 2012 compared with the 18-year average. The spring discharge peak occurred in June, which was about two months later than the 18-year average. Summer 2012 discharge was low, as in the 18-year average. A peak in river discharge occurred in early November 2012, with a value of about twice the 18-year average. A relatively large river discharge also occurred in December 2012.

For a more comprehensive description of 2012 forcing conditions see Libby et al. (2013). They emphasize that 2012 had very warm winter conditions in January and February, very low runoff including lack of a springtime freshet, relatively weak winds but more sustained mid-year upwelling, and stratification of typical strength but which persisted longer than normal in fall. The latter was possibly associated with September and October winds that were weaker than typical, such that strong winds were delayed until November.

3.1.2 Loading of organic carbon, nitrogen, and phosphorous

There are both oceanic and non-oceanic sources of organic materials and nutrients to the Massachusetts Bays system. The oceanic component stems from exchange with adjacent offshore

waters of the Gulf of Maine. These offshore waters are not characterized by particularly high concentrations, but the volume of the exchange is very large. A systemwide budget for nitrogen in the MBS concluded that more than 90% originated offshore (Hydroqual, 2000). Consequently, oceanic input is by far the single largest source of organic materials and nutrients to the system.

Non-oceanic sources include rivers, atmospheric deposition, non-point sources of terrestrial runoff, and point-source sewage outfalls. Among such non-oceanic sources, non-MWRA treatment plants contributed the most (33%) to 2012 organic carbon loading (Figure 3.2a), followed by the MWRA outfall (19%), atmospheric (18%), non-point sources (16%) and rivers (14%). The MWRA outfall represented the largest input (47%) to the 2012 nitrogen load (Figure 3.2b), followed by the atmosphere (29%), non-MWRA point sources (13%), non-point sources (7%) and rivers (4%). For phosphorus loading the MWRA outfall again contributed the largest portion (48%), followed by non-MWRA point sources (29%), non-point sources (15%), river discharge (5%) and atmospheric flux (3%) (Figure 3.2c). Because most of 2012 was very dry (Figure 3.1c), the flow from the MWRA outfall (Figure 3.3a) was low and nearly 100% received secondary treatment, thus loads of carbon and phosphorus were lower than in past years. The load of carbon from the MWRA outfall in 2012 was the lowest of any year from 2005-2012 (Figure 3.3b). The 2012 nitrogen loading from the MWRA outfall was 1% lower than in 2011 and was also slightly lower than other recent years (Figure 3.3c). Similar to carbon but unlike nitrogen, the phosphorus load discharged from the MWRA outfall was 17% lower than the average load from 2005 to 2012 and was the lowest in recent years (Figure 3.3d). Note that for non-MWRA sources, use has been made of the only available dataset (Menzie et al., 1991), for which there are recognized limitations to applicability given than treatment levels at some non-MWRA sources have changed since that study.

3.1.3 UG-RCA open boundary

Bi-weekly forcing on the OBC for UG-RCA is determined using objective analysis (OA) on field survey observations (green, yellow, and black MB stations in Figure 3.4) from the MWRA monitoring program. Results for April 15 and August 15 are representative of the annual cycle, have been examined in reports describing prior years, and thus are presented in Figure 3.5; for ease of comparison the colorscale ranges are the same as in earlier reports. As explained in Zhao et al. (2012), for dissolved organic carbon and biogenic silica, which are no longer being sampled, OBC values are from a seasonal cycle constructed by averaging all prior years' observations. Given the

low frequency of field observations and large distance between the open boundary and observation sites, particularly for the South Passage, the OA-mapped results should be viewed with caution.

Chlorophyll along the south-north transect exhibited similar patterns in April and August, a relatively weak subsurface maximum that is strongest toward the north. April and August patterns for NO_3^- concentration were also similar to each other, generally uniform horizontally and increasing with depth. In April, NO_3^- was relatively low (<4 μM) and uniform above 40 m, while in August, a nutricline appeared in a depth range of 20-40 m with higher values (>8 μM) beneath it. In April, NH_4^+ increased in depth with a sharp vertical gradient at ~10 m below the surface toward the south and deepening to ~20 m in the north. In August NH_4^+ was greatly reduced, <0.5 μM above 40 m. DO was higher in April than in August and decreased southward, with a maximum value in the deeper channel apparently associated with the inflow from the Western Maine Coastal Current (WMCC). The highest DO concentration was >12 mg L^{-1} at the surface in April, and values of ~9 mg L^{-1} or higher extended to about 10 m deep in August. Silicate and phosphate increased with depth in both April and August, and were mostly relatively uniform horizontally with higher values toward the north in April and toward the south in August. In general, particulate organic carbon (POC), nitrogen (PON), and phosphorous (POP) decreased with depth, and toward the south. Dissolved organic carbon (DOC), nitrogen (DON), and phosphorous (DOP) had relatively weak spatial gradients, with weak mid-depth maxima in April DOP and August DON, and a horizontal increase in DOP toward the north in April and toward the south in August.

Interannual variability of OA-mapped OBC forcing is illustrated in Figure 3.6 using nitrate concentration in 2012, 2011, and 2010; the late January and early March dates are included, representing well mixed and early stratified periods respectively, as in prior reports. The 2012 distributions were quite similar to those in 2010, increasing northward and with depth, ranging from about 3-4 μM to 7-9 μM in late January and from about 1-3 μM to ~9 μM in early March. In contrast during 2011 values were relatively higher (8-10 μM) and more spatially uniform in late January, and similar in spatial distribution but with slightly lower values in early March. The North Passage is the major pathway for WMCC water flowing into MB and a potential explanation of the limited phytoplankton growth observed during the 2012 spring season (see e.g., Libby et al., 2013) is that the elevated nitrate concentrations extended less far south, reducing the winter supply of nutrients to MB from the WMCC.

3.2 *Physical fields*

3.2.1 Model-observation comparisons

The purpose of the BEM is assessment of water quality conditions. The physical circulation has strong influence on water quality, so performance of UG-RCA simulations depends on the capability of MB-FVCOM to capture realistic MB physical processes. For this reason, we have assimilated temperature and salinity observations into MB-FVCOM to increase the accuracy of physical fields. Assimilated observations included satellite-derived sea-surface temperature (SST), temperature and salinity profiles from MWRA monitoring surveys, and time series measurements from mooring A01 (Figure 3.4) operated by NERACOOS (Northeast Regional Association of Coastal Ocean Observing Systems).

Figure 3.7 shows comparisons between modeled and observed temperature and salinity at select MWRA monitoring stations spanning MB, grouped for purposes of displaying the results. Stations N01 and N07, located near the MWRA outfall, and station F22 to the northeast, are part of the "northern subset" (the six green stations in Figure 3.4) that appears grouped together in a number of later figures; stations F10, F06, and F13, to the south and near the coast, are in the "southern subset" (the six yellow stations in Figure 3.4) that appears grouped together in a number of later figures. In the station F22 panel of Figure 3.7, the green and pink lines are observations near the surface and bottom respectively from mooring A01 located (see Figure 3.4) about 5 km northeast from F22. Assimilation of SST and hydrographic cast measurements made the modeled temperature and salinity match the observations well. SST assimilation used the nudging method with a time window of 3 days. Most events during which temperature decreased in 2012 lasted for 5-7 days, so the 3-day time window seemed to work well to adjust the model-computed SST to satellite-derived values. As described in Section 2.2 above, the hydrographic data assimilation was improved to address a problem in earlier model runs in which modeled bottom water temperatures and surface salinities showed artificially rapid adjustments (Figure 2.3) to match the observations, which did not represent real physical processes.

The water column was stratified from spring to late fall, with large temperature and salinity differences between the surface and bottom. The brief reduction in stratification at the beginning of June was due to a wind-mixing event (Libby et al. 2013). The largest temperature differences occurred in the middle of July (~day 200), with about 15 °C in the northeast part of the study area

as shown in Figure 3.7 at station F22. Temperature reductions observed in late July, most pronounced in the near-surface records, were due to upwelling (Libby et al. 2013).

Salinity (Figure 3.7) exhibited larger fluctuations near the surface than near the bottom, as expected, particularly at stations N07 and F22 during spring through summer. (For ease of comparison the range of the vertical axis scale of salinity plots in Figure 3.7 is the same as in reports describing prior years, when salinities reached lower values than occurred in 2012.) The lowest salinity occurred in May and June, which was consistent with the freshwater discharge records from the Merrimack River (Figure 3.1) and other MB rivers.

Figure 3.8 and Figure 3.9 show model-observation comparisons for monthly-mean spatial structure of near-surface temperature and salinity. The observed fields are computed using measurements from all stations (black dots) sampled during each month-long period. For most months in MB there was only one one-day survey, though in May and June there were additional surveys; BH stations are sampled weekly or biweekly. The model fields are averaged over the period the corresponding observations span. The assimilation worked well to reproduce observed fields of temperature and salinity. In February, for both observations and model output, temperature was mostly homogeneous and salinity increased in the offshore direction by about 2 across MB. In April, in addition to the salinity gradient, temperature decreased offshore, and model-observation agreement was similar except that model temperatures were colder and more homogenous. In June, temperatures were substantially increased, and spatial structure of temperature and salinity was similar but with a weaker inshore-offshore salinity gradient; the model matched observations adequately. In August SST reached 19–20 °C but with little spatial variation, and the model temperature was higher (by ~1.0 °C) than observed, having a similar inshore-offshore difference as observed but a different spatial pattern with mid-bay maximum. Both model and observed salinity in August had a stronger inshore-offshore gradient, with particularly low values in the northwestern part of the simulation domain and high values offshore. Observed October temperature decreased to around 13.5 °C throughout the study area and the model temperature was slightly warmer, while observed and modeled salinities were comparable to each other with a sharpened inshore-offshore gradient.

3.2.2 Monthly-mean surface sub-tidal currents, temperature, and salinity

The monthly-averaged surface sub-tidal (variations on timescales longer than tidal) current field from January through April (Figure 3.10) was characterized by two major features:

(1) Offshore, an extension of the WMCC flowing south-southeastward from the Western GoM Coast across Stellwagen Bank toward the offshore side of Cape Cod, which was strongest in February and weaker in April; and

(2) A current that bifurcates at the North Passage entrance, with one branch departing from the south-southeastward flow and entering MB southwestward. Water entering MB remained close to the coast and affected the inshore coastal region while moving southward, then turned in a counterclockwise direction and moved offshore eastward to re-join the south-southeastward WMCC extension flow in the northeastern CCB region.

During May through August (Figure 3.11) the monthly-averaged surface currents were essentially dominated by eddies. In May the southeastward current across Stellwagen Bank remained weak and there were two counterclockwise eddies in northern MB. In June the current strengthened and northern MB had a generally clockwise flow that met a counterclockwise circulation spanning southern MB and northern CCB. In July flow weakened, with generally counterclockwise and clockwise motions in northern and southern MB respectively. August flow was generally offshore with the counterclockwise eddy in northern MB still prominent.

September and October circulation was somewhat weaker than August but had similar structure, and the southward near-shore and offshore currents re-intensified in November through December to gradually re-establish the winter-spring pattern (Figure 3.12).

To examine the seasonal variability of water properties, we present the model surface temperature (Figure 3.13) and salinity (Figure 3.14) fields at the end of each month. Recall, time series of surface and bottom temperatures and salinities (Figure 3.7) indicated that the water was seasonally stratified in MB; the end-of-month surface fields reveal more complete spatial structure. Temperature in January and February was colder (~4°C) inshore, particularly in CCB, and warmer (~6°C) offshore. In March, temperature was relatively homogeneous (~6°C) across the domain and slightly colder (~4°C) inshore near the Merrimack River mouth. In April, the entire region warmed to ~10°C except in the north where Merrimack discharge helped sustain colder temperatures (~6°C). Increased heat flux led to temperatures of 14°–18°C in May and 14°–20°C in June. In June, temperatures were higher in the south, lower in the north, and lowest along the northern coast where the river inflow influence persisted. In July and August temperatures rose by ~2°C and the spatial pattern remained similar, with the cold northern coast region smaller and extending less far south. During fall, temperatures fell due to heat loss through the surface (15–17°C, 7–13°C, 9-

11°C, and 7-11°C in September, October, November, and December respectively) with cooler temperatures inshore.

The model surface salinity distribution (Figure 3.14) in January through April included freshest water in a broad inshore band north of Cape Ann, which connected to a narrow inshore band extending south throughout MB. In May and June southwesterly wind prevailed, pushing low-salinity water offshore by Ekman transport, and although there were three modest freshwater discharge events (Figure 3.1) the salinity gradients across the region were generally weak. In June through August, river flow was very low and salinities were 30 or higher, with a weak increase northward and offshore. In late September, northwesterly wind drove onshore Ekman transport which rebuilt a salinity gradient across the inshore areas, particularly off the month of the Merrimack River. This gradient intensified, with low salinities confined to near-shore regions, during November and December due to freshwater discharge peaks.

3.2.3 Comparison with previous years' simulations

The monthly-mean surface current, temperature, and salinity at the end of April and September were selected as examples to illustrate inter-annual variations by comparing 2012 with 2011 (Figure 3.15 and Figure 3.16). In April (Figure 3.15 upper panels), the flow field in 2012 was characterized by bifurcating currents as described above, while in 2011 there was a relatively strong clockwise eddy near the coast south of Cape Ann, which shifted the bifurcation to the south and limited the water entering MB at its northern boundary. In 2012 the counterclockwise circulation around the perimeter of MB and extending in to CCB was more pronounced than in 2011. In September (Figure 3.15 lower panels), the 2012 circulation was generally weak with a single counterclockwise eddy in central/northern MB, while the 2011 flow included numerous alternating eddies between Cape Ann and Cape Cod. In summary, a prominent difference between the two years was increased shoreward movement of GoM water towards MB during spring 2012.

Surface temperatures in 2012 were considerably warmer (by ~2°C) in April, and colder (by ~1°C) in September, relative to 2011 (Figure 3.16). Offshore surface waters were considerably fresher in 2012 than in 2011. However, in CCB the surface salinity in April was about 1 higher in 2012 than in 2011. This difference is consistent with the relatively low river discharges observed in early spring of 2012.

3.3 *Water quality fields*

3.3.1 Model fields including comparisons to observations

Model-observation correlation and regression analyses of key variables—including surface chlorophyll, NO_3^-, SiO_3^{2-}, NH_4^+, and bottom DO concentration (mg L^{-1}) and DO percent saturation—from all stations outside BH (including stations shown in black, as well as the northern and southern subsets of stations, see Figure 3.4) are presented in Figure 3.17. There is no meaningful correlation between model for near-surface chlorophyll or for silicate. The model greatly underestimates the chlorophyll when its concentration is higher than about 2 μg L^{-1}. For NO_3^- near the surface, high observed values tended to be associated with high modeled values, but there is a high degree of scatter in model results corresponding to lower NO_3^- values. Overall the model tended to overestimate the corresponding nitrate values, although the range of values is similar between model and data. The correlation coefficient was 0.87 for surface nitrate. For near-surface ammonium, there is no clear relationship at higher concentrations, and the model tended to exceed observations toward the low end of the concentration range. A better-defined model-data relationship is seen for DO, including a correlation coefficient of 0.83 for bottom DO. However, model DO tended to exceed the concentration and saturation of DO at low values and be lower than them at high values. The DO saturation was not directly modeled, rather it was calculated based on temperature, salinity and DO concentration; biases in the simulation of these different parameters could all influence the accuracy of DO saturation estimates.

The remainder of this section describes the 2012 annual progressions of key model variables, including plots that facilitate visual comparisons to observations. Many individual figures show results from subsets of all stations in each of three geographic domains (as shown in Figure 3.4): “northern subset” (F22, N04, N01, N18, Outfall/N21, and N07), “southern subset” (F15, F13, F10, F06, F29, and F01), and “harbor subset” (024, 139, 140, 142, 124, and F23).

3.3.1.1 Chlorophyll

Model chlorophyll showed less variation over the year than observations, and less surface-bottom difference (Figure 3.18 to Figure 3.20). The model spring bloom peak was lower than observations at most of the northern and southern subset stations. Model chlorophyll showed increases in spring and fall, but the low amplitudes and short durations cannot be described as dominant blooms. An underestimation of chlorophyll concentration is consistent with the overestimation of NO_3^- concentration seen in the regression plots (Figure 3.17). This feature was

also reported in prior model assessments and suggests that the RCA parameterization for nutrient uptake might need to be re-evaluated. It is also interesting to note that modeled chlorophyll in bottom waters never reaches the very low levels seen in summer field measurements, generally remaining above 1 μg L^{-1} throughout the study area all year.

The vertical distribution of model chlorophyll along a west-east transect (see Figure 3.4) across the outfall to the model boundary is shown in Figure 3.21. As expected, summer chlorophyll concentrations were generally higher in the upper layer. In January, vertical mixing and light limitation kept chlorophyll levels low except near the open boundary. In February there was an inshore-offshore chlorophyll gradient, from ~6 μg L^{-1} offshore to ~2 μg L^{-1} in western MB. Peak values occurred in March and were generally uniform vertically, with elevated levels in western and eastern MB and the highest concentration of the year near the open boundary. As vertical stratification developed, a surface or subsurface chlorophyll maximum persisted across the transect through October, after which the vertical variation in chlorophyll was less pronounced.

3.3.1.2 Dissolved inorganic nitrogen

Modeled and observed dissolved inorganic nitrogen (DIN) showed typical seasonal variation near the surface and bottom at most of the monitoring stations (Figure 3.22 to Figure 3.24). DIN was generally depleted in surface waters during March and April due to consumption by phytoplankton, remained at low levels in summer through early fall, and was then replenished in late fall and winter by vertical mixing. In contrast to surface waters, DIN in the bottom layer stayed at a relatively high level through the summer and fall seasons; a vertical gradient in DIN concentration occurred in the model and observations at most of the monitoring stations. Observed low springtime near-surface and near-bottom DIN concentrations were captured by the model.

At the outfall during two springtime surveys observed DIN levels were highest near the surface, in contrast to other stations (Figure 3.22). The simulation did not capture this feature, which is likely associated with the details of circulation within the zone of initial dilution (e.g. Blumberg et al., 1996), and if so would not be expected to be represented particularly well in the model.

At some stations the model underestimated the observed DIN concentration in the bottom layer (Figure 3.22, Figure 3.23). For example, observed summer DIN reached up to 7 μM in bottom waters at western MB stations F06 and F13, in water depths of about 32 m and 28 m respectively. Near-bottom depths at these stations are below the euphotic zone where nutrient uptake by phytoplankton does not occur. It is possible the model underestimation of DIN at depth there is due

to local nutrient sources not captured well by the model, such as groundwater sources (Becker, 1992, Jiang et al. 2007) which the model bases on historical estimates without inclusion of geographic variations.

At most BH stations, including F23 at the harbor mouth, the magnitudes and seasonal cycles of DIN in the model were similar to observations (Figure 3.24). Nutrient depletion affected the full water column and vertical gradients were small. Simulated near-bottom DIN concentrations were higher at stations 024 and 124, at the inner harbor mouth and in southeastern BH in Hingham Bay respectively, a vertical gradient that was not observed in the field data.

In end-of-month snapshots on the west-east transect across the outfall (Figure 3.25), the DIN signature of the outfall plume was concentrated at depth throughout the year. Near-surface DIN was lowest from March to September as expected in association with stratification, and higher during the generally higher mixing levels in other months.

3.3.1.3 Primary productivity

Model primary productivity is shown in Figure 3.26 at three monitoring stations (F23, N04, and N18) where observations of primary productivity (not shown) had been made in past years. Ongoing field sampling no longer includes primary productivity measurements. The vertical axis ranges are set for ease of comparison to reports on earlier years. Instead of typical peaks for spring and fall blooms, in 2012 primary productivity increased gradually in spring, remained at moderate levels through summer, and decreased abruptly in late fall. It was not particularly higher at station N18, close to the MWRA outfall, than at the other stations.

3.3.1.4 Dissolved and particulate organic nitrogen

Model-observation agreement was modest for seasonal variations and vertical distributions of DON (Figure 3.27 to Figure 3.29) and PON (Figure 3.30 to Figure 3.32). Modeled DON showed little seasonal variation, in contrast to modeled PON, which had moderate values from spring through late summer and low values during winter. Model PON showed short-term fluctuations with limited amplitudes, rather than dominant spring or fall bloom events. In both model and observations, there was no anomalous signal near the outfall in either DON or PON, showing that the organic nitrogen pools were essentially controlled by internal dynamics within the water column and not detectably altered by outfall effluent.

Model DON along the west-east transect (Figure 3.29) was relatively uniform vertically and slightly higher from January to June than from July to December, with peak values at the offshore boundary during August and September. Model PON along the west-east transect (Figure 3.32) was highest and nearly vertically uniform during March, and had horizontal layers with subsurface or surface maxima and lower deep values during other months, except for November through January when values were lower and more vertically uniform.

3.3.1.5 Particulate organic carbon

Model-observation agreement was weak for seasonal variations and vertical distributions of POC (Figure 3.33 and Figure 3.34). Observed seasonal variations in surface POC were different at different sites, with comparable spring and summer/fall peaks at some sites (for example F22 and F06), higher summer/fall peaks at some sites (for example N18, F13), and less pronounced peaks at other sites (for example N01, N07). In contrast, seasonal variations in model POC were generally the same across all sites and displayed two dominant events, one in early spring and one in late summer. Observed deep POC varied little seasonally but was generally substantially lower that surface values. In contrast, model deep POC exhibited seasonal variations in parallel with model surface POC, and was higher than surface POC during most of the year.

Model POC on the west-east transect (Figure 3.35) was relatively low in January and May through July. High POC occurred in February through April, with peak values near the surface and offshore. From August through December POC levels were moderate with spatial structure generally vertically layered, near-surface maxima, and peak values offshore.

3.3.1.6 Dissolved oxygen

Fairly good agreement was found between simulated and observed DO (Figure 3.36 and Figure 3.37). The seasonal cycle (peak in spring, decrease through summer to minimum in late fall, then increase) was reasonably well reproduced by the model. The model had a noticeable bias toward underestimation near the surface and overestimation near the bottom, compared to observations. As noted above (Figure 3.17) the correlation between modeled and observed DO concentrations was 0.75 near the surface and 0.83 near the bottom, with root-mean square (RMS) error of ~0.87 and ~0.68 mg L^{-1}, respectively.

The model captured the timing of the DO peak in late March, but considerably underestimated the maximum DO concentration. Observed near-surface DO was unusually high at several stations

during spring 2012 (Figure 3.38), for example reaching more than 13 mg L^{-1} at F22 and N04, stations where in 2011 it never exceeded 12 mg L^{-1}. At stations F22 and N04, the model-computed maximum near-surface DO concentrations were 11.4 mg L^{-1} and 11.1 mg L^{-1}, about 1.6 mg L^{-1} and 2.2 mg L^{-1} lower than the observations, respectively (Figure 3.36, upper frames). Similar model-observation differences were also found at stations N01 and N18 (Figure 3.36, middle frames) as well as at stations F15, F13, F10 and F06 (Figure 3.37).

The model did not capture the observed longer-than-typical duration of low DO near-bottom concentrations in fall 2012. An analysis (by R. Geyer in Appendix A of Libby et al., 2013) of MWRA field survey DO observations, averaged across all stations sampled in the region over survey years 1992-2011, noted that DO in 2012 was very low compared to the long term average and lower than all prior years during much of the year. To confirm and expand on these results we did a similar calculation using monthly averages (Figure 3.39). The long-term mean and range of values (black line and gray shaded area) is based on all stations sampled 1992-2010. An average across the subset of stations sampled in 2012 (blue line) makes clear that DO was unusually low. When the average is computed using the subset of those stations excluding BH, the result (red line) is somewhat higher, which is due to the unusually high 2012 springtime DO peak in MB that was not seen in BH. Model results (green line) averaged over the same station locations as used in the latter calculation reveal that although the model seasonal cycle was generally similar to observations it failed to capture the observed late duration of low bottom DO.

Model DO on the west-east transect (Figure 3.40) showed the same general patterns as those found in previous years. Concentrations are highest in spring and lowest in late summer, with values near the surface higher than near the bottom. In 2012 the vertical gradient in model DO did not weaken in winter as much as in many prior years.

Variability of DO in MB is controlled by physical and biogeochemical processes. Physical processes include advection, vertical mixing, re-aeration, and lateral diffusion, while biogeochemical processes are photosynthetic production, phytoplankton respiration, oxidation of organic carbon, sediment oxygen demand (SOD) and nitrification. High DO values in spring reflect photosynthesis production through phytoplankton growth, while remineralization of organic substances keeps DO low in summer and fall (e.g., Tian et al., 2009). On the basis of UG-RCA simulations validated against observations for the period 1992-2010, Xue et al. (2012) concluded that DO variability in northern MB is dominated by horizontal advection associated with the

western GoM coastal current while in southern MB, particularly within CCB, a well-defined circulation retention mechanism causes longer residence times and DO variation is controlled predominantly by local biogeochemical processes.

Xue et al. (2014) further investigated mechanisms controlling DO and concluded that a dominant factor is re-aeration, or air-sea interaction, as governed partly by vertical mixing and partly by DO over/under-saturation. DO saturation depends on temperature and salinity as well as oxygen concentration, and is a useful quantity to help understand the relative influence of temperature on DO compared to photosynthesis; percent saturation above 100% can result from photosynthetic production. We computed DO saturation from observations of DO concentration, temperature, and salinity using the approximate relation given in equation 2.3 of Zhao et al. (2012). Comparisons between this result and modeled DO saturation (Figure 3.41 to Figure 3.43) reveal a similar pattern at most MB stations. In winter, DO saturation levels are modest and vertical mixing keeps them nearly vertically uniform; in spring, photosynthesis increases surface values, which reach a maximum in early summer. Then both surface and deep values both gradually decrease through late fall or early winter, when they are homogenized again. The model underestimated the saturation value at most stations in 2012, just as found by Zhao et al. (2012) for simulations of 2011, which could indicate that photosynthetic oxygen production is underestimated by the model.

For most stations in BH, observed DO saturation (Figure 3.43) varied only weakly seasonally and vertically, compared to MB. Model DO saturation in BH captured this variability at most stations, with the exception of 024 and 124 where the model DO saturation was quite similar to that in MB. Model DO saturation along the west-east transect (Figure 3.44) was most uniform vertically in November through January, took peak values in March and April extending along the full transect and nearly throughout the water column, and in other months was mostly horizontally uniform with a gradient from high values at the surface to lower values at depth.

To help improve understanding of the relative importance of processes governing DO in the model, annual cycles of DO flux components were computed for both 2011 and 2012 in the manner of Xue et al. (2014), but here averaged across the UG-RCA domain (Figure 3.45). The total DO flux is the sum of components due to reaeration, advection, oxidation, photosynthesis-respiration, and SOD. The annual cycle of net flux is generally similar during the two years. Relative to 2012, in 2011 the photosynthesis-respiration flux was substantially more positive, and the oxidation flux was substantially more negative. Nonetheless, in the late summer of both years, the total flux is

quite similar, as it is mainly the difference between these two terms (photosynthesis-respiration and oxidation), and they tend to balance each other as discussed by Xue et al. (2014).

3.3.1.7 Sediment fluxes

Model sediment nutrient fluxes and sediment oxygen demand (SOD) are shown in Figure 3.46 and Figure 3.47, at BH and MB stations (Figure 3.4; BH02, BH03, BH08A, MB01, MB03 and MB05) where flux measurements (not shown) had been made in earlier years. Ongoing field sampling no longer includes benthic fluxes. Vertical axis ranges are set for ease of comparison to reports on earlier years. Ammonium fluxes were higher during summer and early fall at BH stations as compared with MB stations, indicating that in the model remineralization contributed a substantial share to the increased nutrient supplies in summer in BH. A similar pattern was observed for SOD, with low flux at MB stations and high flux in BH during summer and fall.

3.3.1.8 Summary

In summary, the UG-RCA 2012 simulation captured many of the observed seasonal and vertical variations of an array of key parameters examined here. Among them, agreement of the model with observations was generally strongest for DIN and DO, modest for chlorophyll, DON and PON, and poor for DOC. Notable differences of model fields with observations included underestimation of spring and fall bloom chlorophyll concentrations, overestimation of MB bottom chlorophyll and BH surface and bottom chlorophyll during the summer, overestimation of bottom POC in MB, and underestimation of MB surface DO in spring. The model typically does not capture the extremes of observed values, and at most stations has smaller surface-bottom differences than observed.

3.3.2 Comparison with previous years' simulations

We now compare UG-RCA simulations for 2010, 2011 and 2012 in order to provide context for inter-annual variability in the model. Overall, the 2012 chlorophyll simulation differed from those of 2010 and 2011 in that it had a no clear spring or fall bloom (Figure 3.48). The 2010 model chlorophyll had a spring bloom reaching more than 4 $\mu g\ L^{-1}$ in April and a relatively large fall bloom reaching more than 5 $\mu g\ L^{-1}$. The 2011 model chlorophyll had no noticeable spring bloom, a peak in the winter season, and two small fall blooms over a two-week period during September.

The DIN seasonal cycle was generally similar among the three years, with high values in winter, low values in summer and replenishment in late fall (Figure 3.49). Values in 2012 were

lower than in 2010 and 2011 during the winter-spring decrease, and slightly higher than them in early fall.

For bottom DO concentration (Figure 3.50) and bottom DO saturation (Figure 3.51), in all three years high values occurred during the spring phytoplankton bloom and low values occurred in late summer and early fall. In 2012, DO concentration was about 1 mg L^{-1} lower in February and March than in 2010 and 2011, then somewhat higher than them in April, with a similar pattern in DO saturation. At most stations the fall replenishment of DO concentration and saturation occurred slightly earlier, and at a faster rate, in 2012 and 2010 compared to 2011. This contrasts the longer than typical 2012 late summer and early fall low DO conditions observed (Libby et al., 2013).

4. Scenario experiment and sensitivity experiment

In this section, we describe a scenario experiment and a sensitivity experiment. The scenario experiment is the same as in prior MWRA modeling reports, using simulations without and with MWRA effluent to assess the potential influence of the MWRA outfall on MB water quality and ecosystem function during 2012. The sensitivity experiment examines the influence of the advection of water flowing in at the northern boundary on the model-simulated DO concentration in the interior, particularly in northern MB.

4.1 *Scenario experiment: Effect of outfall effluent*

We refer to the simulation described above, with the MWRA outfall present, as the "control" and to the sensitivity-analysis simulation without the outfall as the "non-sewage" run. We compared the chlorophyll, DIN, and DO between the two simulations. The control and non-sewage simulations had nearly identical intensities and seasonal variations of chlorophyll concentration (Figure 4.1). The seasonal cycle of surface DIN was also similar in the two simulations (Figure 4.2). In summer they were almost identical while in winter the non-sewage case had lower surface DIN concentration than the control. In bottom DIN (Figure 4.3) the non-sewage case was notably lower than the control at stations near the outfall and very similar at other stations. The DO results (Figure 4.4 and Figure 4.5) were practically identical for the two simulations.

These results for 2012 are consistent with prior non-sewage scenario runs (HydroQual 1995; Jiang and Zhou 2006b; Tian et al. 2009; Chen et al. 2010; Tian et al. 2010, Zhao et al. 2011, 2012). They are also in keeping with the conclusion drawn by MWRA that the effect of the outfall on MB is confined to within about 10-20 km and consists mainly of elevated ammonium levels there,

based on comparing field observations between pre-diversion (prior to relocation of the outfall to MB from BH) and post-diversion periods. While the outfall influences nutrients in its immediate vicinity, it does not have a notable influence on system-wide chlorophyll or DO.

To investigate the extent of the difference between the two runs for ammonium—the most abundant form of nitrogen in the outfall discharge—we plotted the spatial distribution of the difference between bottom-layer ammonium in the control and non-sewage cases at the end of each month (Figure 4.6). We also plotted the ammonium difference (Figure 4.7) at the end of each month, along the west-east transect through the outfall (shown in lower right of Figure 4.5). Generally, as in past years, the bottom ammonium difference (Figure 4.6) was perceptibly higher in summer months than in winter months, as expected due to effluent trapping by summer stratification. Also, as in past years, months when dispersal of the plume extended larger distances occurred in winter. In the west-east transects (Figure 4.7) the plume was confined vertically by stratification more so in summer than winter, as expected. In these end-of-month snapshots, the plume did not extend as near to the surface in winter as it did in past years.

To summarize, the no-outfall scenario simulation for 2012 indicated similar results as in prior years. The outfall plume influence typically remains within about 20 km of the outfall, and concentrated in the deeper part of the water column except in winter. Dispersal of the plume can occur over longer horizontal distances during winter, but both light and vertical mixing are unfavorable to phytoplankton growth at that time. Consequently, the conclusion that there are no ecologically important influences of the outfall on biomass or DO distributions is supported.

4.2 *Sensitivity experiment: Northern boundary DO*

The sensitivity experiment described here investigates the influence on DO inside MB of the model open boundary condition (OBC) value of DO. To set the stage we recall that, at stations outside BH, the 2012 UG-RCA simulation considerably underestimated the peak surface DO in spring and overestimated the summer/fall DO minima (Figure 3.36 and Figure 3.37), and that inflow to MB from the WMCC on the northern boundary was stronger in spring of 2012 than in spring 2011 (Figure 3.15). In addition we note that F26 and F27, two stations close to the boundary at the northeastern portion of the domain, have not been sampled since 2010. This leads to the hypothesis that, were DO samples near F26/F27 available in 2012, and were they to have been substantially higher than those from other more interior stations that were sampled, they could have influenced the OA mapping yielding a higher DO at the OBC and thus led to better model

agreement with the observed high spring DO. A similar hypothesis applies to potential improvement of model agreement with the low DO observations during fall.

To investigate this we conducted two sensitivity experiments. In Experiment A we included DO records from NERACOOS mooring A01 in the OA analysis for the OBC. Mooring A01 is located northeast of the outfall but not as far northeast as stations F26/F27 (Figure 3.4). In Experiment B we created a synthetic F27 record by adding the model-observation difference (about 2 mg L^{-1}) in DO concentration at F22 (the station nearest to F26/F27 that was sampled in 2012) to the station F22 record, and included that result in the OA analysis. The two experiments are used together to illustrate the range of impact of the DO boundary condition on simulated DO in MB.

Figure 4.8 shows the different Experiment A and B OBC results at the boundary point closest to F27, along with that of the base run described in Section 3 above. Somewhat surprisingly, including mooring A01 in the OA mapping (Experiment A) led to an OBC with a spring DO peak about 1 mg L^{-1} lower (Figure 4.8). Consequently, simulated DO in experiment A (Figure 4.9) disagreed even more strongly with surface observations at interior stations in spring of 2012 than the base run did. This demonstrated that DO in the interior of MB is strongly influenced by the DO boundary condition. It also suggested that, for springtime, if higher DO at F26/F27 was responsible for higher interior MB DO, a large DO gradient between mooring A01 and F26/F27 must have been present.

We have no 2012 observations from F26/F27, so to examine the maximum influence of a higher DO boundary value we adjusted it in Experiment B as follows. The model-observation difference of the spring peak at F22 was about 1.7 mg L^{-1} and at station N04 farther toward interior MB it was over 2.3 mg L^{-1}. We constructed a synthetic station F27 record representative of these differences by adding 2 mg L^{-1} to each surface DO value at F22, and then included this as a synthetic station F27 in the OA-mapping. The resulting DO boundary value had the same time-variation pattern, but the maximum value was increased by about 1.2 mg L^{-1} (Figure 4.8). Re-running the UG-RCA with this adjusted DO boundary condition led to visible improvements in simulated surface DO in the northern MB region (Figure 4.10), although the model still underestimated the peak values. The bottom DO, which is overestimated by the model, was slightly worsened by the inclusion of assumed higher values at the boundary. As in the recent analysis by Xue et al. (2012), this result suggests that the northern boundary DO value is critically important, though not sufficient, to ensure simulation accuracy in interior northern MB.

Finally, it should be noted that spatial differences in surface DO concentrations as high as 2 mg L^{-1} between the stations F26/F27 and station F22 were never observed in the sixteen years when both stations were measured by the MWRA monitoring program. The largest difference observed was 1.5 mg L^{-1}, during two of 100 surveys over that time period. Thus Experiment B represents an unlikely set of conditions, in which F22 and the synthetic F27 differ by more than has ever been observed, and can be viewed as an upper bound for influence of the OBC on the interior.

5. Summary

The UMass Dartmouth Marine Ecosystem Dynamic Modeling laboratory simulated hydrodynamic and water quality parameters including dissolved oxygen for calendar year 2012 in MBS using the unstructured grid model system MB-FVCOM/UG-RCA. The methods were as in the prior year's simulation (described in Zhao et al., 2012) but with two substantive changes: (a) code upgrades to the most recent version of FVCOM, and to associated interfaces between it and UG-RCA, and (b) improved data assimilation that reduces abrupt temporal changes in temperature and salinity that had previously been occurring near sampled times of assimilated observations.

The hydrodynamic model reproduced observations of temperature and salinity and captured tidal and subtidal currents well. The modeled seasonal cycle of stratification, more dominantly temperature-driven in 2012 than some other years due to the lower than average river runoff and hence weaker salinity variability in 2012, agreed well with observations. Movement of GoM water in to MB in the area south of Cape Ann during spring was more pronounced in 2012 than in 2011.

The water quality simulation captured general patterns in seasonal variations and vertical structure of many observed fields. In general the model showed a smaller range of values, and smaller surface-bottom differences during the stratified season, when compared to observations. Well-known observed features in the seasonal cycle and vertical structure of DIN were evidenced by the model, namely the spring/summer reduction in shallow concentrations due to phytoplankton uptake and later fall replenishment due to enhanced mixing when stratification breaks down. However, modeled chlorophyll did not show dominant blooms at any point during the year, in contrast to observations that showed typical spring and fall blooms. This could be because the model GoM water, which appears to have moved into MB during springtime more strongly than in a typical year, had lower concentrations than observed due to limitations associated with the OBC methodology. Model deep chlorophyll was consistently higher than observations during summer. The model captured the gross features of the seasonal cycle of DO, with peaks in spring when

shallow values increase due to phytoplankton growth, continuous decreases through summer and early fall, and replenishment during the winter mixed period. However it missed the observed high springtime concentrations, and the late fall extended duration of low bottom DO. Model DON and PON showed modest agreement with observations, while model POC did not capture well the seasonal variations or the vertical structure of observations and was biased high at depth. In summary, model-observation agreement was generally strongest for DIN and DO, modest for chlorophyll, DON and PON, and poor for DOC.

In order to assess the potential influence of the MWRA outfall on MB system-wide ecosystem function, results of the base simulation were compared to a scenario simulation in which effluent from the MWRA outfall was removed. In 2012, as in simulations of previous years, the influence of the effluent was demonstrated to be confined to within about 10-20 km of the outfall, and to consist mainly of increased ammonium concentrations there. In summer the influence is more confined in the deeper water column, and minimally dispersed horizontally, in association with stronger stratification and weaker circulation due to reduced winds. Conversely the enhanced vertical mixing and stronger currents during the more windy unstratified winter conditions means the signature of the effluent extends nearer to the surface, and can be dispersed over longer ranges. However, the low light availability and low temperatures during winter mean phytoplankton growth, the most likely system attribute to potentially respond to elevated ammonium levels, remains weak. Consequently the effluent is shown to have no perceptible effect on system-wide ecosystem functionality such as phytoplankton growth or oxygen levels.

Because the model did not capture well the anomalously high 2012 observed MB spring surface DO concentrations, the influence of DO forcing at the northeastern model boundary was investigated using sensitivity simulations. In experiments A and B respectively the OA mapping of DO to the OBC was made to incorporate (a) mooring A01 time series observations and (b) synthetic values chosen to represent the highest range of past observations. Contrary to initial expectations, experiment A degraded model-observation agreement. This suggests there may have been DO variations on short horizontal spatial scales near mooring A01 and the northeastern boundary, though past observations indicate spatial gradients of sufficiently large magnitude are rare. Experiment B gave better model-observation agreement near the surface but caused small increases to model-observation mismatch at depth. Both experiments demonstrate that advection is an important influence on DO in interior MB and that simulation accuracy can be strongly

determined by DO on the OBC near the northeastern boundary. This implies that the quantity and quality of DO observations there, and the methodology for using them to determine the OBC, are key factors controlling model DO performance.

References

Becker S. 1992. The seasonal distribution of nutrients in Massachusetts and Cape Cod Bays. Masters Thesis, University of New Hampshire, Durham. 127pp.

Beardsley, R., E.E. Adams, D. Harleman, A. Giblin, J.R. Kelly, J.E. O'Reilly, and J.F. Paul, 1995. Report of the MWRA hydrodynamic and water quality model evaluation group. MWRA Enviro. Quality Dept. Misc. Rpt. No. ms-37. Boston: Massachusetts Water Resource Authority. 58pp.

Blumberg A., Ji Z. and Ziegler C.K., 1996, Modeling outfall plume behavior using a far field model, *J. Hydraulic Engineering*, **112**: 610-616.

Chen C., B. Beardsley, G.W. Cowles, J. Qi, Z. Lai, G. Gao, D. Stuebe, Q. Xu, P. Xue, J. Ge, R. Hu, R. Ji, R. Tian, H. Huang, H. Wu, H. Lin, Y. Sun, and L. Zhao, 2013. An Unstructured grid, Finite-Volume Community Ocean Model-FVCOM User Community-FVCOM user manual, School for Marine Science and Technology, University of Massachusetts Dartmouth, New Bedford, Fourth Edition. SMAST/UMASSD Technical Report-13-0701, 404pp.

Chen C, Beardsley R, Xu Q, Mickelson MJ, Tian R, Xue P, Cowles GW, Rothschild BJ. 2009. The Massachusetts and Cape Cod Bays hydrodynamic model: 2006-2007 simulation. Boston: Massachusetts Water Resources Authority. Report 2009-10. 77pp.

Chen C., Tian R., Beardsley R.C., Qi J. and Xu Q. 2010. Modeling 2008 in Massachusetts Bay using an upgraded unstructured-grid Bays Eutrophication Model. Boston: Massachusetts Water Resources Authority. Report 2010-15. 127pp.

Geyer, W.R. 2013. Physical Processes Influencing Massachusetts Bay, 2012. Appendix to Libby et al. 2013, "2012 Water column monitoring results", Boston: Massachusetts Water Resources Authority. Report 2013-15.

HydroQual, 1993. A water quality model for Massachusetts and Cape Cod Bays. Boston: Massachusetts Water Resources Authority. Report 1993-05. 222pp.

HydroQual, 1995. A water quality model for Massachusetts and Cape Cod Bays: Calibration of the Bay Eutrophication Model (BEM). Boston: Massachusetts Water Resources Authority. Report 1995-08. 402pp.

HydroQual, 2000. Bays Eutrophication Model (BEM): modeling analysis for the period 1992-1994. Boston: Massachusetts Water Resources Authority. Report 2000-02. 158pp.

HydroQual. 2001a. Addendum to "Bays Eutrophication Model (BEM): modeling analysis for the period of 1992-1994". Boston: Massachusetts Water Resources Authority. Report 2001-13. 60 pp.

HydroQual, 2001b. Boundary sensitivity for the Bays Eutrophication Model (BEM). Boston: Massachusetts Water Resources Authority. Report 2001-14. 90pp.

HydroQual. 2001c. Analysis of the addition of a third algal group to the Bays Eutrophication Model (BEM) kinetics. Boston: Massachusetts Water Resources Authority. Report 2001-15. 110pp.

HydroQual, Inc. and Signell R.P. 2001. Calibration of the Massachusetts and Cape Cod Bays Hydrodynamic Model: 1998-1999. Boston: Massachusetts Water Resources Authority. Report 2001-12. 170pp.

HydroQual. 2002a. Sensitivity of the Bays Eutrophication Model (BEM) to changes in algal model coefficients. Boston: Massachusetts Water Resources Authority Report 2002-16. 236pp.

HydroQual. 2002b. Addendum to the 1998-1999 hydrodynamic modeling report. Boston: Massachusetts Water Resources Authority. Report 2002-17. 82pp.

HydroQual, Inc. 2003. Bays Eutrophication Model (BEM): modeling analysis for the period 1998-1999. Boston, Massachusetts Water Resources Authority. Report 2003-03. 318pp.

HydroQual, 2004. "User's Guide for RCA, Release 3.0", Hydroqual, Inc, New Jersey.

Jiang M, and Zhou M. 2003. Massachusetts Bay hydrodynamic model and water quality model results in 1998-99: comparison report between HydroQual and University of Massachusetts Boston runs. Boston: Massachusetts Water Resources Authority. Report 2003-10. 42pp.

Jiang M. and Zhou M. 2004a. Calibration of the Massachusetts and Cape Cod Bays hydrodynamic model: 2000-2001. Boston: Massachusetts Water Resources Authority. Report 2004-08. 71pp.

Jiang M. and Zhou M. 2004b. Bays Eutrophication Model (BEM) model verification for the period: 2000-2001. Boston: Massachusetts Water Resources Authority. Report 2004-09. 90pp.

Jiang M. and Zhou M. 2006a. The Massachusetts and Cape Cod Bays hydrodynamic model: 2002-2004 simulation. Boston: Massachusetts Water Resources Authority. Report 2006-12. 128pp.

Jiang M. and Zhou M. 2006b. Massachusetts Bay Eutrophication Model: 2002-2004 Simulation. Boston: Massachusetts Water Resources Authority. Report 2006-13. 126pp.

Jiang M. and Zhou M. 2007. User's guide to the water-quality part of the Bays Eutrophication Model (BEM). Boston: Massachusetts Water Resources Authority. Report 2007-09. 36pp.

Jiang, M., G. T. Wallace, M. Zhou, S. Libby and C. D. Hunt, 2007. Summer formation of a high-nutrient low-oxygen pool in Cape Cod Bay, USA, *J. Geophys. Res*., **112**, C05006, doi:10.1029/2006JC003889.

Jiang M. and Zhou M. 2008a. The Massachusetts and Cape Cod Bays hydrodynamic model: 2005 simulation. Boston: Massachusetts Water Resources Authority. Report 2008-12. 58pp.

Jiang M, and Zhou M. 2008b. Massachusetts Bay Eutrophication Model: 2005 simulation. Boston: Massachusetts Water Resources Authority. Report 2008-13. 82pp.

Libby PS, Borkman DG, Geyer WR, Turner JT, Costa A, Mickelson MJ. 2013. 2012 Water column monitoring results. Boston: Massachusetts Water Resources Authority. Report 2013-15. 39pp. plus appendices.

Menzie CA, Cura JJ, Jr, Freshman JS, Potocki B. 1991. Boston Harbor: estimates of loadings. Boston: Massachusetts Water Resources Authority. Report 1991-04. 108pp.

Tian, R.C., Chen C.S., Xu Q.C., Xue P.F., Cowles G.W., Beardsley R. and Rothschild B. 2009. Massachusetts Bay Eutrophication Model: 2006-2007 Simulation. Boston: Massachusetts Water Resources Authority. Report 2009-11. 147pp.

Tian, R.C., Chen, C., Zhao, L.Z., Xue, P., Leo, W.S., Mickelson M.J. 2010. Modeling 2009 in Massachusetts Bay using the unstructured-grid Bays Eutrophication Model. Boston: Massachusetts Water Resources Authority. Report 2010-22. 100pp.

Xue, P., C. Chen, and R. C. Beardsley, 2012. Observing system simulation experiments of dissolved oxygen monitoring in Massachusetts Bay. *J. Geophys. Res.*, 117, C05014, doi:10.1029/2011JC007843.

Xue, P., C. Chen, J. Qi, R. C. Beardsley, R. Tian, L. Zhao, and H. Lin, 2014. Mechanism studies of seasonal variability of dissolved oxygen in Mass Bay: A multi-scale FVCOM/UG-RCA application. *Journal of Marine Systems*. 131, 102-119.

Zhao L, Tian R, Xue P, Chen C, Leo WS, Mickelson MJ. 2011. Modeling 2010 in Massachusetts Bay using the unstructured grid Bay Eutrophication Model. Boston: Massachusetts Water Resources Authority. Report 2011-09. 118 p.

Zhao, L.Z., Chen, C., Leo, W.S. and Mickelson M.J. 2012. Modeling 2011 in Massachusetts Bay using the unstructured-grid Bays Eutrophication Model. Boston: Massachusetts Water Resources Authority. Report 2011-13. 135pp.

Table 1.1 Bays Eutrophication Model (BEM) technical and historical development documentation.

Model-focused MWRA Technical Reports to date, chronological order. General topic, highlighted aspects of content, and citation with MWRA technical report number. (When this table is viewed electronically, citations are hyperlinked to the MWRA online Technical Reports list for easy access and download of PDF files.)

HDM = Hydrodynamic model, WQM = water quality model, BEM = HDM+WQM.

Topic	*Highlighted aspects of content*	*Citation*
Phase I		
BEM model design and initial calibration	Both HDM and WQM by Hydroqual; Adapting Chesapeake formulations; "Aggregated" grid for WQM; Appendix A, water column kinetics; Appendix B, sediment model	Hydroqual 1993 (TR 1993-05)
BEM calibration; 1989-1991, 1992 periods	HDM by USGS (ECOM-si); MB focused; Simulated Oct 1989 – Apr 1991 and Jan-Dec 1992; Sensitivity to WQM open boundary condition (OBC); Initial projection/scenario runs	Hydroqual 1995 (TR 1995-08)
BEM assessment by Model Evaluation Group	Summarizes all HDM & WQM components, including detail on sediments module; Assesses strengths, weaknesses, recommends most fruitful applications	Beardsley et al, 1995 (TR 1995-ms-37)
BEM simulation 1992-94	Re-ran 1992 period; Systemwide budgets for nitrogen and nutrients; Model assessed in relation to inter-annual changes in fall bloom, spring and summer dissolved oxygen (DO)	Hydroqual 2000 (TR 2000-02)
BEM calibration using 1998-99 simulation	Detailed description of HDM; Improved (spatially varying) light attenuation; New OAX (objective analysis) determination of OBC forcing; Re-ran 1992-94 period	Hydroqual & Signell 2001 (TR 2001-12)
WQM: OBC, parameters, Grid aggregation	[Addendum to Hydroqual 2000] Improved method for OBC; Review of changes to kinetic model parameter choices in earlier simulations, and effects of grid aggregation	Hydroqual 2001a (TR 2001-13)
WQM boundary sensitivity	Sensitivity to DO and DIN on open boundary	Hydroqual 2001b (TR 2001-14)
WQM third algal group	Discusses improvements & limitations associated with adding third (Autumn) algal group	Hydroqual 2001c (TR 2001-15)
WQM algal model coefficients	Sensitivity study of coefficients in Laws-Chalup formulation; Reviews history of past coefficient values used, and changes made	Hydroqual 2002a (TR 2002-16)
HDM: Mixing, surface flux, OBC, GoM model	[Addendum to Hydroqual & Signell 2001] Discusses vertical mixing, surface heat flux, light attenuation, relaxation times used on OBC, and Gulf of Maine model	Hydroqual 2002b (TR 2002-17)
BEM verification, 1998-99 simulation period	Aggregation terminated; BC forcing method explained in more detail; Review of Harbor & Outfall Monitoring observations; Sensitivity to 3rd algal group and to nutrient recycling rates	Hydroqual 2003 (TR 2003-03)
Phase II		
BEM: comparing Hydroqual, UMB runs	HDM & WQM both by UMB; Summary of MB physical/ biological oceanography; Compared HDM pre/post-UMB using 1992-94, compared WQM pre/post-UMB using 1998-99	Jiang and Zhou 2003 (TR 2003-10)

(**Table 1.1**, continued)

Topic	*Highlighted aspects of content*	*Citation*
Phase II, continued		
HDM calibration	Improved OBC forcing from "manual"/"tuning" to sea level & T/S observations using geostrophic method; describes summertime upwelling/downwelling	Jiang and Zhou 2004a (TR 2004-08)
BEM simulation period 2000-01	Incorporates improved HDM OBC method; Used improved attenuation coefficient in BH; Sensitivity to lag in zooplankton grazing; High-nutrient low-oxygen conditions in CCB	Jiang and Zhou 2004b (TR 2004-09)
HDM: 2002-04 simulation	Regional model tidal forcing; nudging assimilation of mooring currents, T/S observations; Model-observation comparisons; Sensitivity to additional vertical grid levels	Jiang and Zhou 2006a (TR 2006-12)
WQM: 2002-04 simulation	Rates quality of different years' nutrients observations used in OBC; Improves wind mixing/aeration formulation; Compares Laws-Chalup to Platt ("standard")	Jiang and Zhou 2006b (TR 2006-13)
User's Guide to WQM	Explains all boundary point source forcing (including MWRA effluent); Summary of model equations and parameters (Appendix A); Explains differences between RCA-v2.0 and v3.0	Jiang and Zhou 2007 (TR 2007-09)
HDM 2005 simulation	New tidal elevation forcing; Improved BC observations; Model summer up/downwelling weaker than observed; Winter cooling/mixing, freshwater plumes, eddies off Cape Ann	Jiang and Zhou 2008a (TR 2008-12)
WQM 2005 simulation	Examines processes governing nutrients, dissolved oxygen (DO); Emphasizes roles of events in river flow and winds; No-outfall scenario run discussed	Jiang and Zhou 2008b (TR 2008-13)
Phase III		
HDM 2006-07 simulation	Introduces spatially variable wind forcing, finer grid resolution, assimilation at OBC; Compares ECOMsi to FVCOM; Notes poor response to cooling events	Chen et al., 2009 (TR 2009-10)
WQM 2006-07 simulation	Shows improvement of model-obs DO agreement associated with spatially varying winds; Discusses scenario run with no outfall; Final RCA-v2.0-based simulation	Tian et al., 2009 (TR 2009-11)
BEM 2008 simulation	First use of FVCOM and (RCA-v3.0-based) UG-RCA, nested in regional FVCOM; Compares RCA v2.0 and v3.0 using 2006; Implements total irradiance vs PAR scaling; Compares 2006 & 2008 simulations; Sensitivity to reduced monitoring sampling sites; No-outfall scenario run	Chen et al., 2010 (TR 2010-15)
BEM 2009 simulation	Provides in-depth explanations of all methods; Compares 2009 forcing conditions and bloom/DO responses to earlier years; No-outfall scenario run	Tian et al., 2010 (TR 2010-22)
BEM 2010 simulation	Compares 2010 forcing conditions and bloom/DO responses to earlier years; No-outfall scenario run	Zhao et al., 2011 (TR 2011-09)
BEM 2011 simulation	Compares 2011 forcing conditions and bloom/DO responses to earlier years; No-outfall scenario run	Zhao et al., 2012 (TR 2012-13)

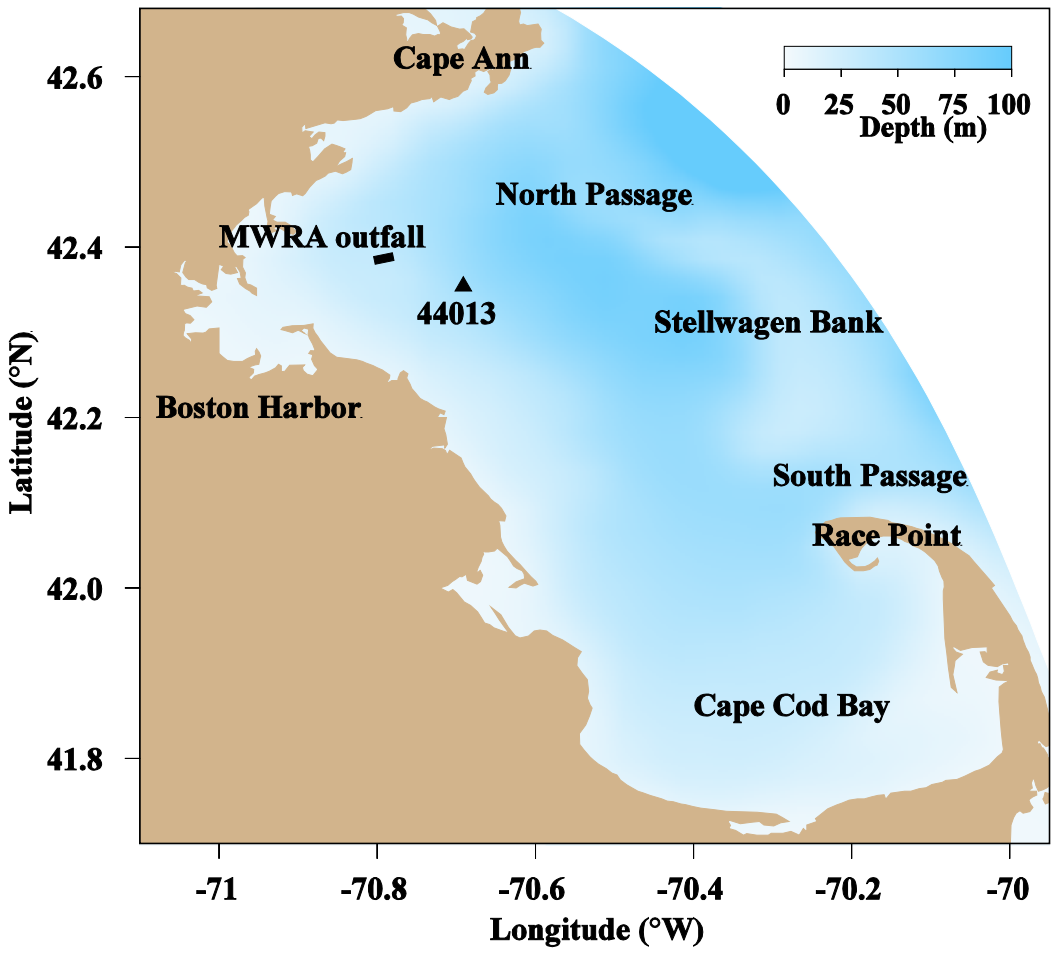

Figure 1.1 The Massachusetts Bay system (MBS) and location of the MWRA outfall.

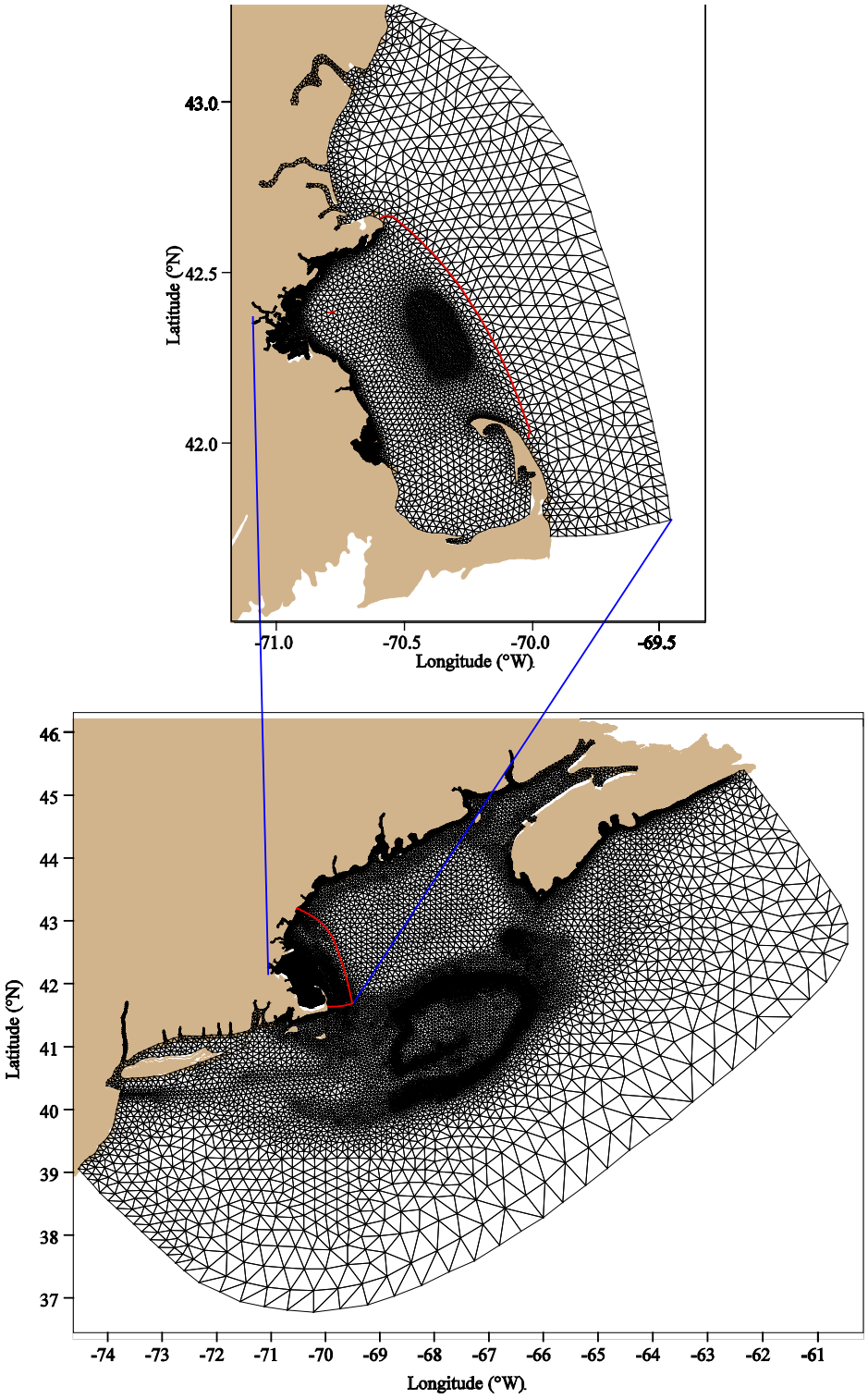

Figure 2.1 Model grids.

Lower panel: Gulf-of-Maine FVCOM grid; the red line shows the nested domain of Massachusetts Bay FVCOM. Upper panel: higher-resolution grid for MB-FVCOM; the red line shows the domain of the water quality model UG-RCA, which does not extend as far east as the MB-FVCOM grid.

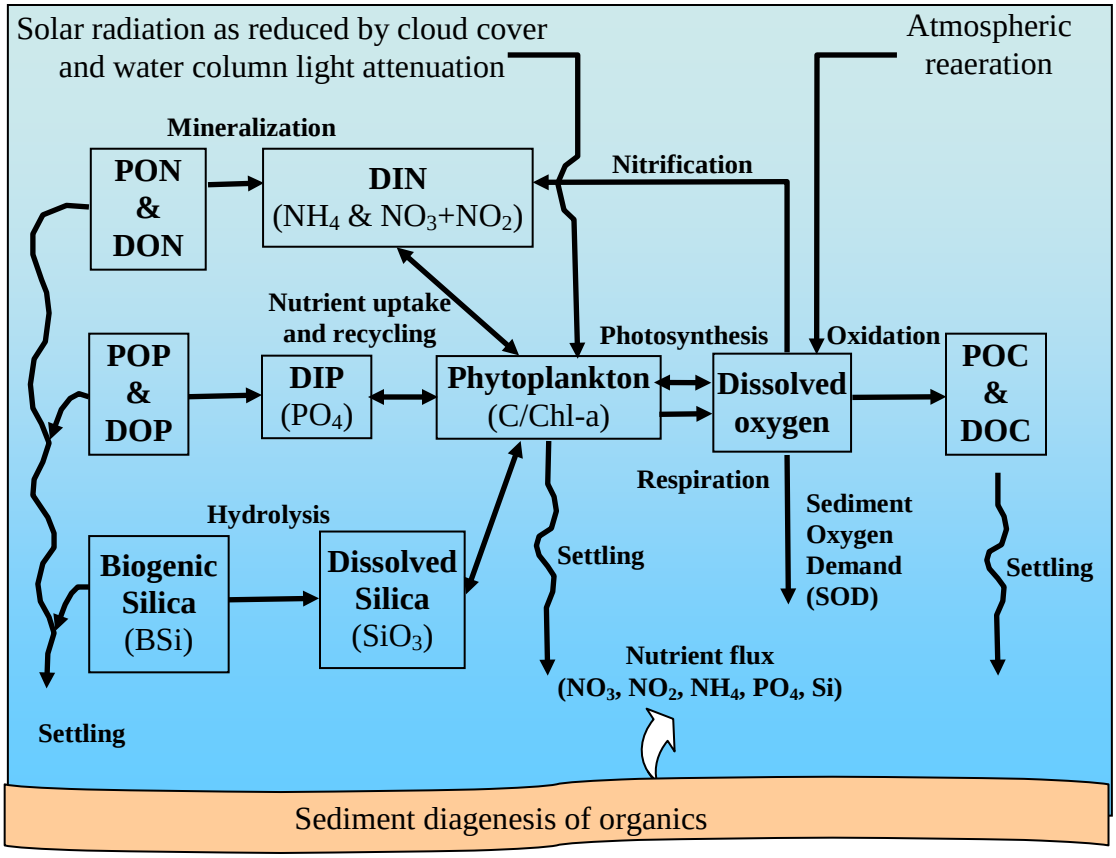

Figure 2.2 Schematic of water quality model (reproduced from Hydroqual, 2004).

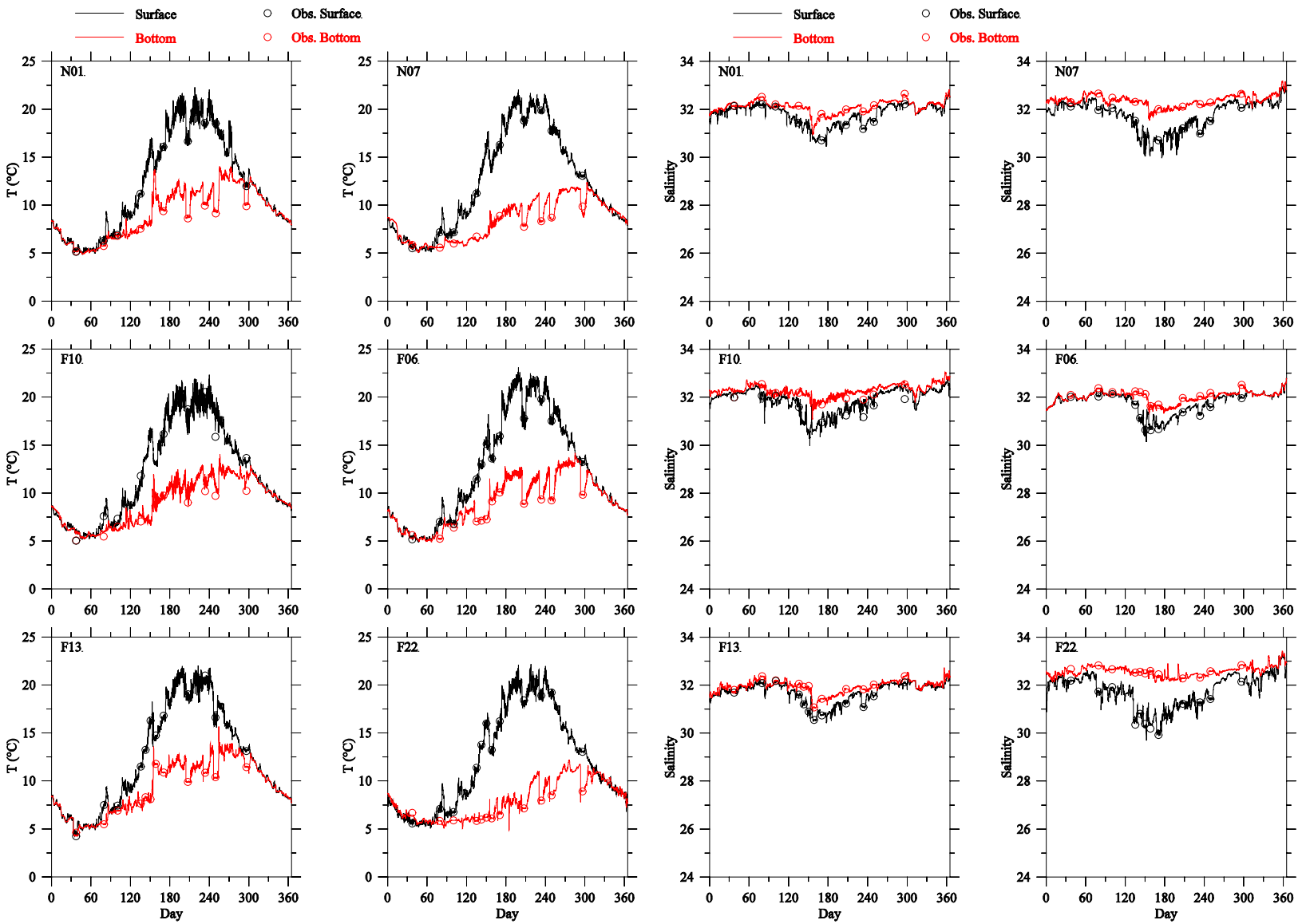

Figure 2.3 Example of model-observation comparisons for temperature (left) and salinity (right), prior to improved data assimilation method.

Abrupt changes in simulation values occur near times when moored observations were assimilated. Compare to Figure 3.7, which results from the improved method and shows much less abrupt changes.

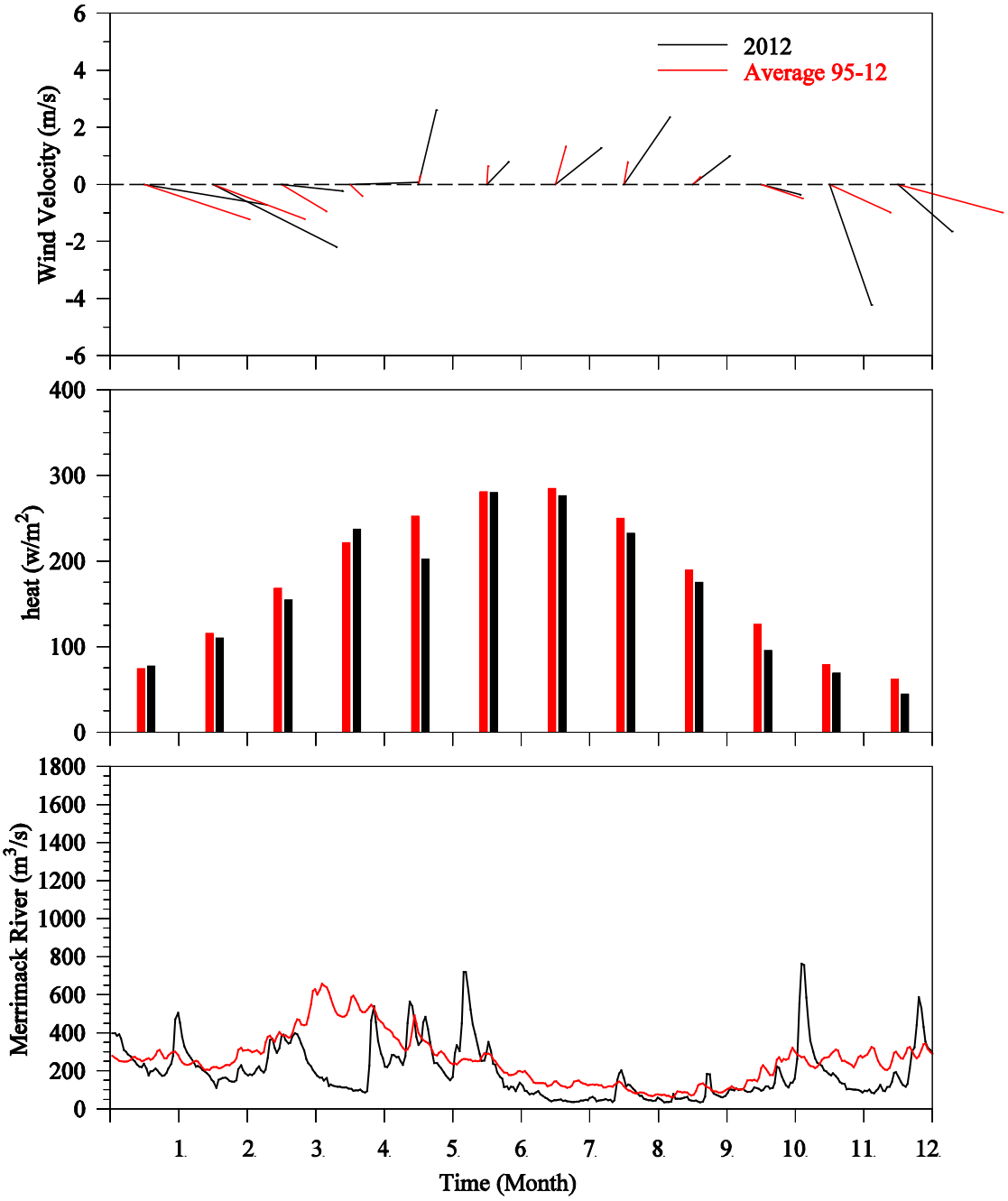

Figure 3.1 Monthly-averaged wind (upper panel) and heat flux (mid panel) and daily-averaged discharge from Merrimack River in 2012 (black) and the 18-year (1995-2012) average (red).

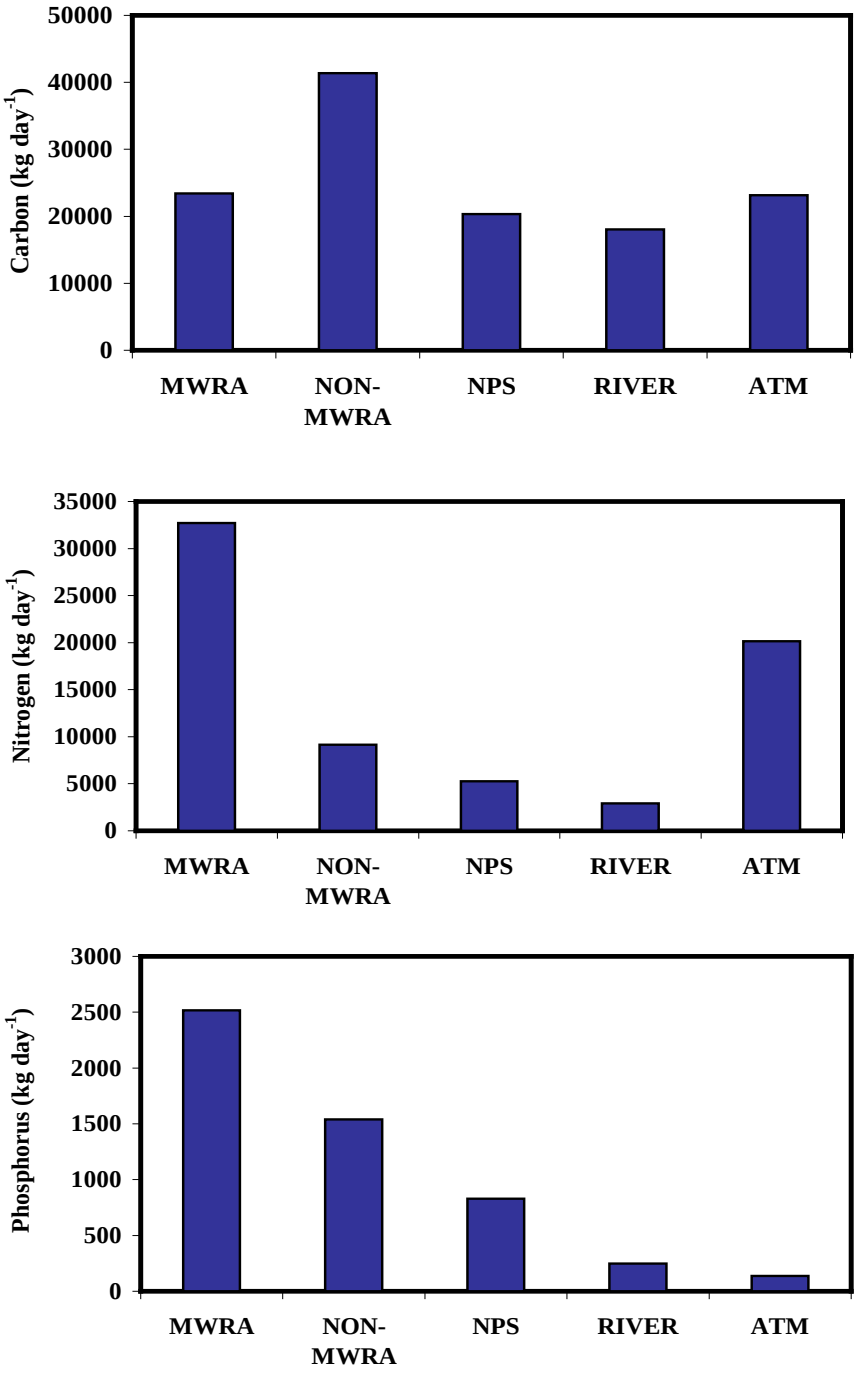

Figure 3.2 Mean daily loads of carbon, nitrogen and phosphorus from non-oceanic sources in 2012.

MWRA: MWRA outfall; Non-MWRA: Non MWRA point sources; NPS: Non-point sources; River: River loadings; ATM: Atmospheric input.

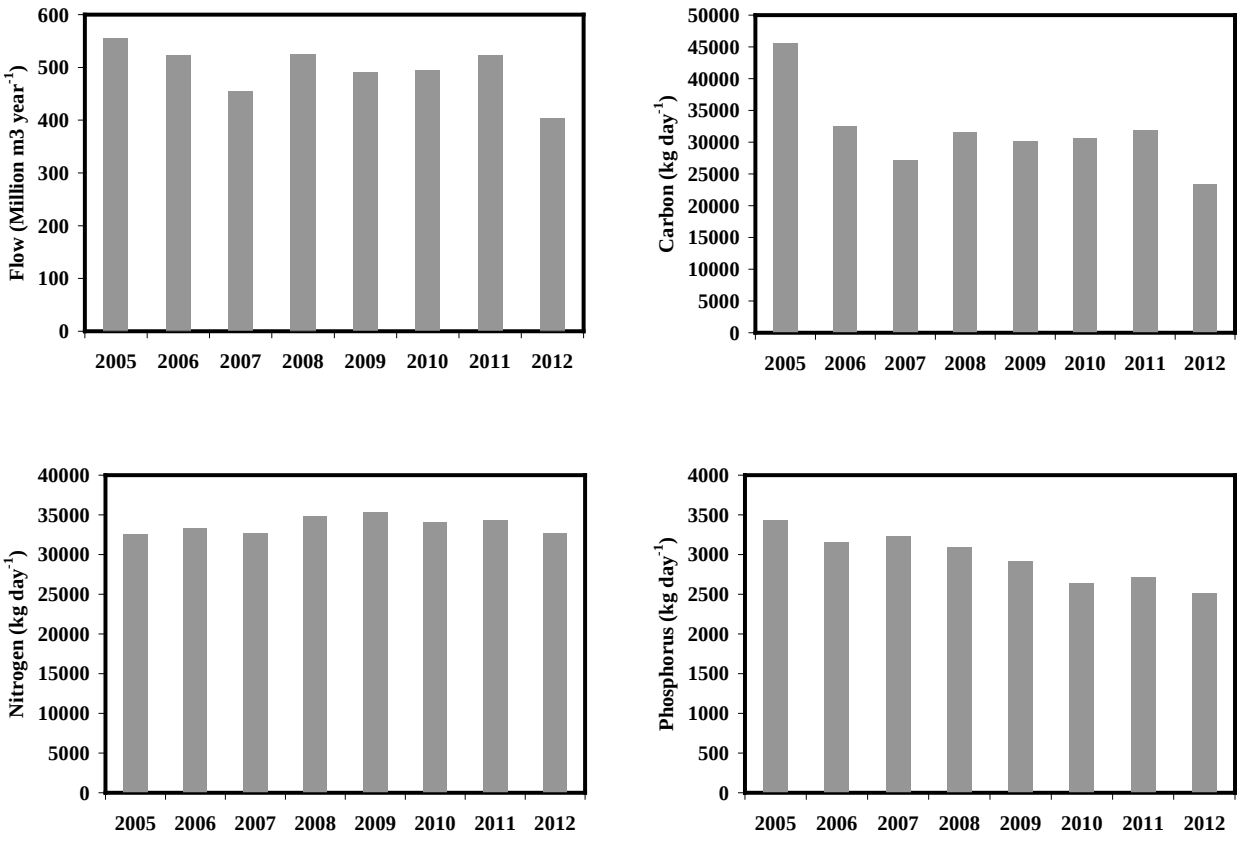

Figure 3.3 MWRA outfall mean annual flow and daily carbon, nitrogen and phosphorus loads 2005-2012.

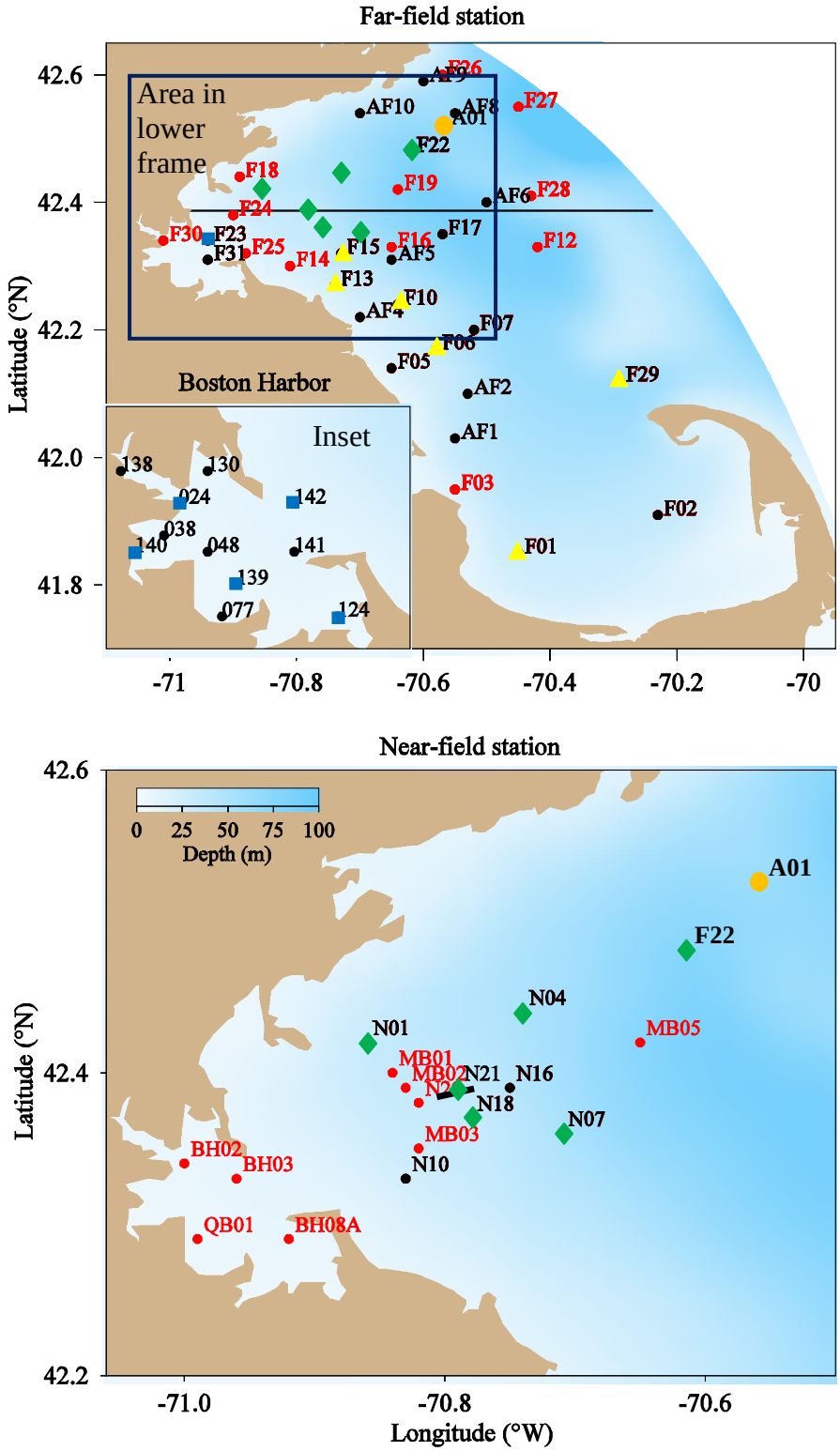

Figure 3.4 Station locations, including northern subset (green), southern subset (yellow), harbor subset (blue).

All green, yellow, blue, and black stations were sampled in 2012; red stations were sampled in past years but not in 2012. **Upper frame:** Farfield (prefix F) and *Alexandrium* Rapid Response Study (prefix AF) stations; lower left inset, Boston Harbor stations (numeric names). Black west-east line: vertical section in later plots. **Lower frame:** Nearfield (N) stations and sediment flux study stations (prefixes BH for Boston Harbor, MB for Massachusetts Bay, and QB for Quincy Bay). NERACOOS mooring site is A01 (orange).

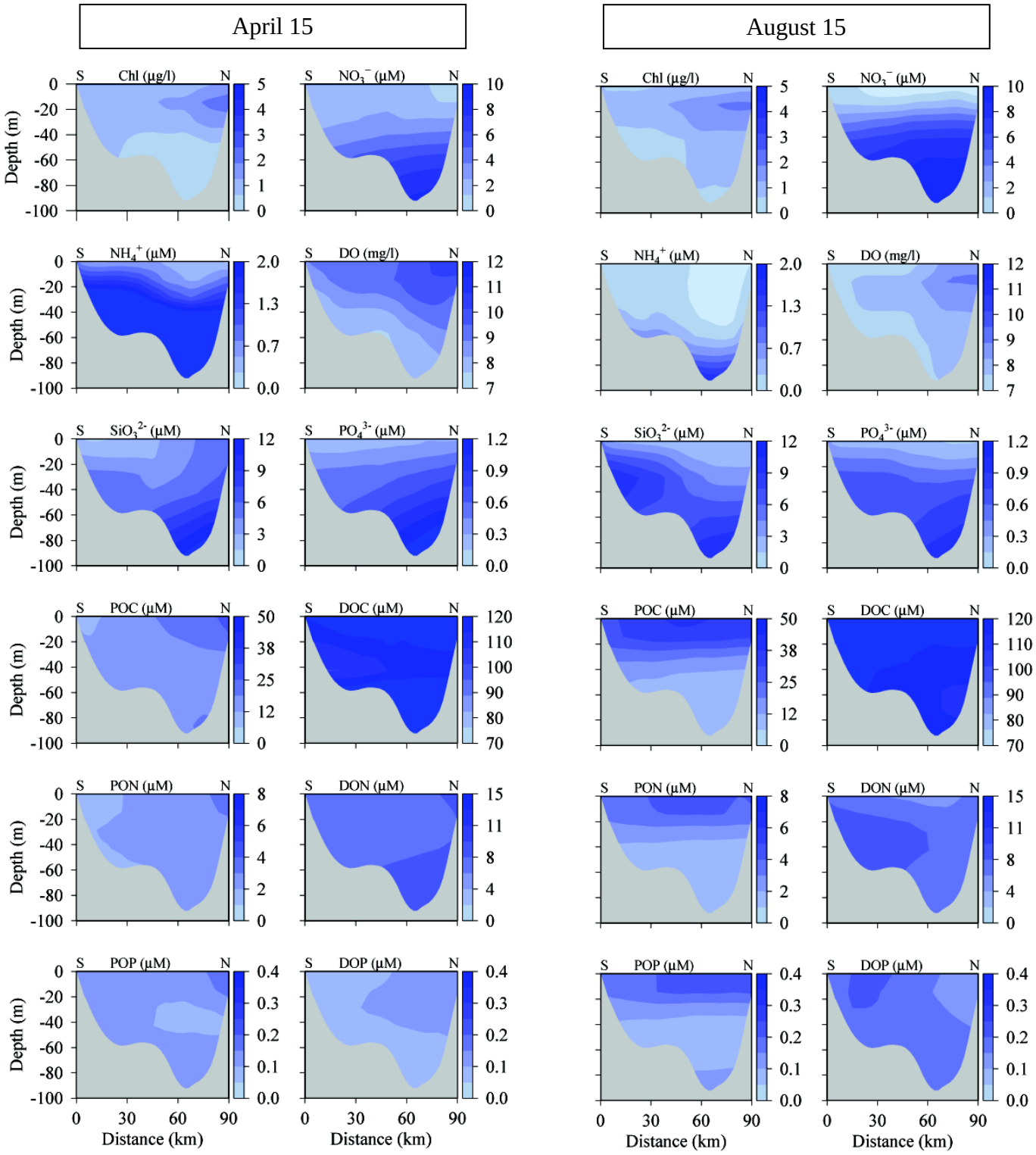

Figure 3.5 Open boundary chlorophyll, nutrients, DO and organics concentrations.

April 15 (left 2 columns) and August 15 (right 2 columns), 2012. Horizontal axis is distance along transect from Cape Cod (south S) to Cape Ann (north N).

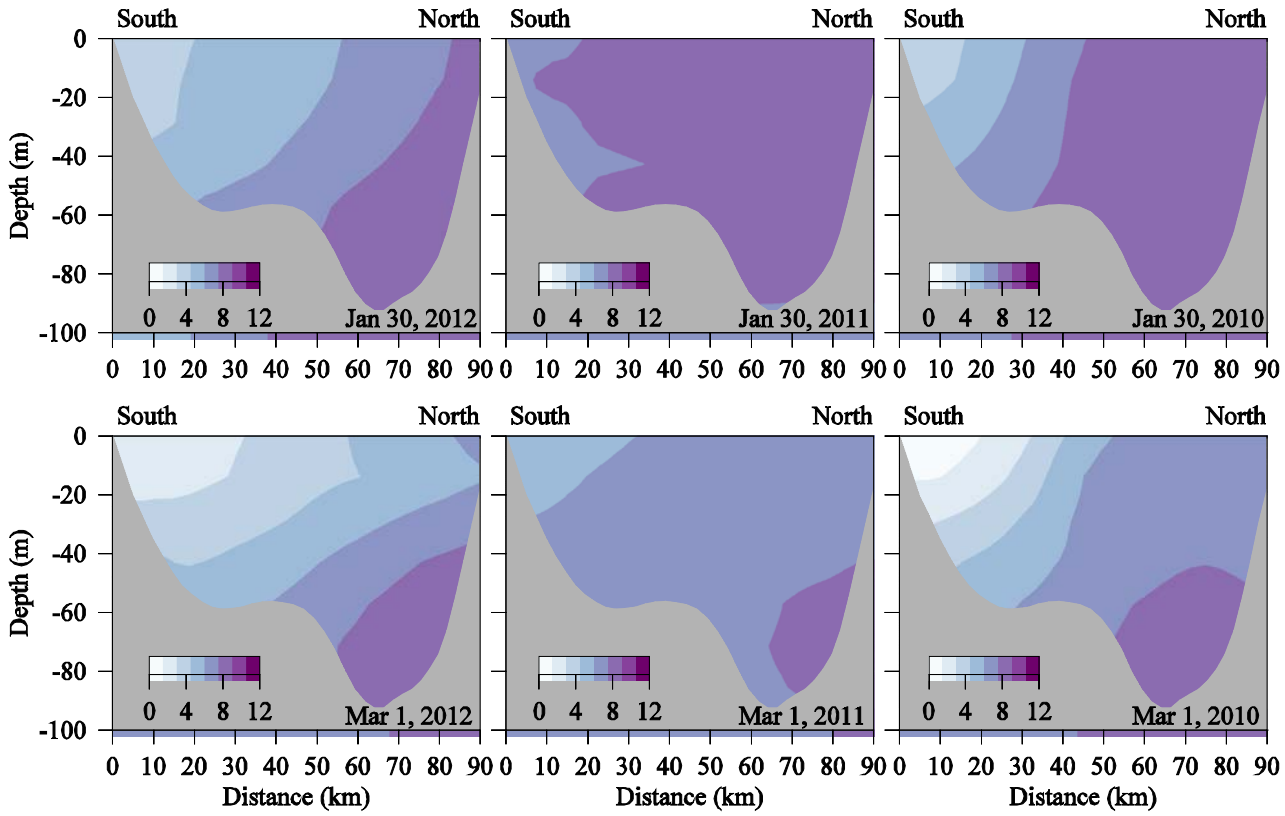

Figure 3.6 Inter-annual variations in open boundary nitrate (μM). 2012 (left), 2011 (middle) and 2010 (right) in winter. January 30 (upper) and March 1 (lower).

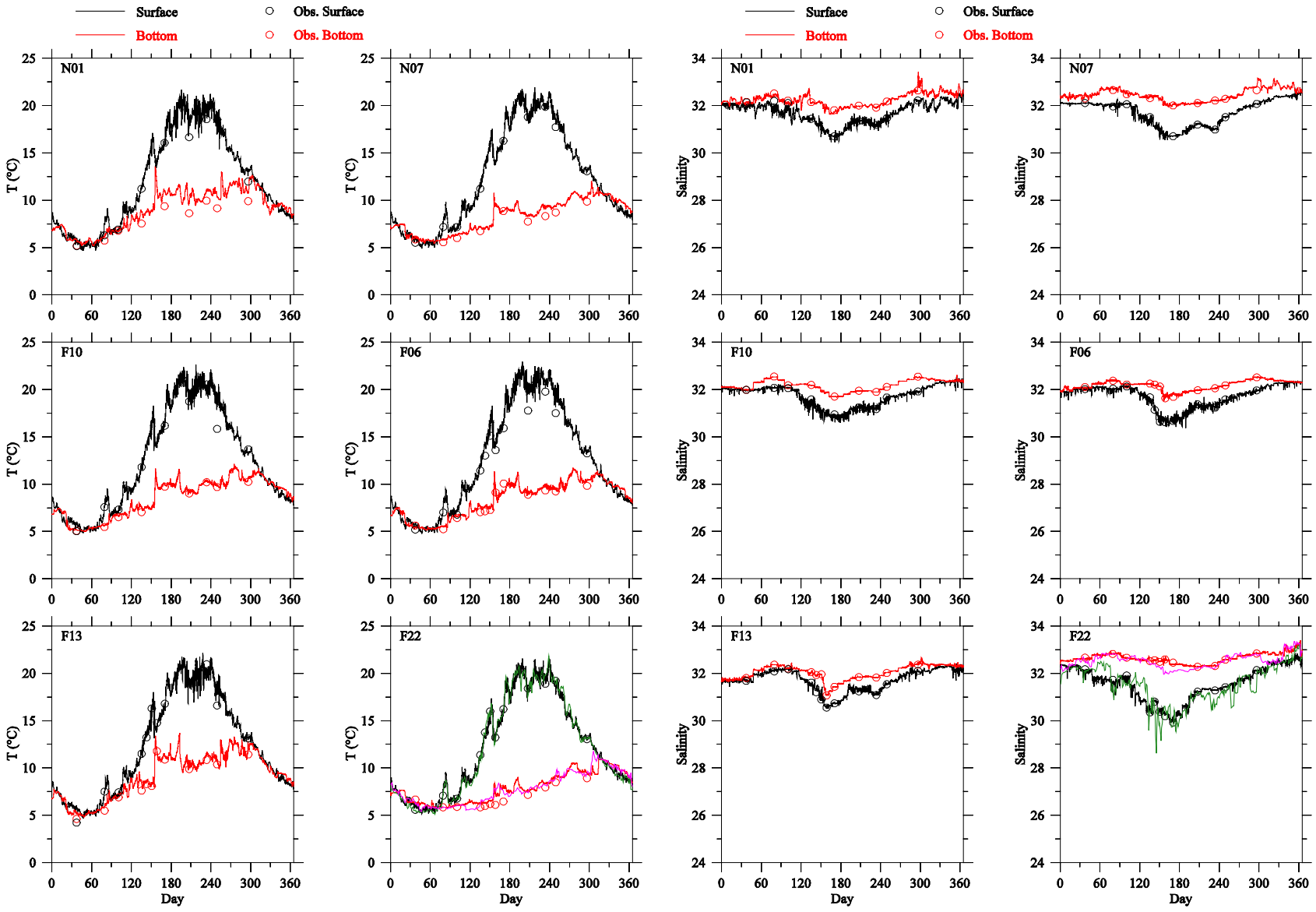

Figure 3.7 Temperature and salinity: observed (circles) and modeled (line) at select northern/southern subset stations in 2012. Mooring A01 observations are green (near-surface) and pink (near-bottom) lines in F22 panels.

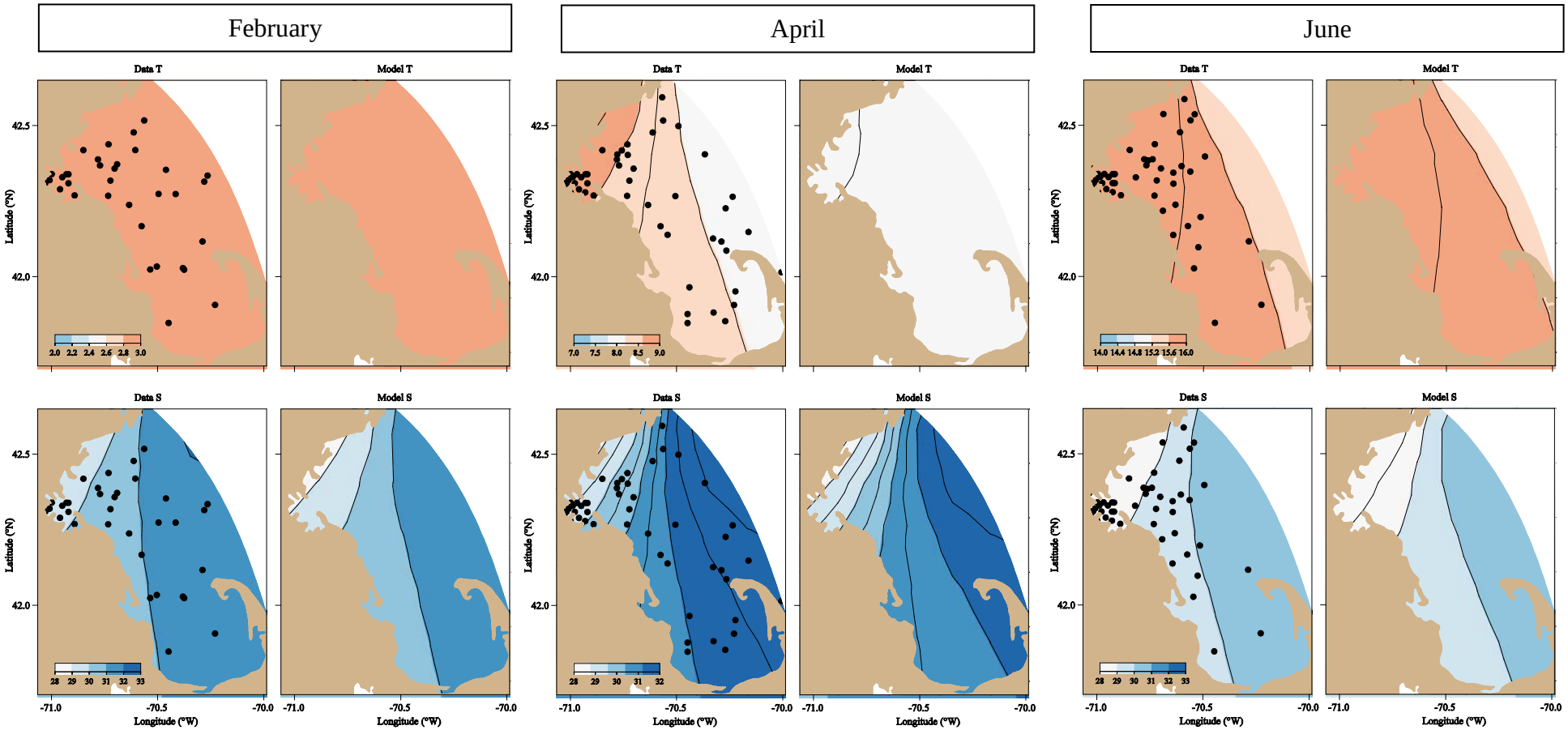

Figure 3.8 Near-surface temperature (upper, ^{o}C) and salinity (lower, PSS), Feb (left group), Apr (middle group), and Jun (right group). Observed (left in each pair) and model (right in each pair).

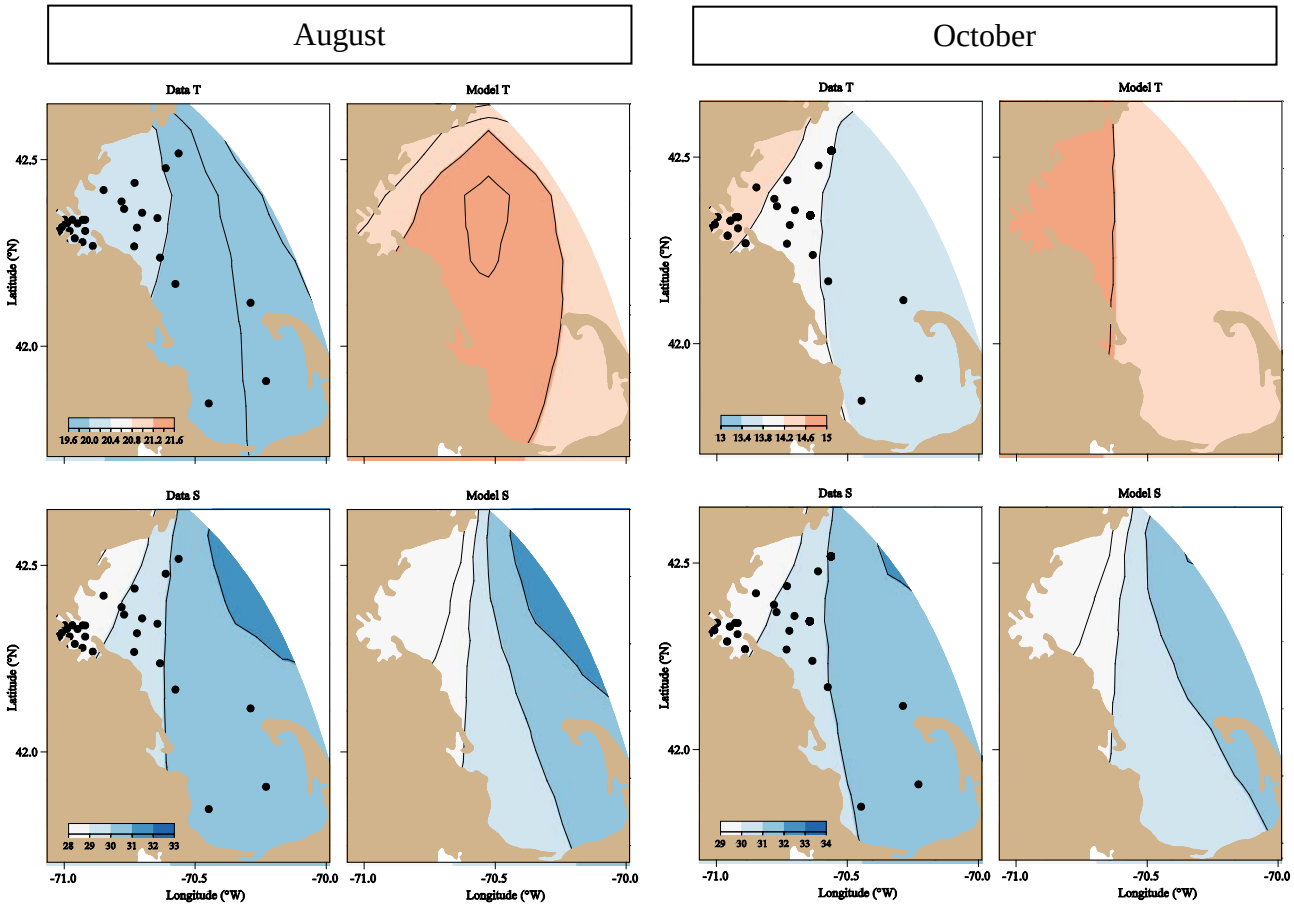

Figure 3.9 Near-surface temperature (upper, ^{o}C) and salinity (lower, PSS), Aug (left group), and Oct (right group). Observed (left in each pair) and model (right in each pair).

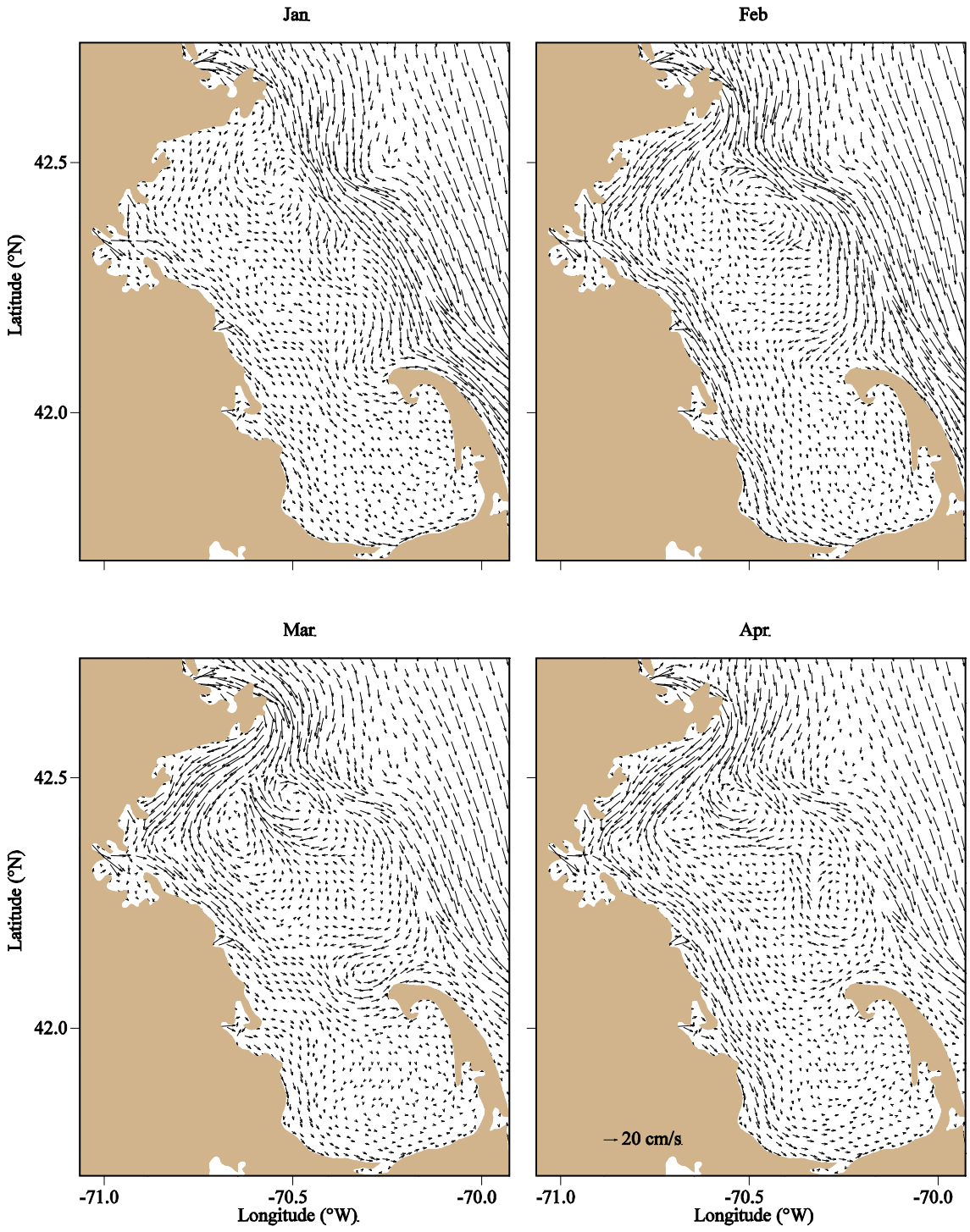

Figure 3.10 Monthly-mean model surface currents: Jan to Apr 2012.

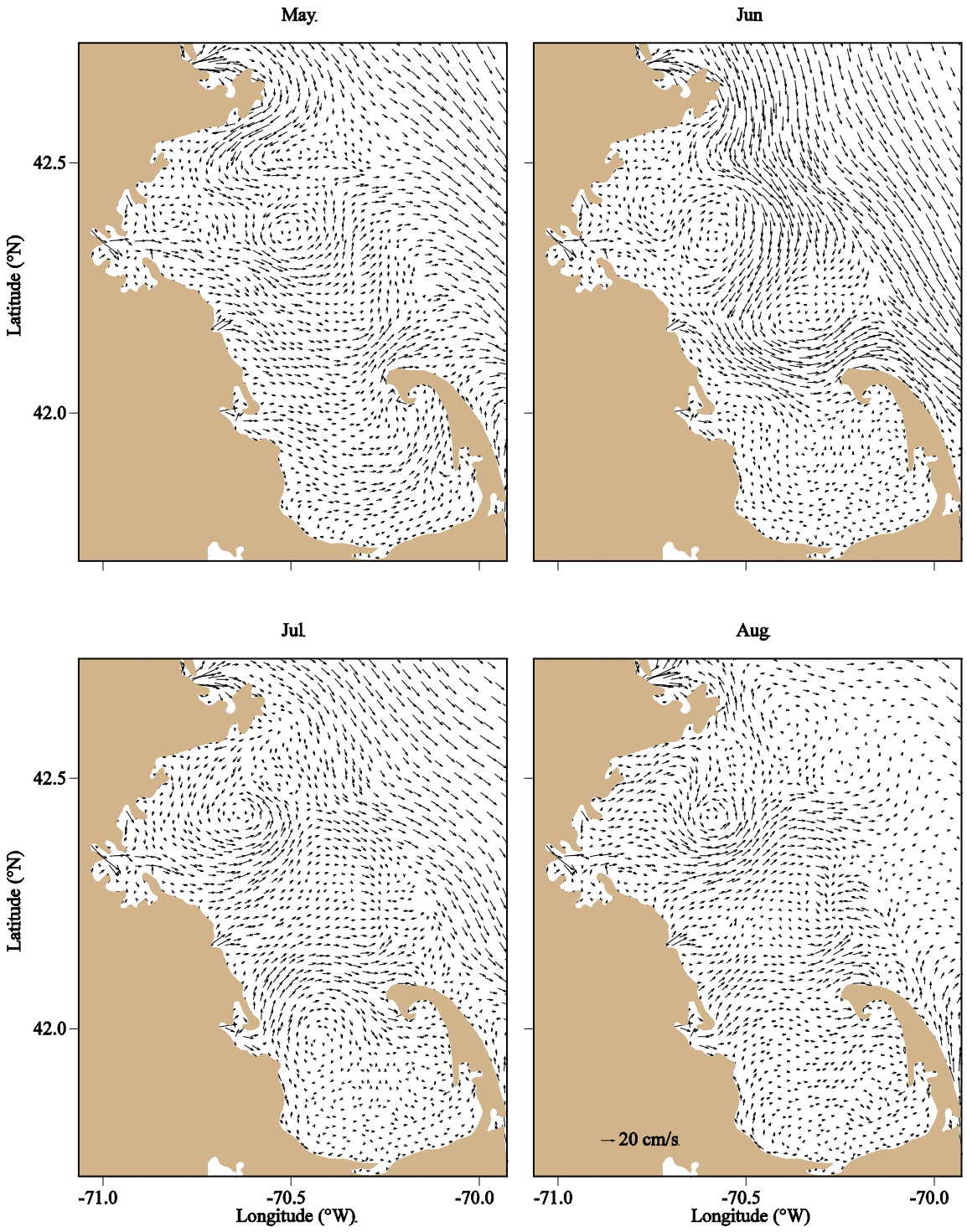

Figure 3.11 Monthly-mean model surface currents: May to Aug 2012.

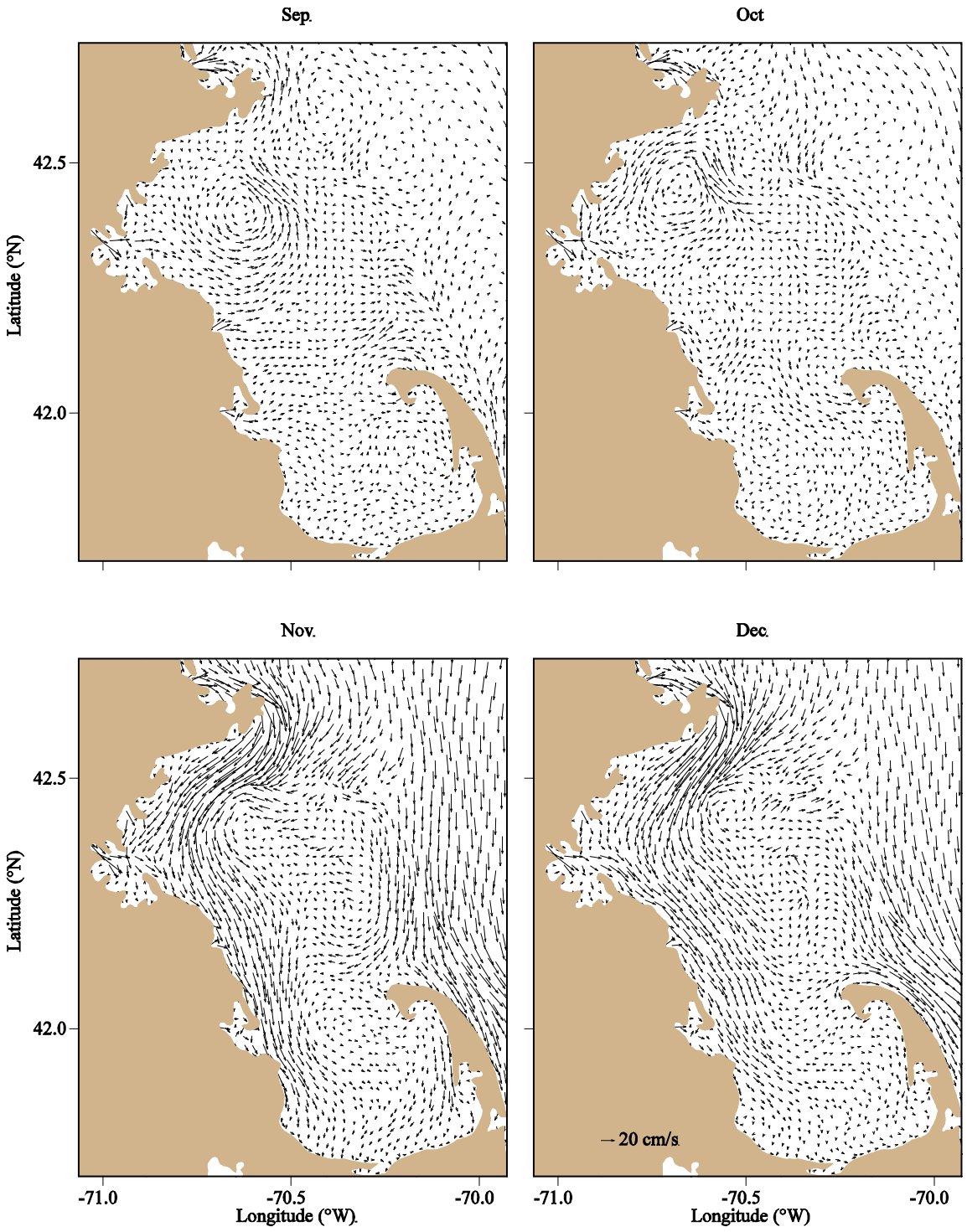

Figure 3.12 Monthly-mean model surface currents: Sep to Dec 2012.

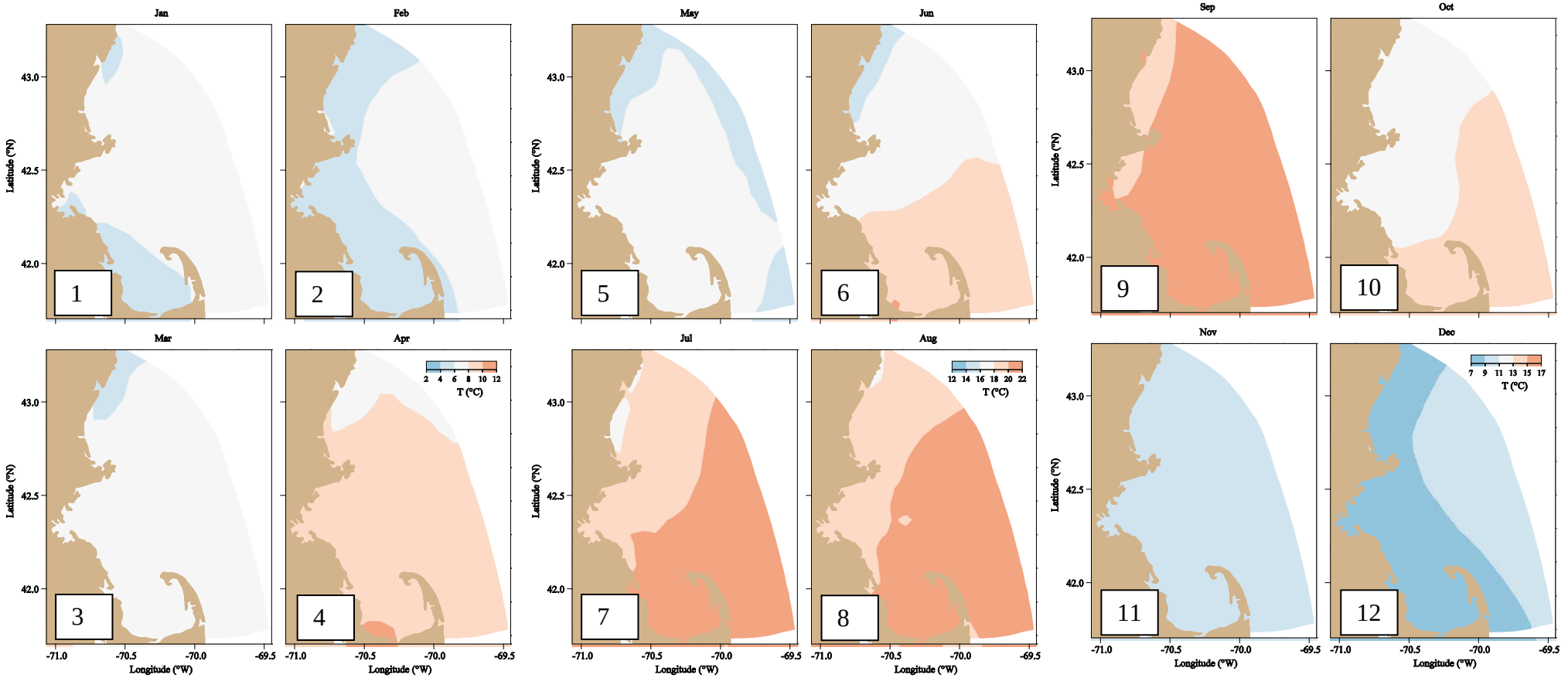

Figure 3.13 Model surface temperature at the end of each month of 2012.

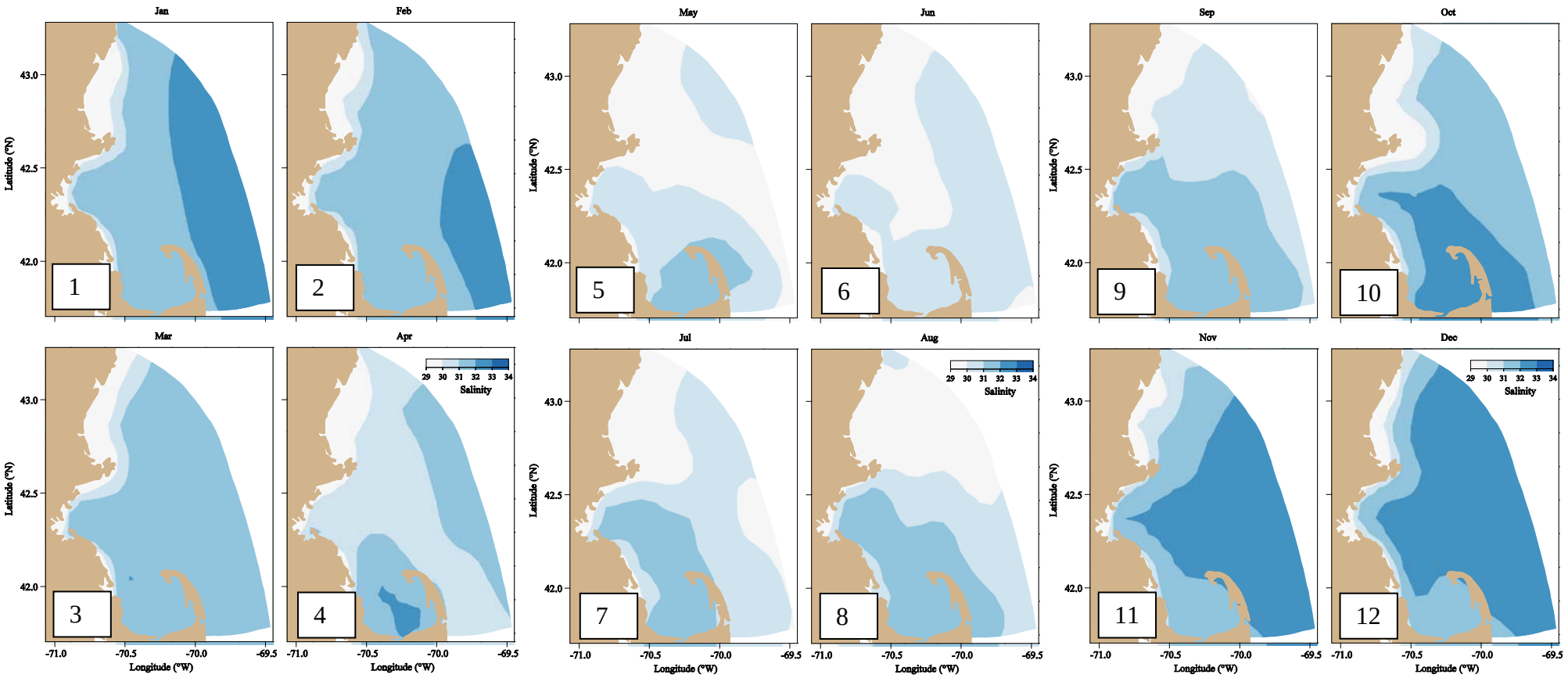

Figure 3.14 Model surface salinity at the end of each month of 2012.

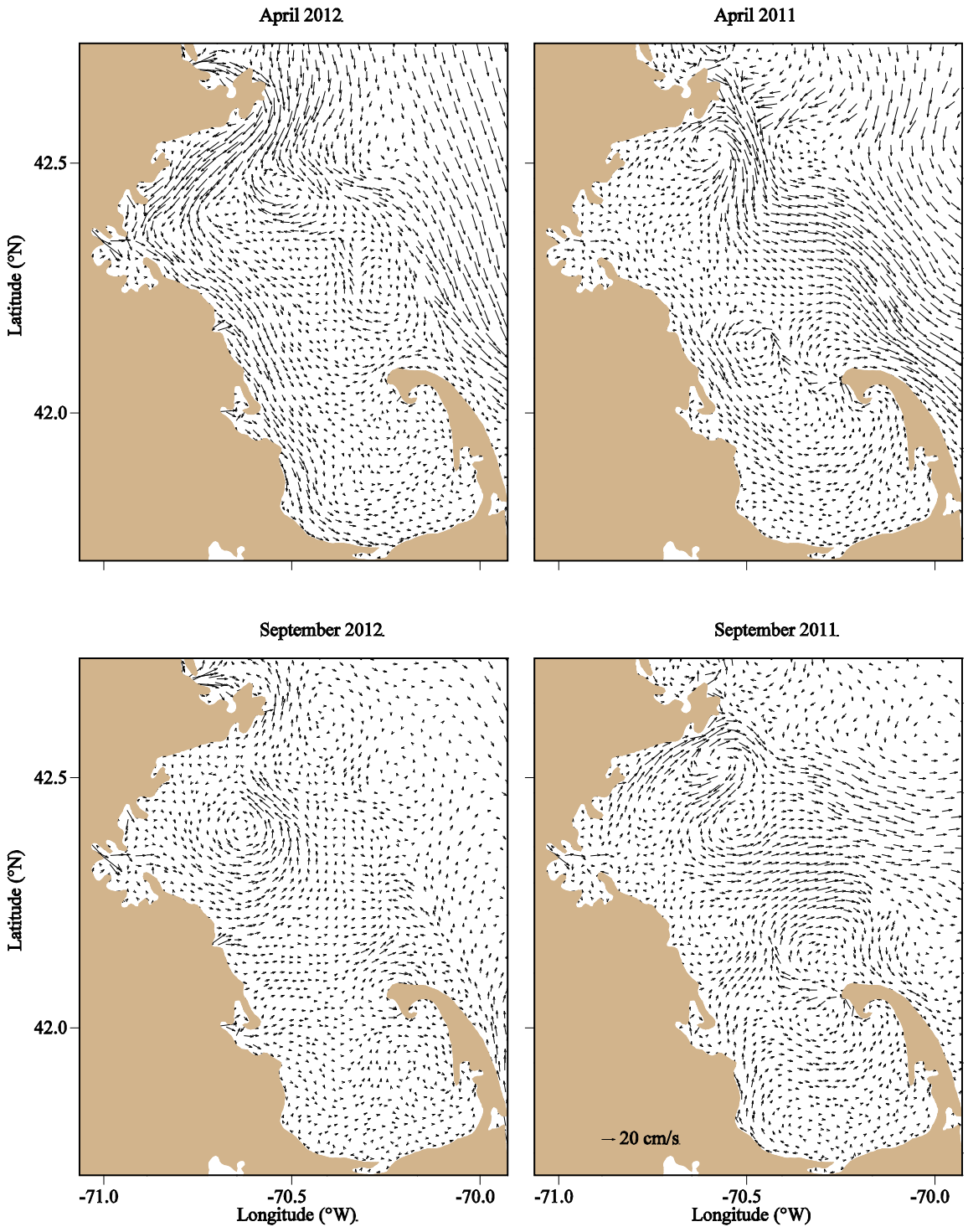

Figure 3.15 Inter-annual variation in monthly-mean surface currents: Apr (upper) and Sep (lower) during 2012 (left) and 2011 (right).

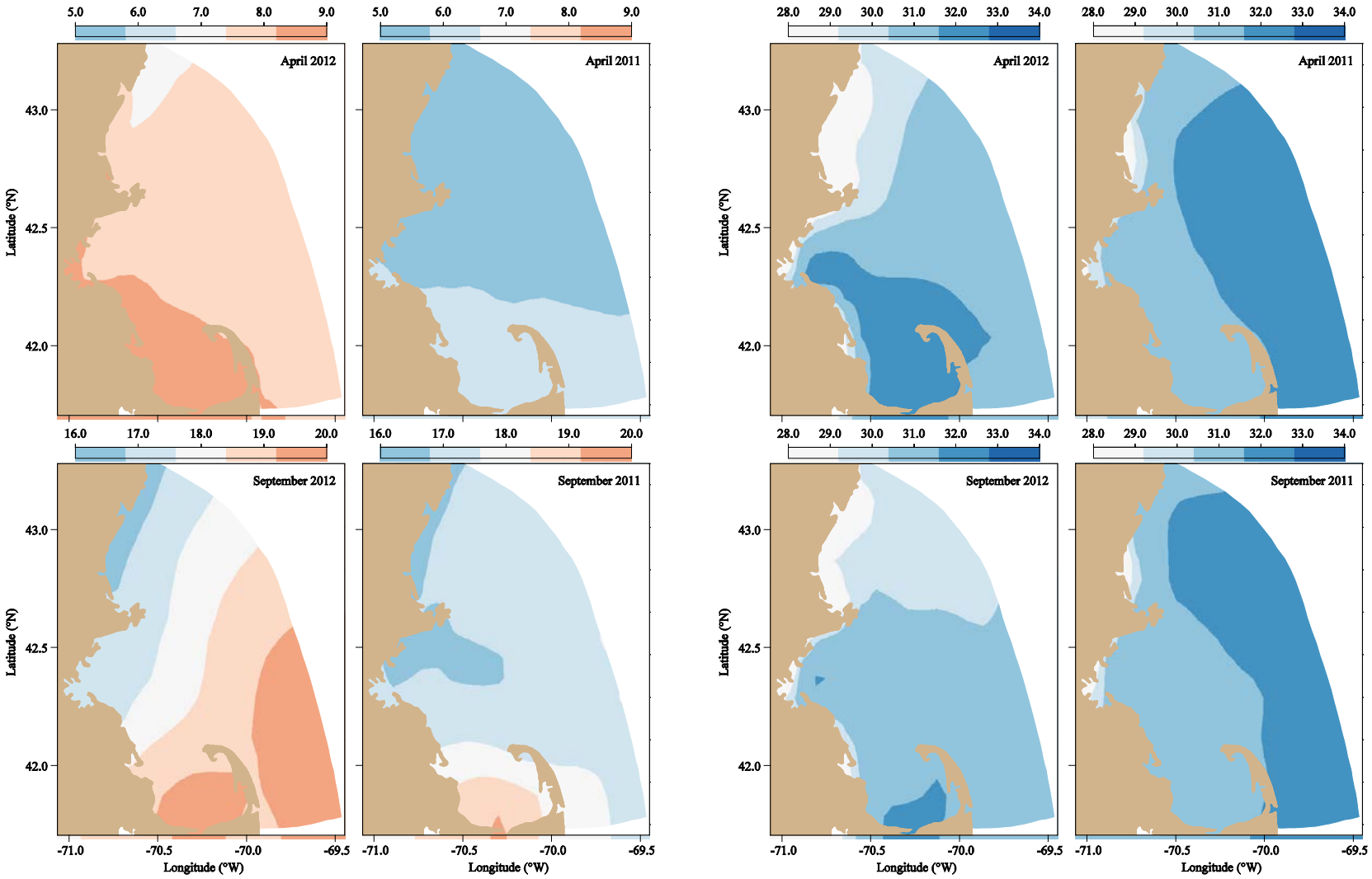

Figure 3.16 Inter-annual variation in monthly-mean surface temperatures (left group, ^{o}C) and salinities (right group, PSS): Apr (upper) and Sep (lower) during 2012 (left) and 2011 (right).

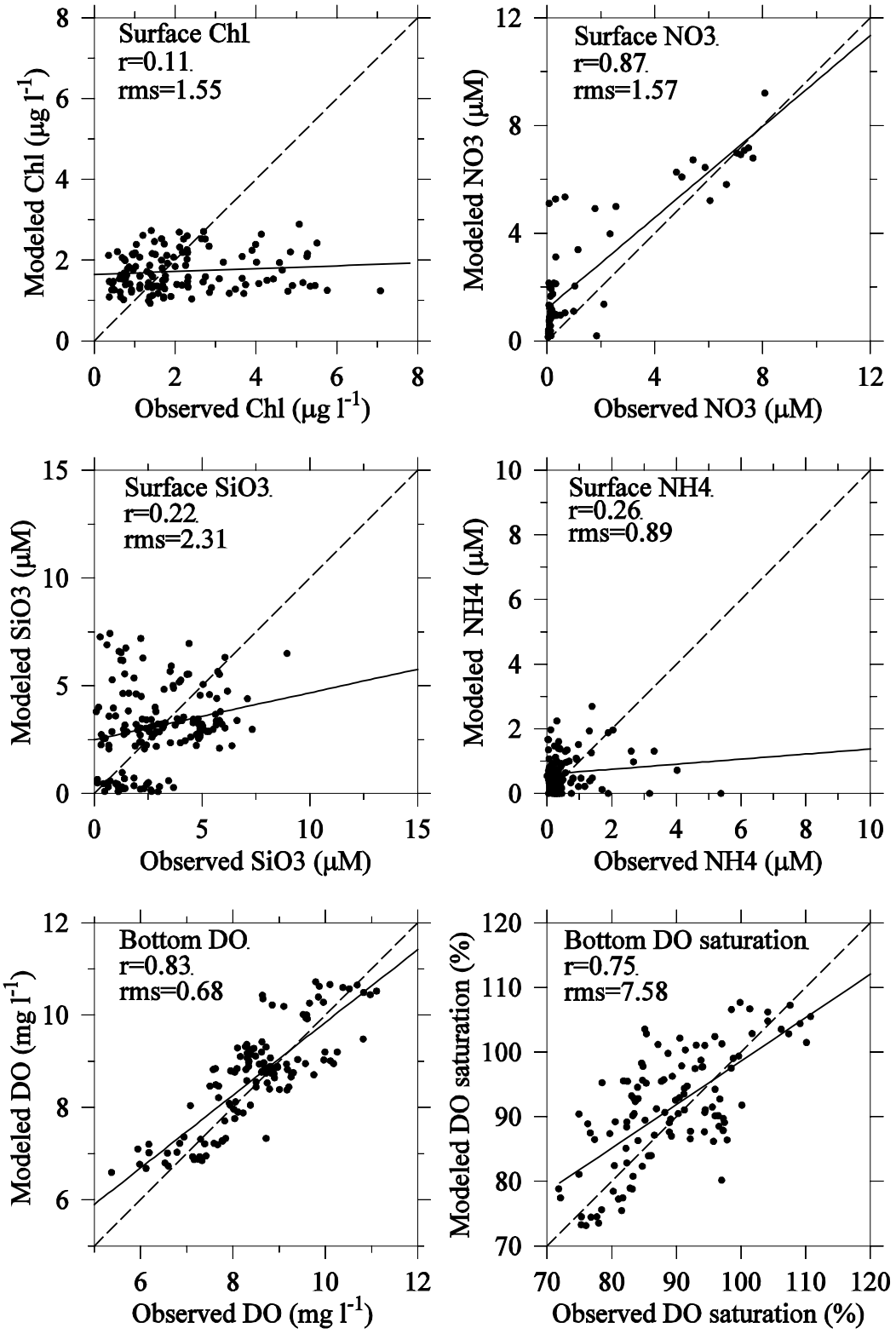

Figure 3.17 Model-observation correlations and regressions (solid lines) of key parameters, all stations outside BH, 2012.

Dashed lines indicate equality between observed and modeled results.

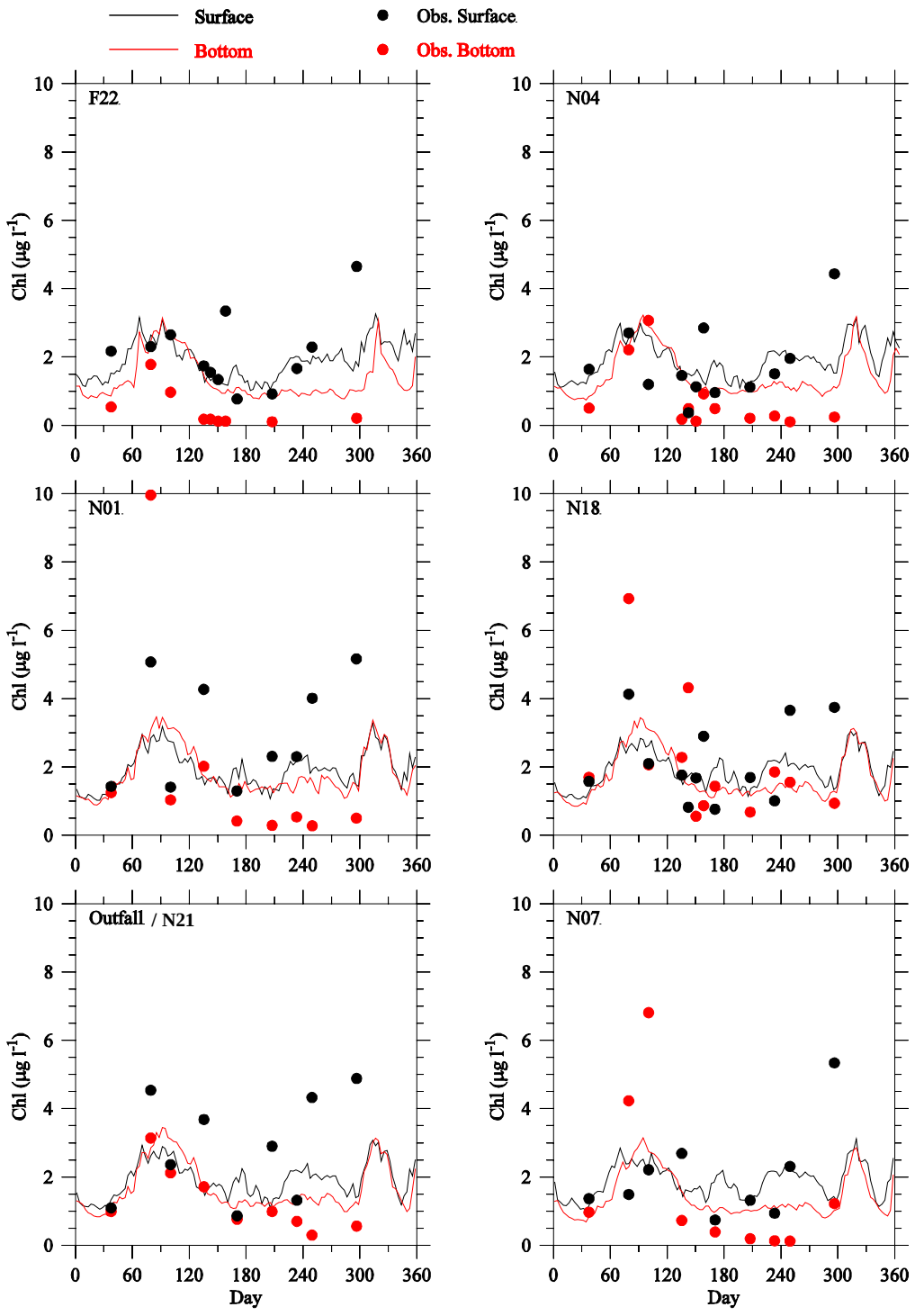

Figure 3.18 Chlorophyll: observed (dots) and modeled (lines) at northern subset stations in 2012.

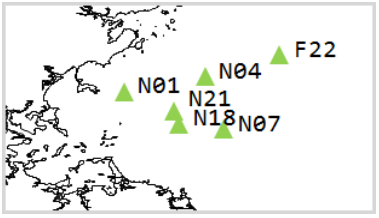

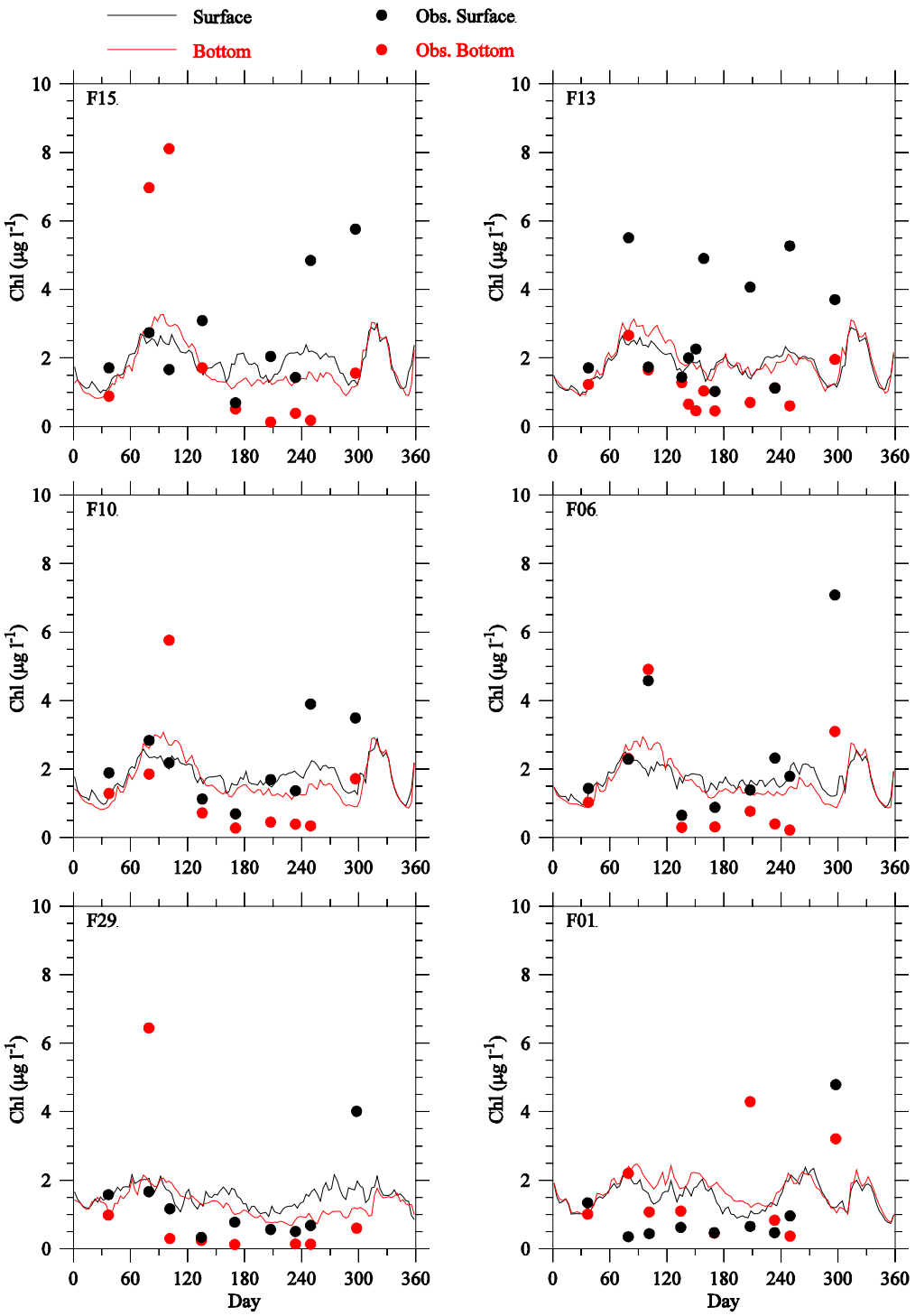

Figure 3.19 Chlorophyll: observed (dots) and modeled (lines) at southern subset stations in 2012.

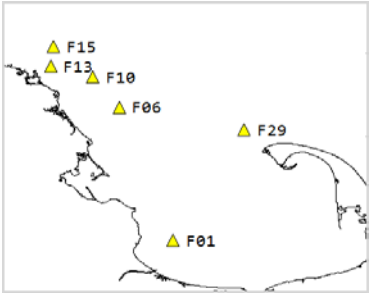

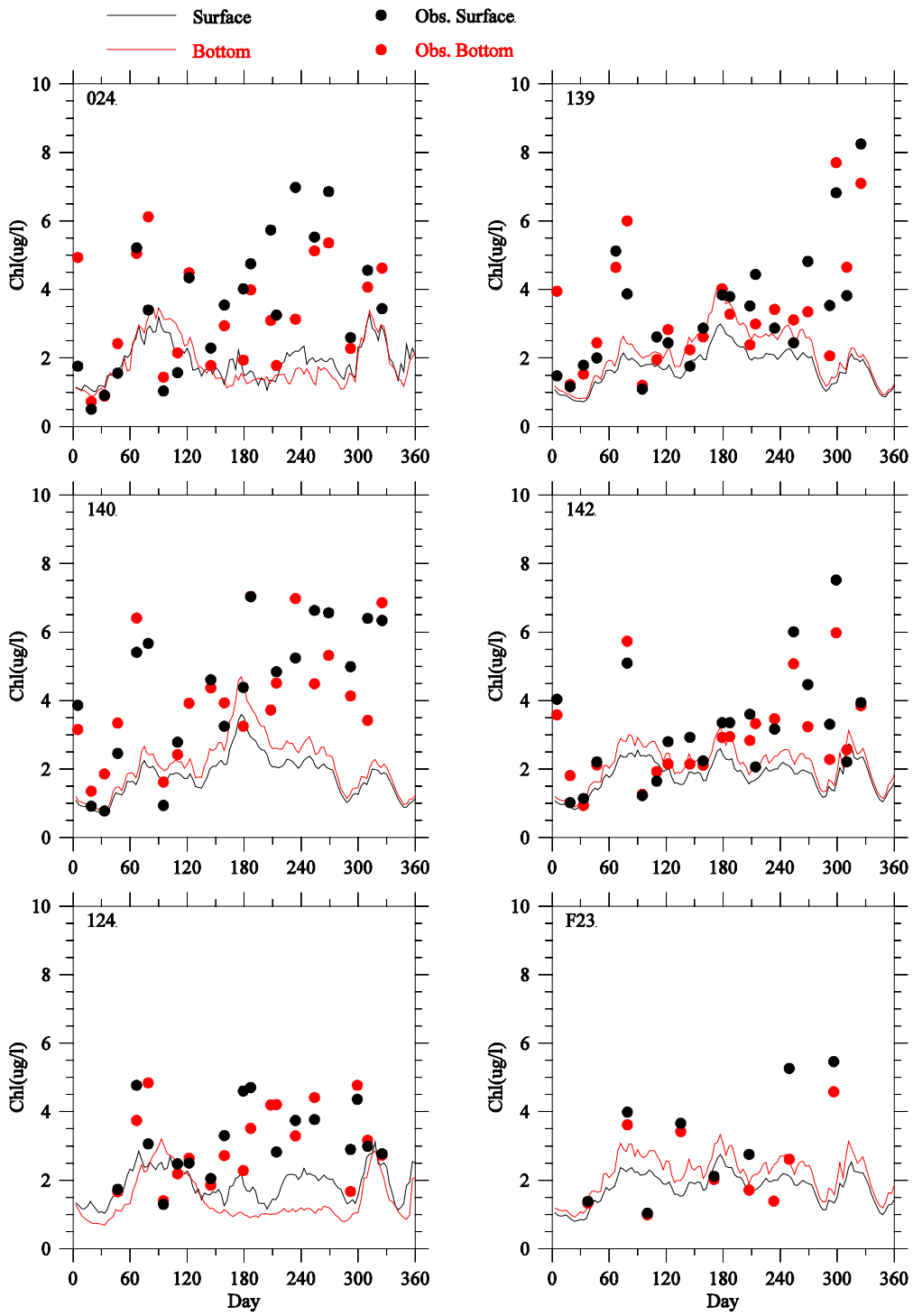

Figure 3.20 Chlorophyll: observed (dots) and modeled (lines) at harbor subset stations in 2012.

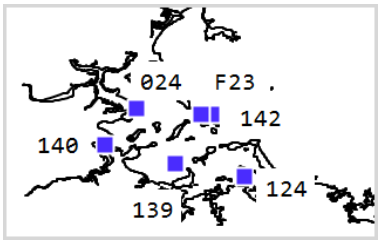

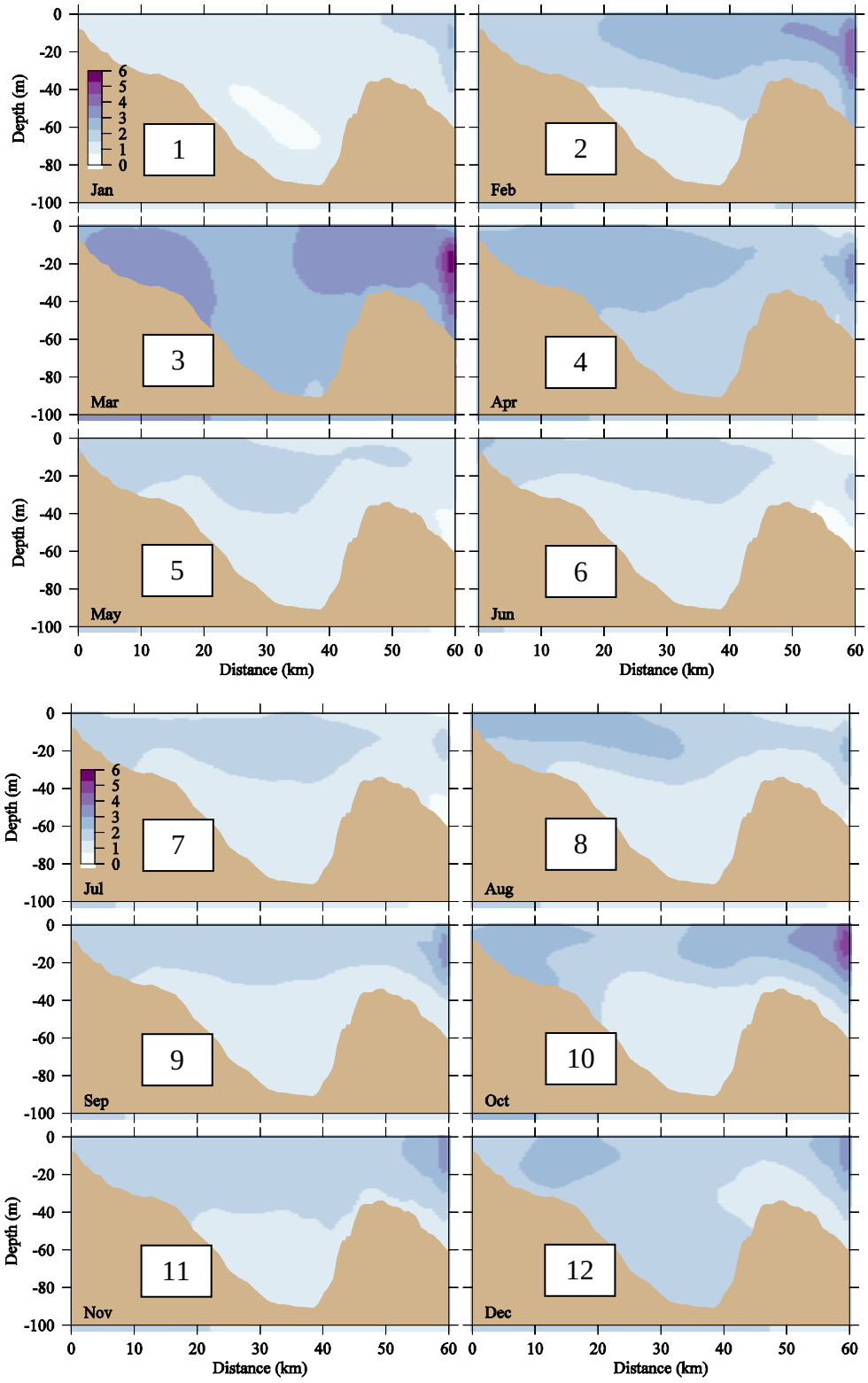

Figure 3.21 Model chlorophyll (μg L^{-1}): west-east transect through MWRA outfall, end of each month, 2012.

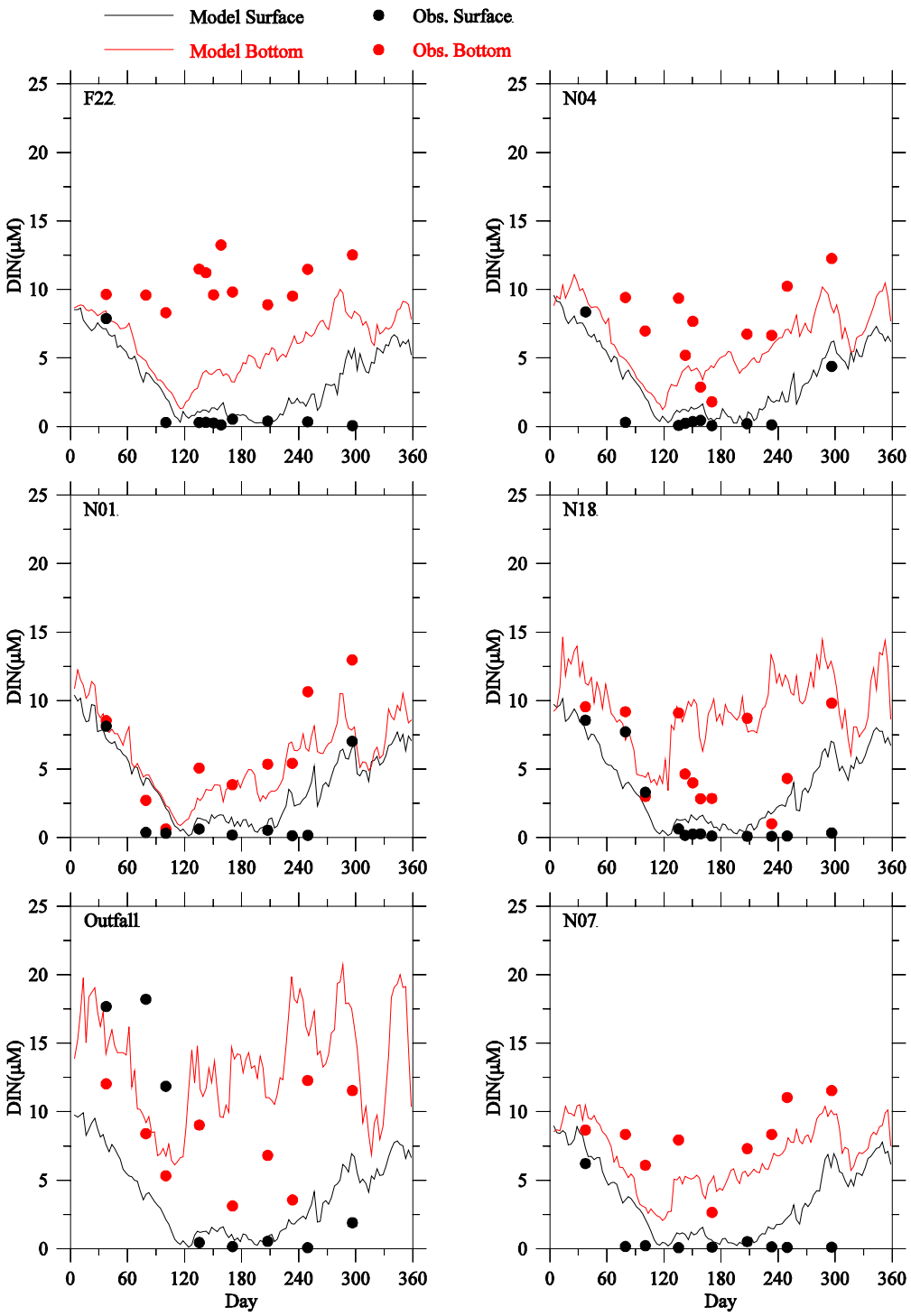

Figure 3.22 DIN: observed (dots) and modeled (lines) at northern subset stations in 2012.

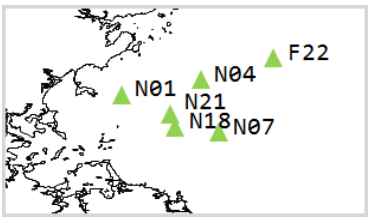

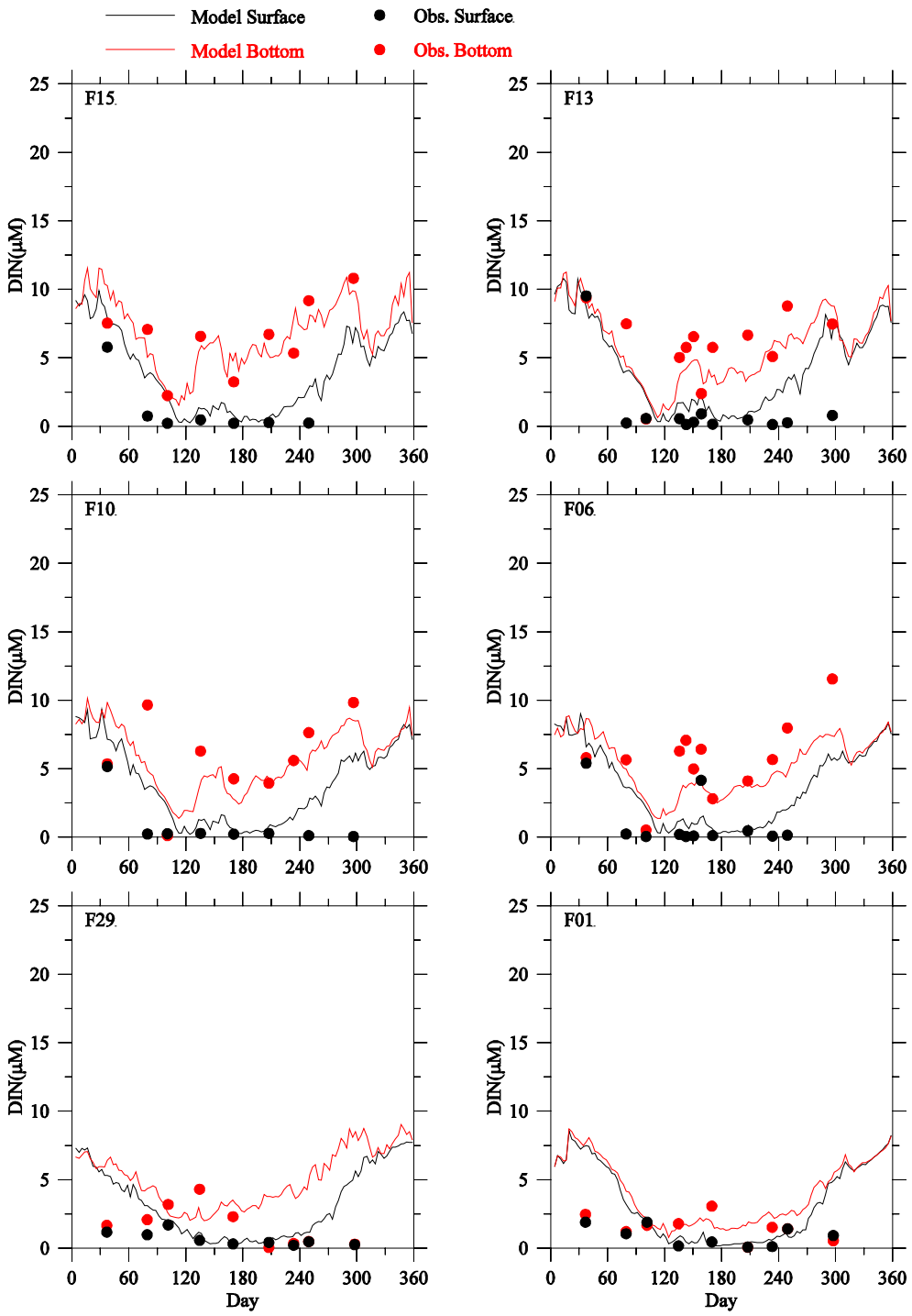

Figure 3.23 DIN: Observed (dots) and modeled (lines) at southern subset stations in 2012.

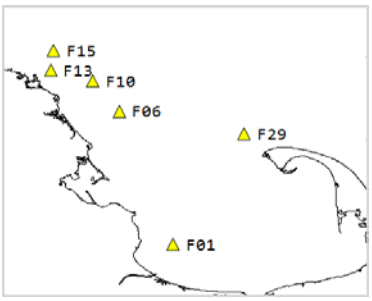

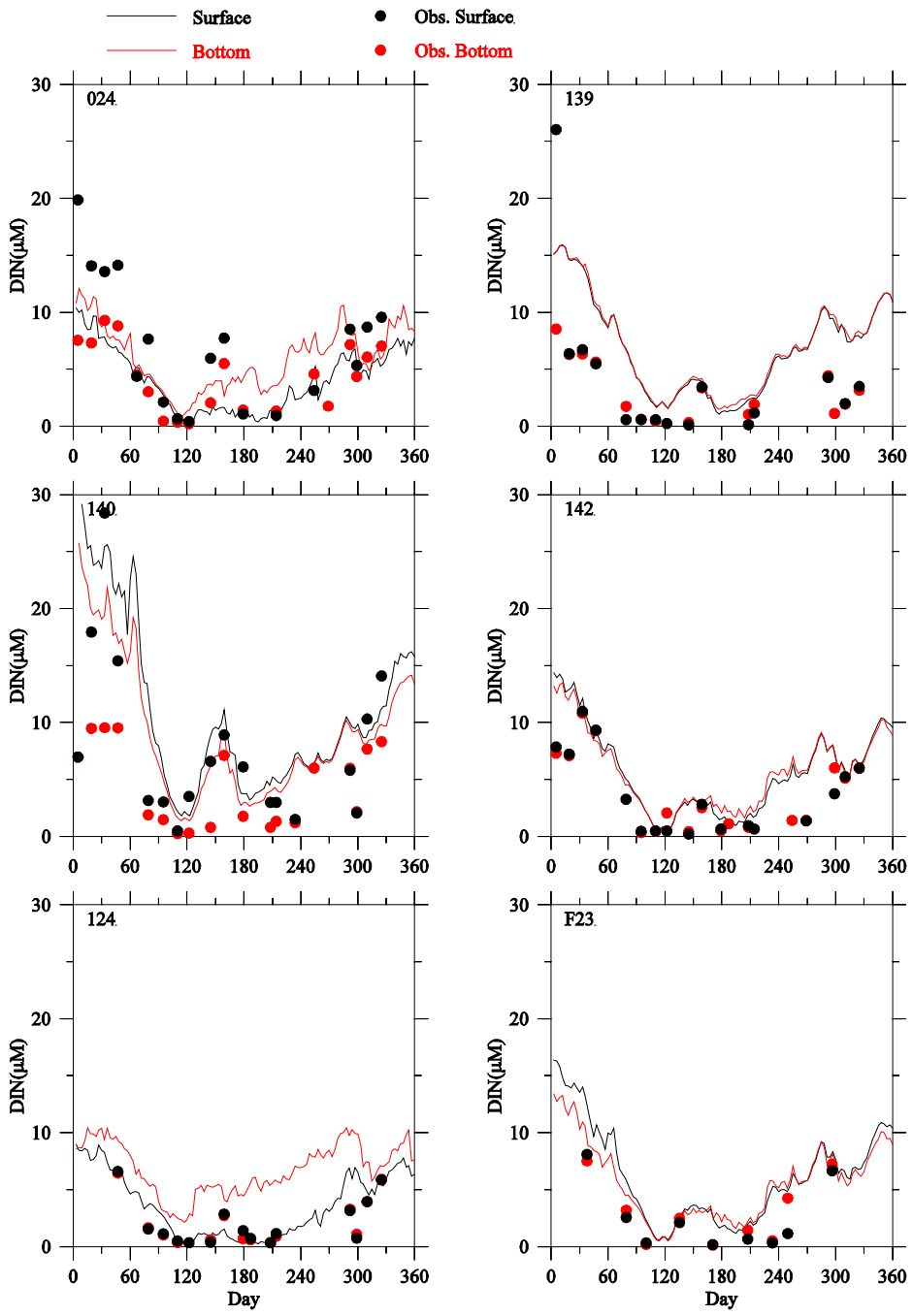

Figure 3.24 DIN: observed (dots) and modeled (lines) at harbor subset stations in 2012.

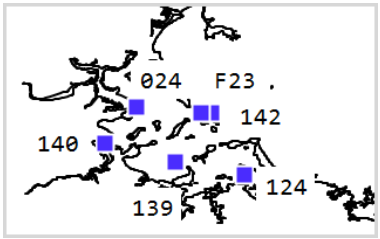

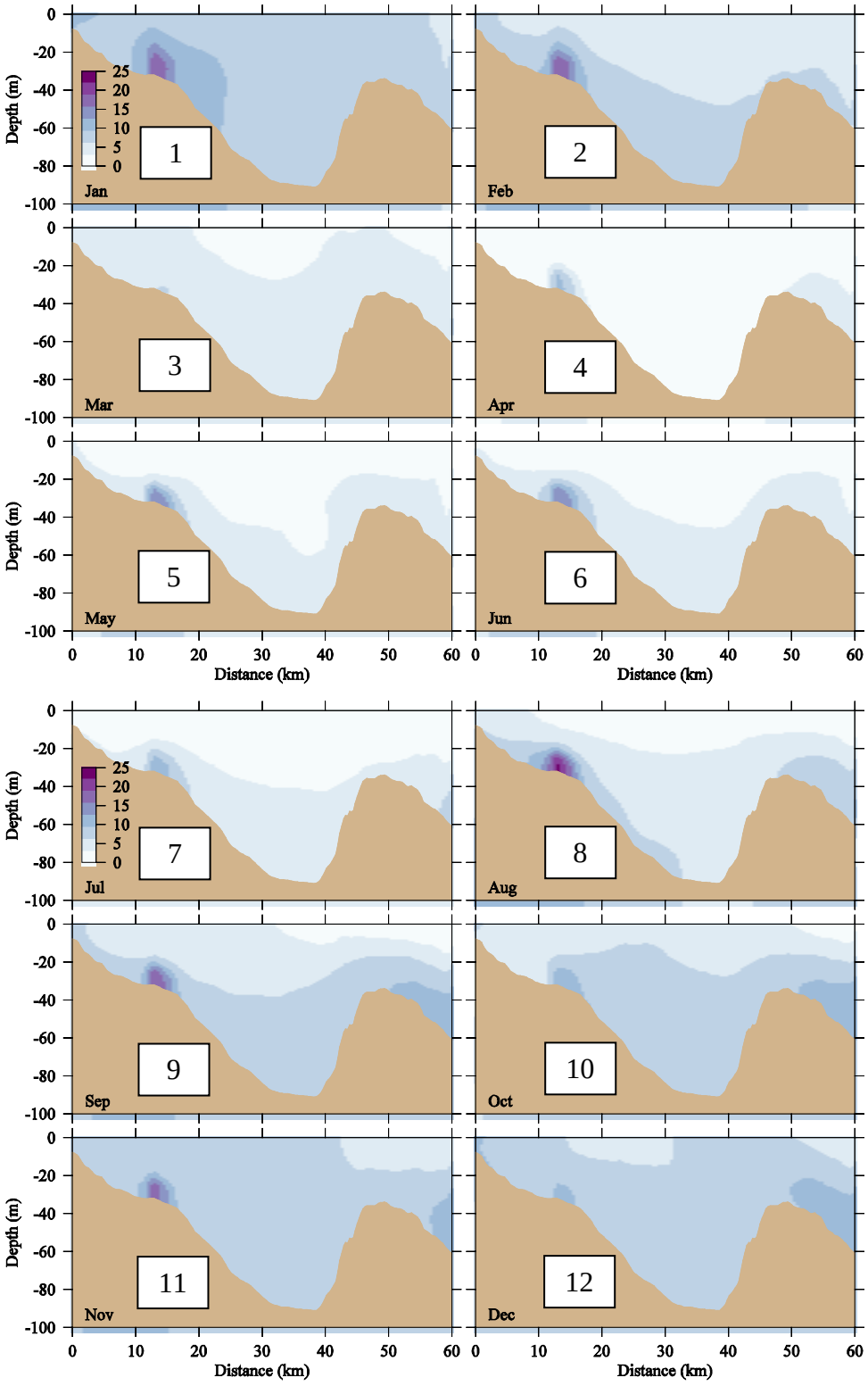

Figure 3.25 Model DIN (μM): west-east transect through MWRA outfall, end of each month, 2012.

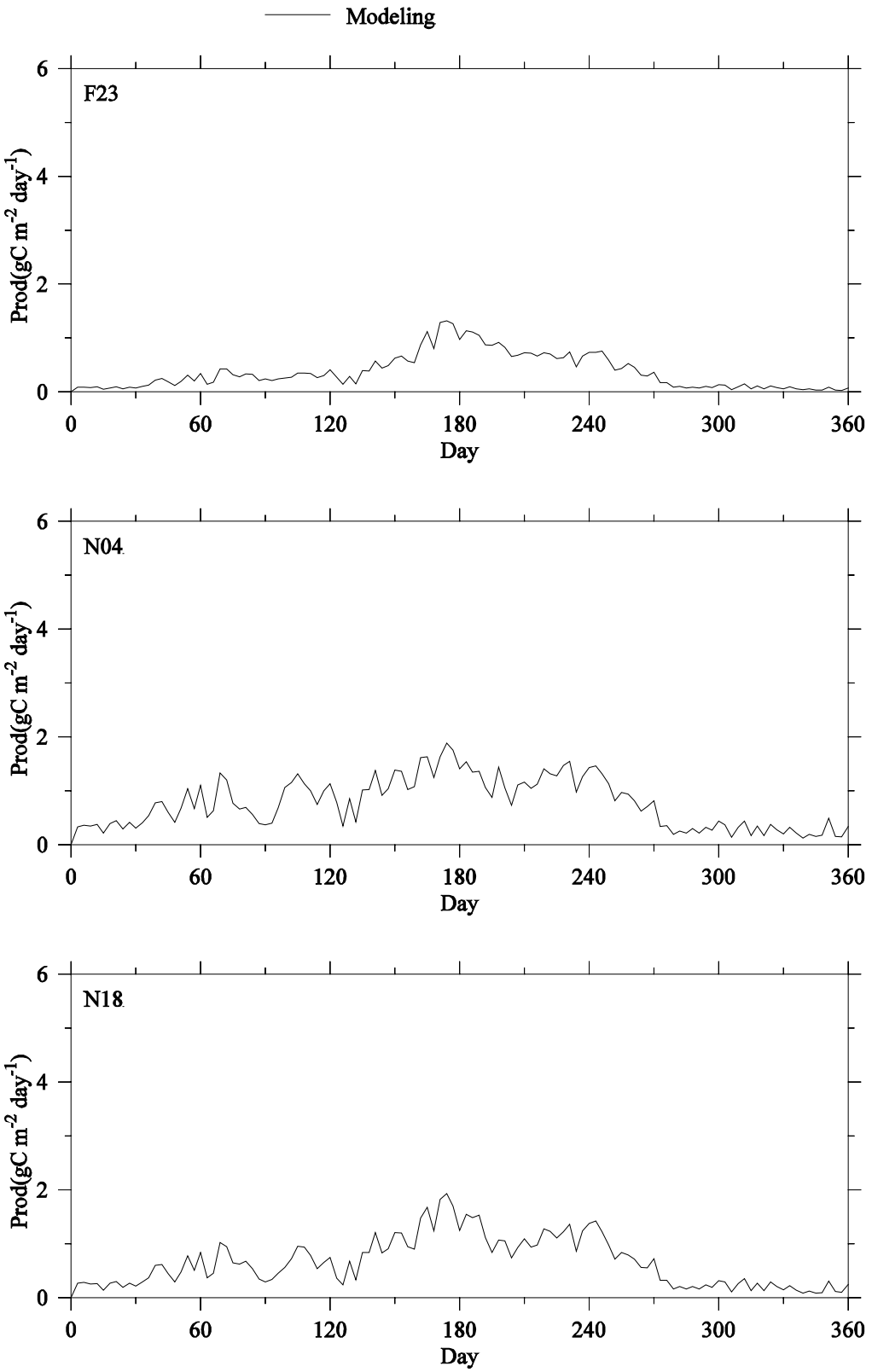

Figure 3.26 Model primary production time series, vertically integrated, select northern/harbor subset stations in 2012.

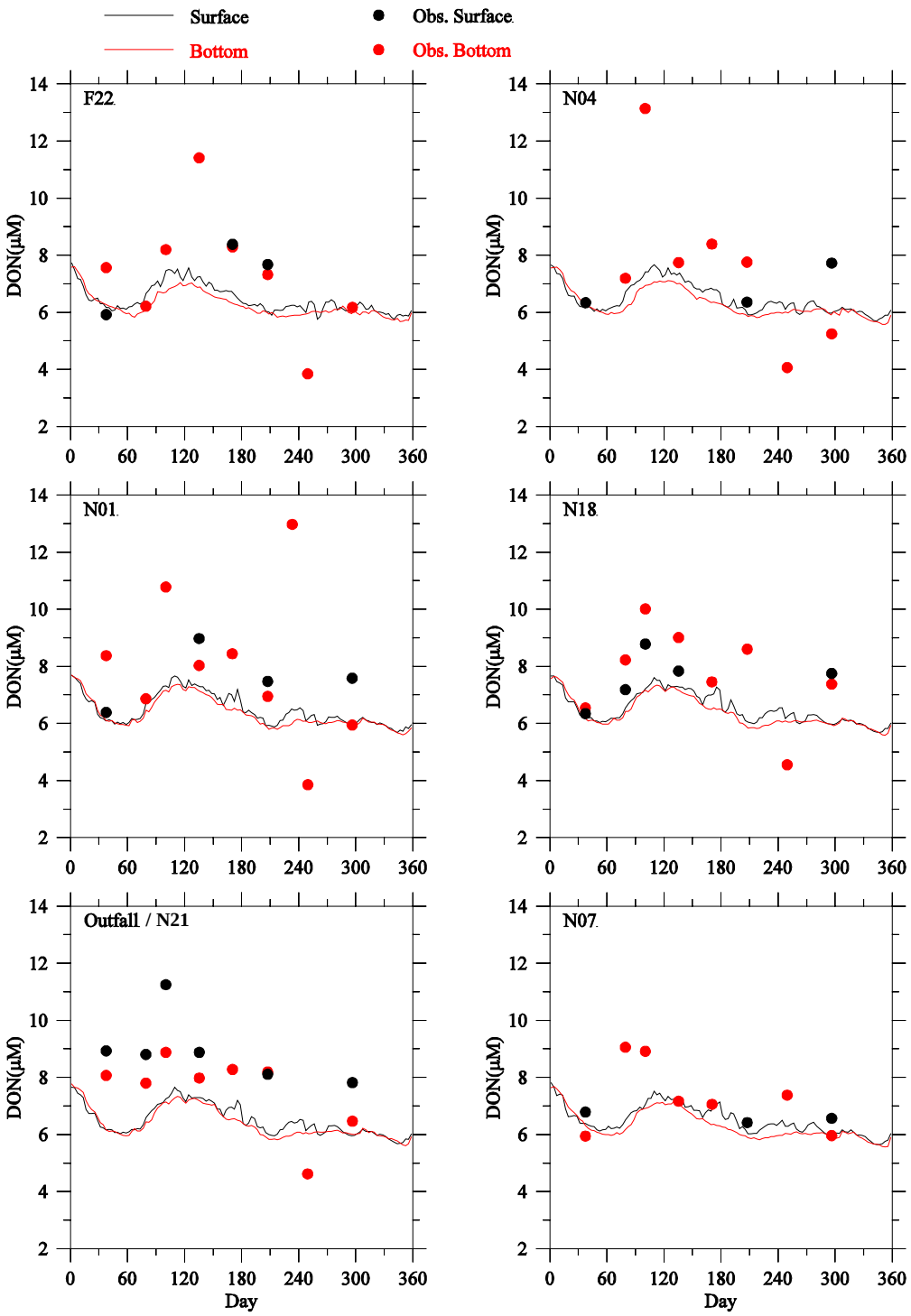

Figure 3.27 DON: observed (dots) and modeled (lines) at northern subset stations in 2012.

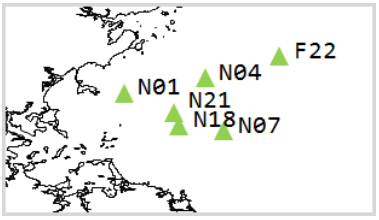

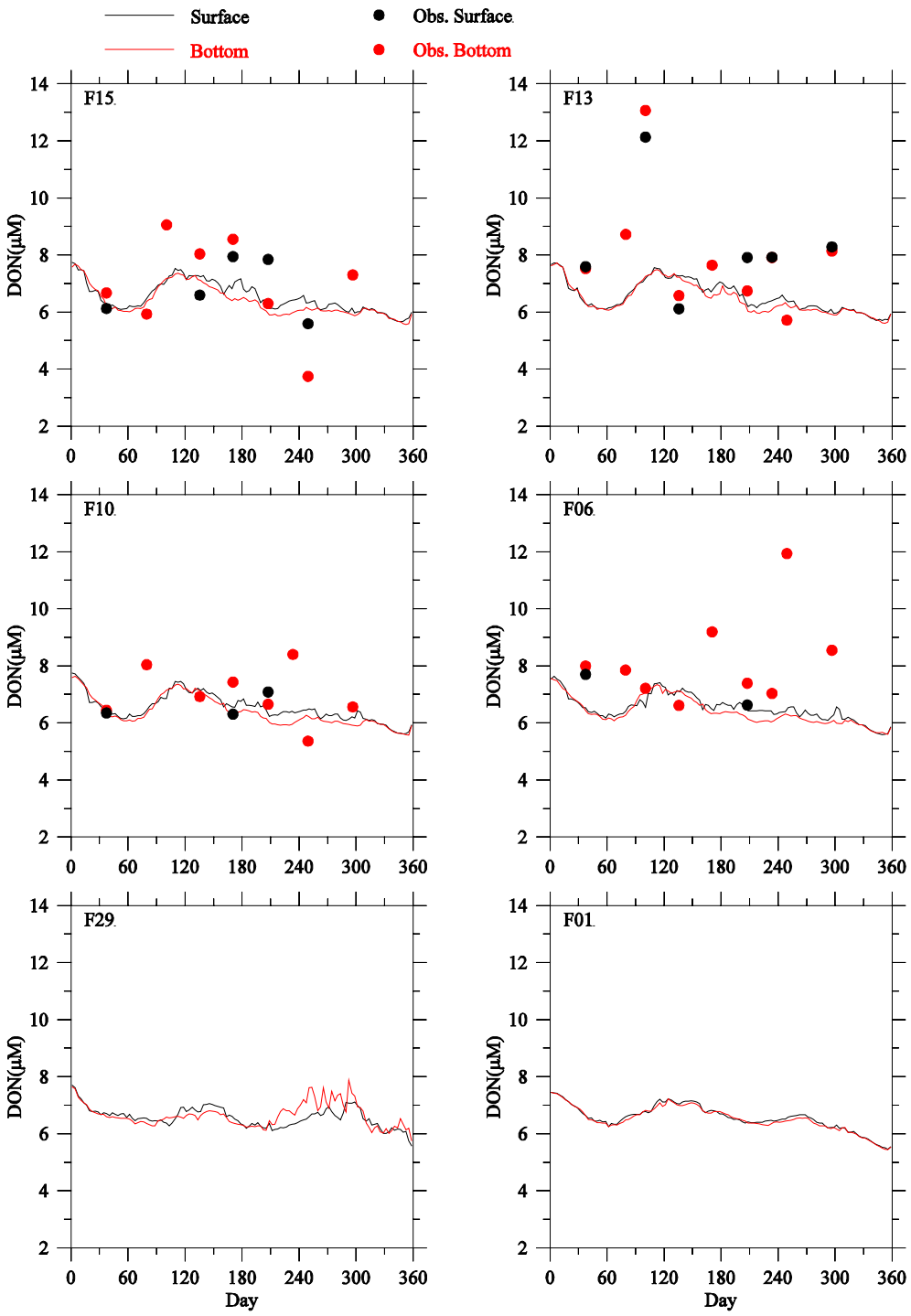

Figure 3.28 DON: observed (dots) and modeled (lines) at southern subset stations in 2012.

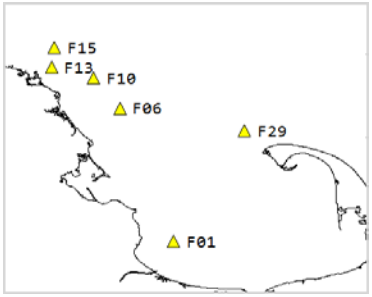

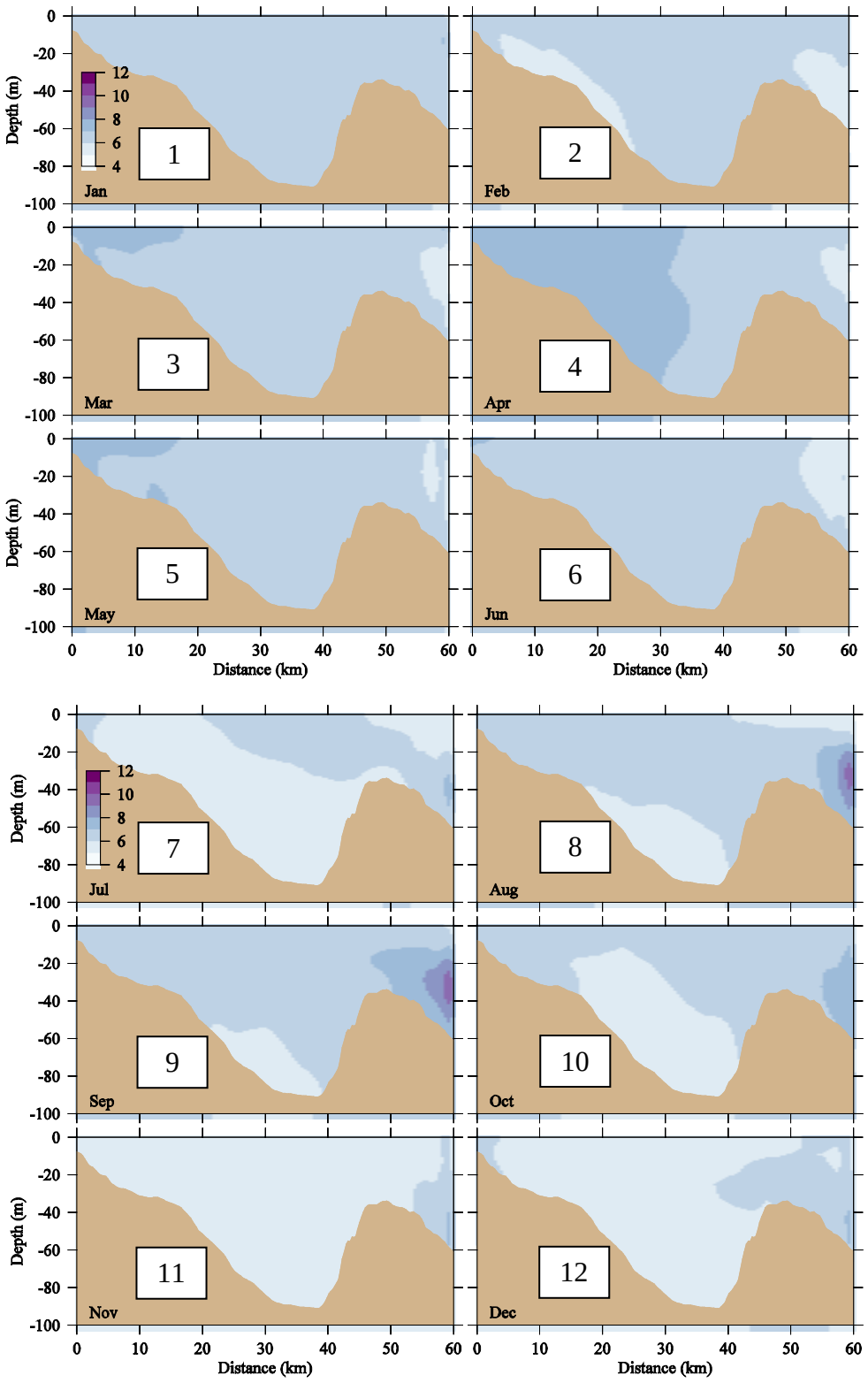

Figure 3.29 Model DON (μM): west-east transect through MWRA outfall, end of each month, 2012.

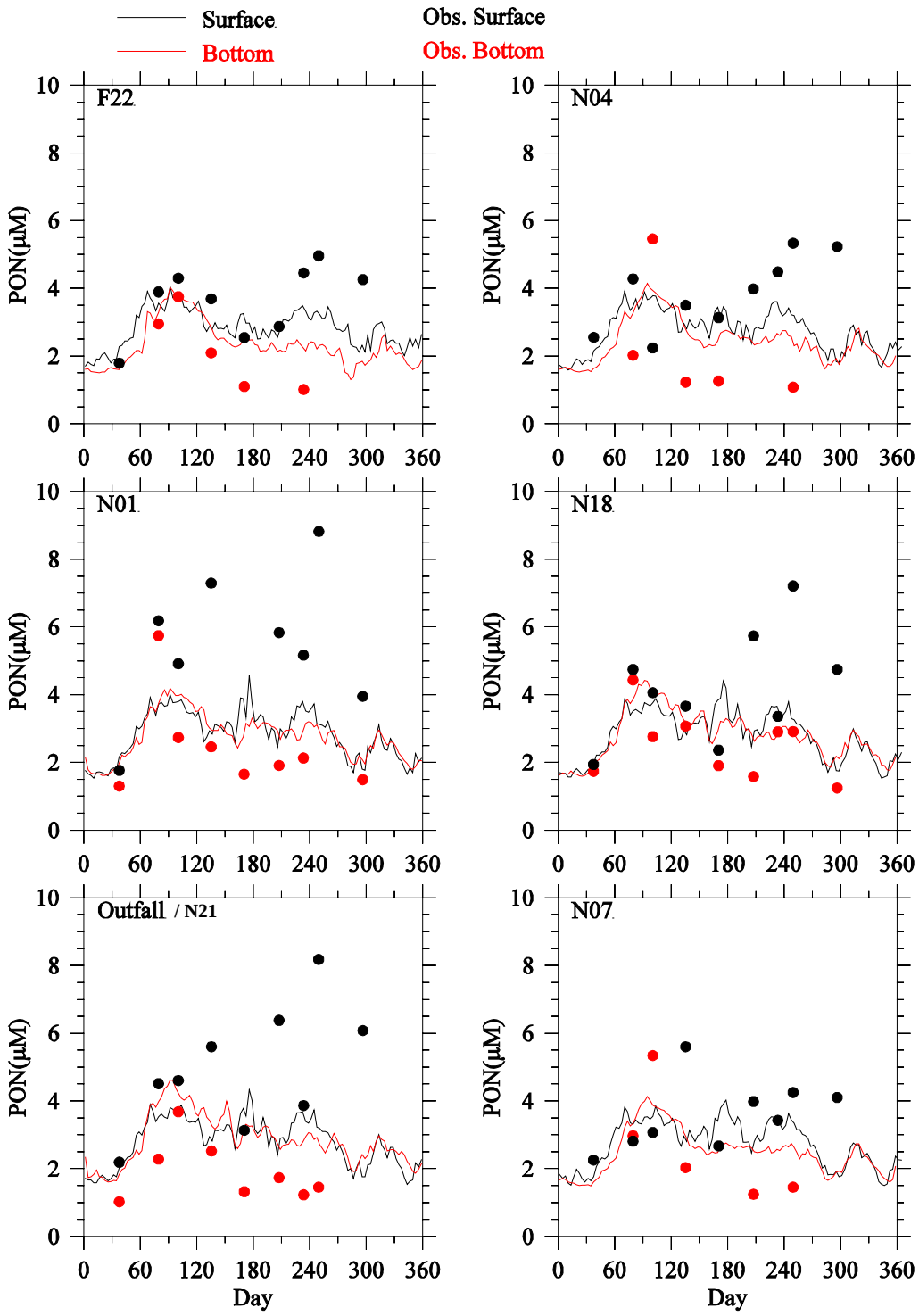

Figure 3.30 PON: observed (dots) and modeled (lines) at northern subset stations in 2012.

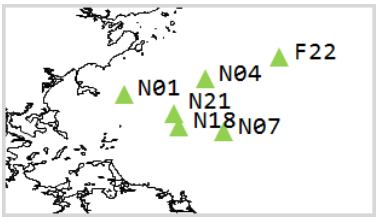

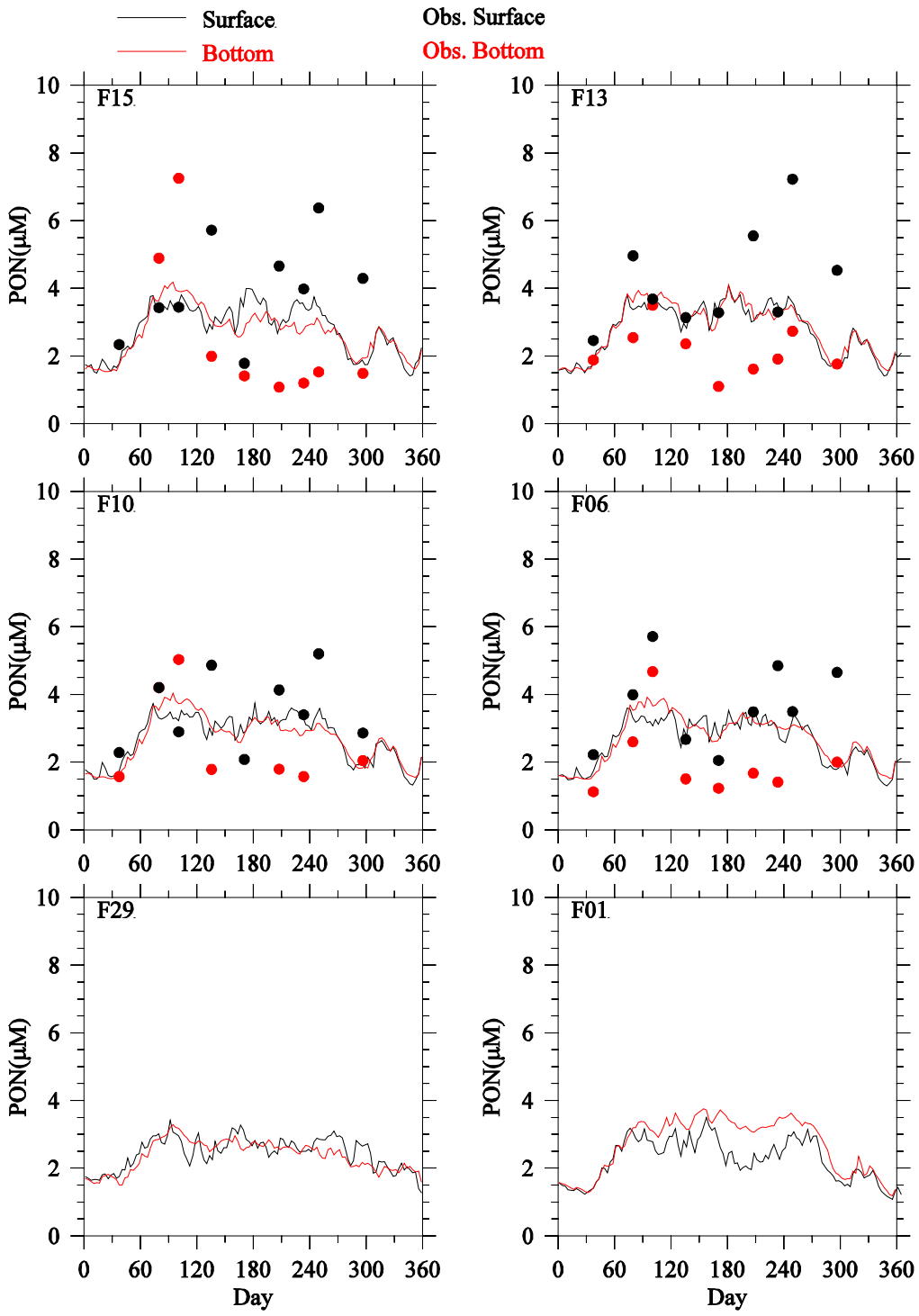

Figure 3.31 PON: observed (dots) and modeled (lines) at southern subset stations in 2012.

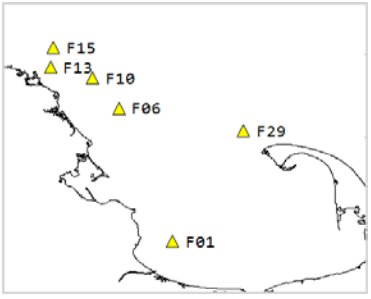

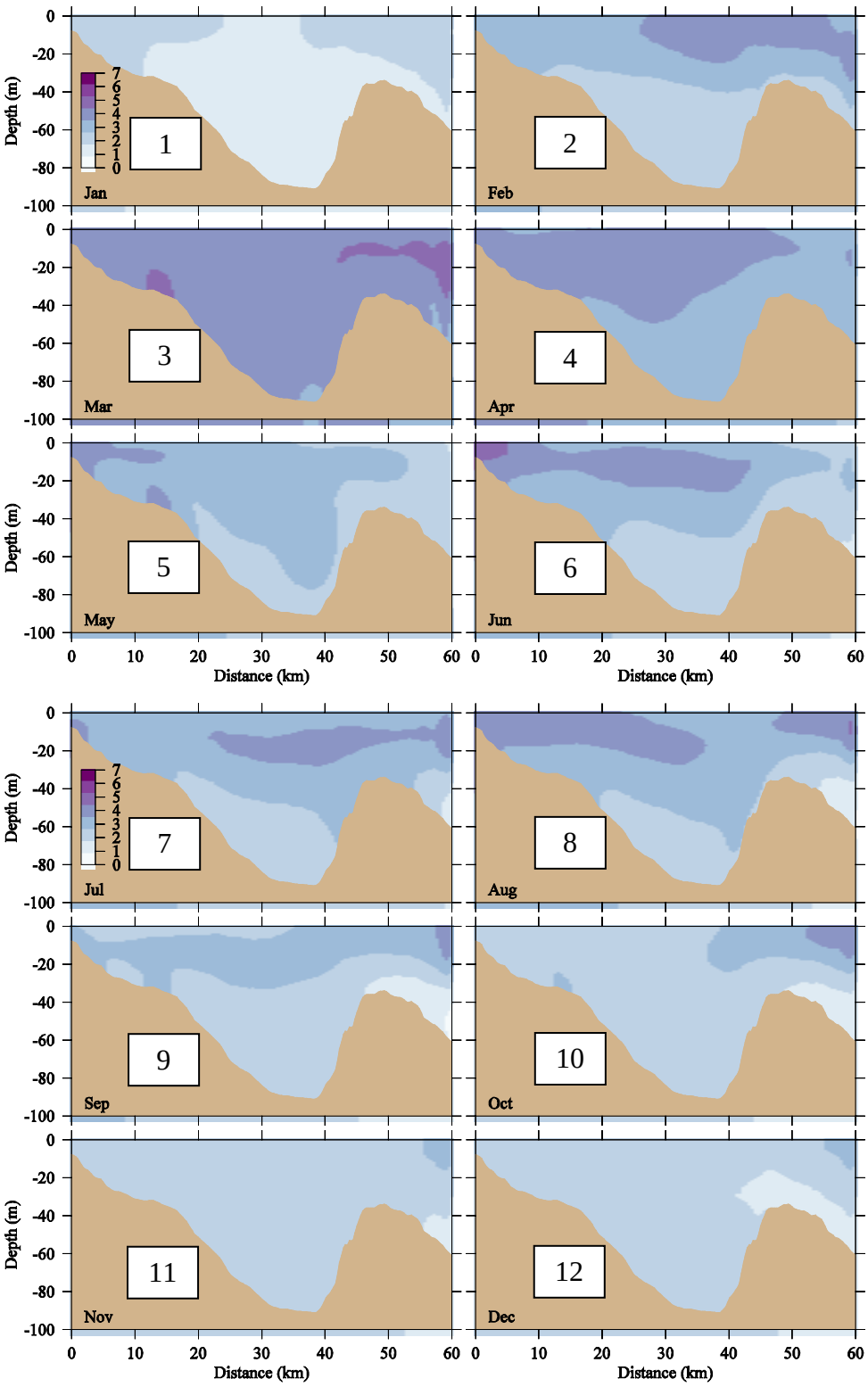

Figure 3.32 Model PON (μM): west-east transect through MWRA outfall, end of each month, 2012.

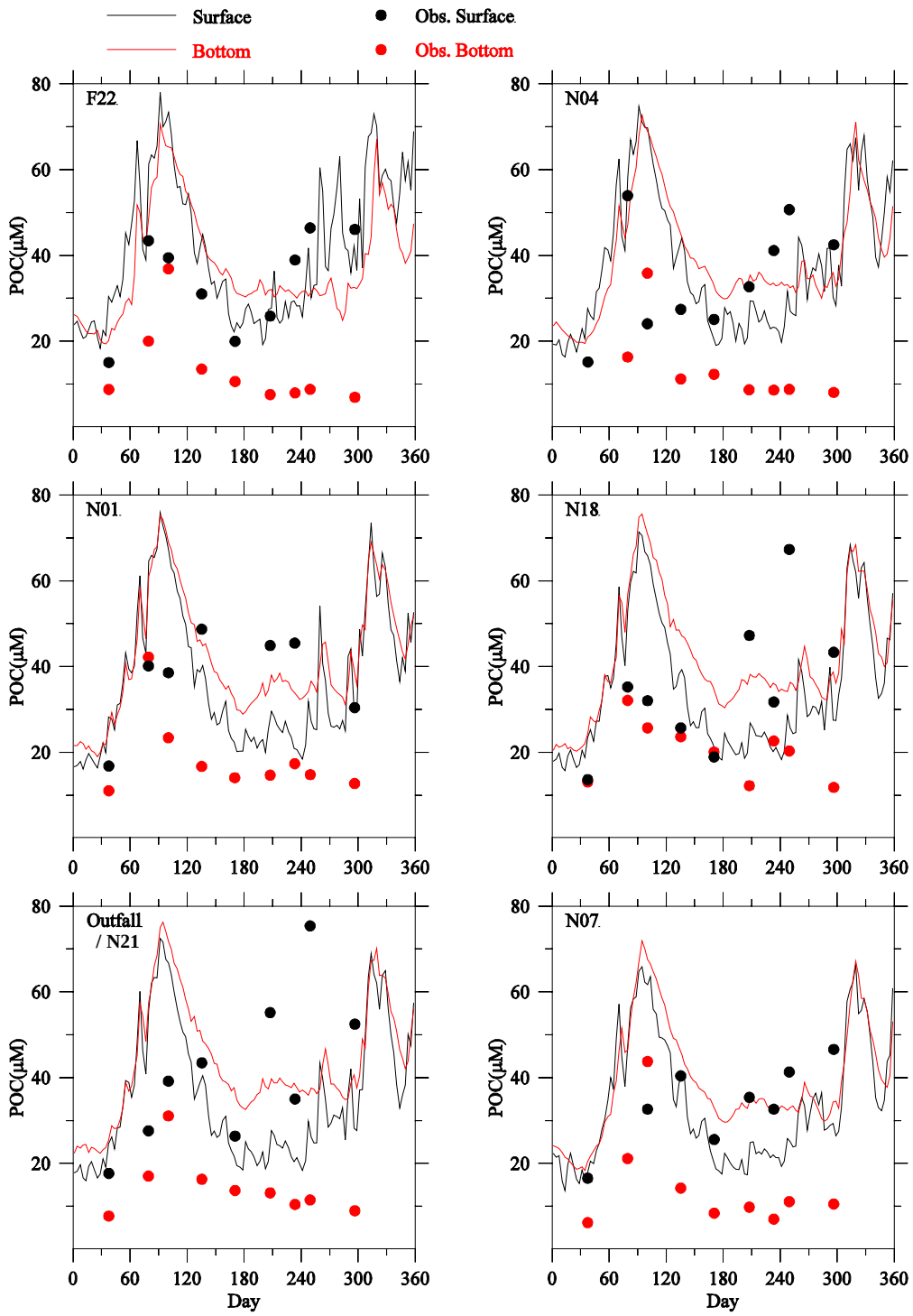

Figure 3.33 POC: observed (dots) and modeled (lines) at northern subset stations in 2012.

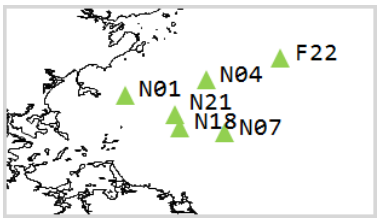

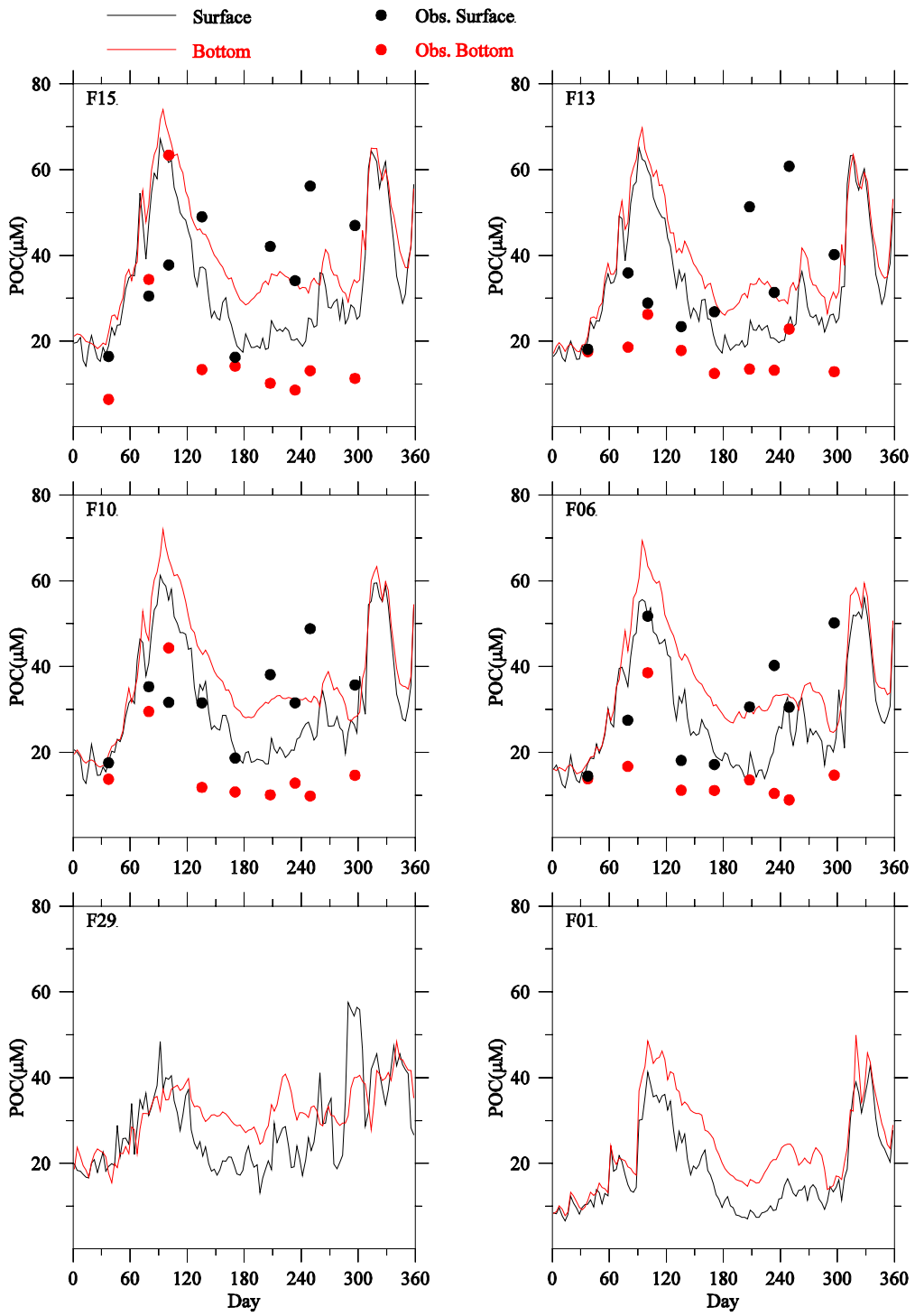

Figure 3.34 POC: observed (dots) and modeled (lines) at southern subset stations in 2012.

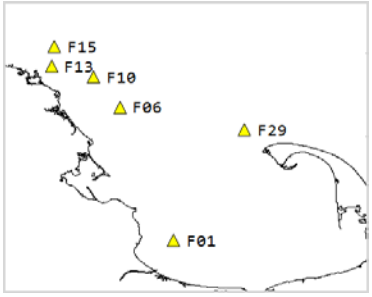

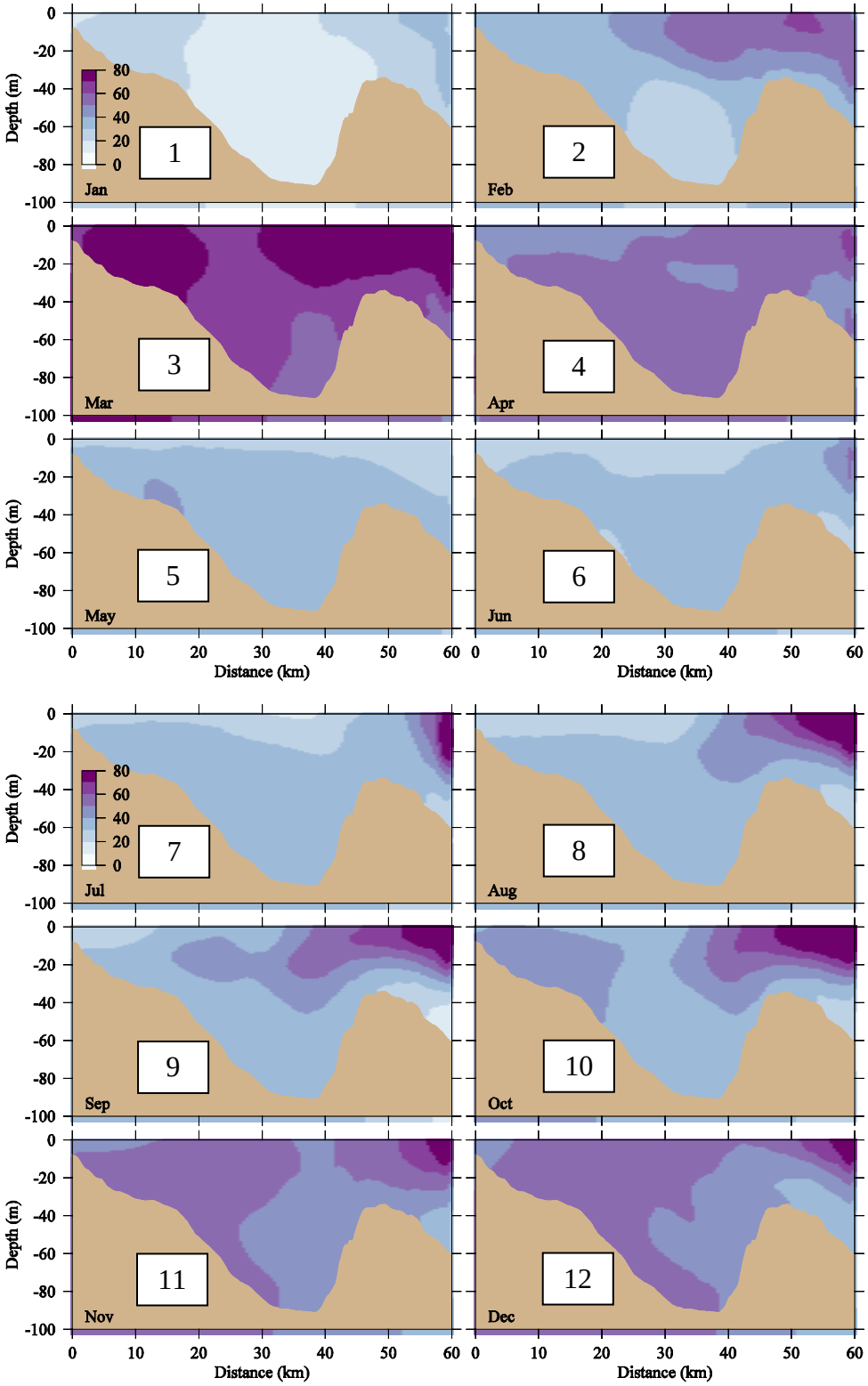

Figure 3.35 Model POC (µM): west-east transect through MWRA outfall, end of each month, 2012.

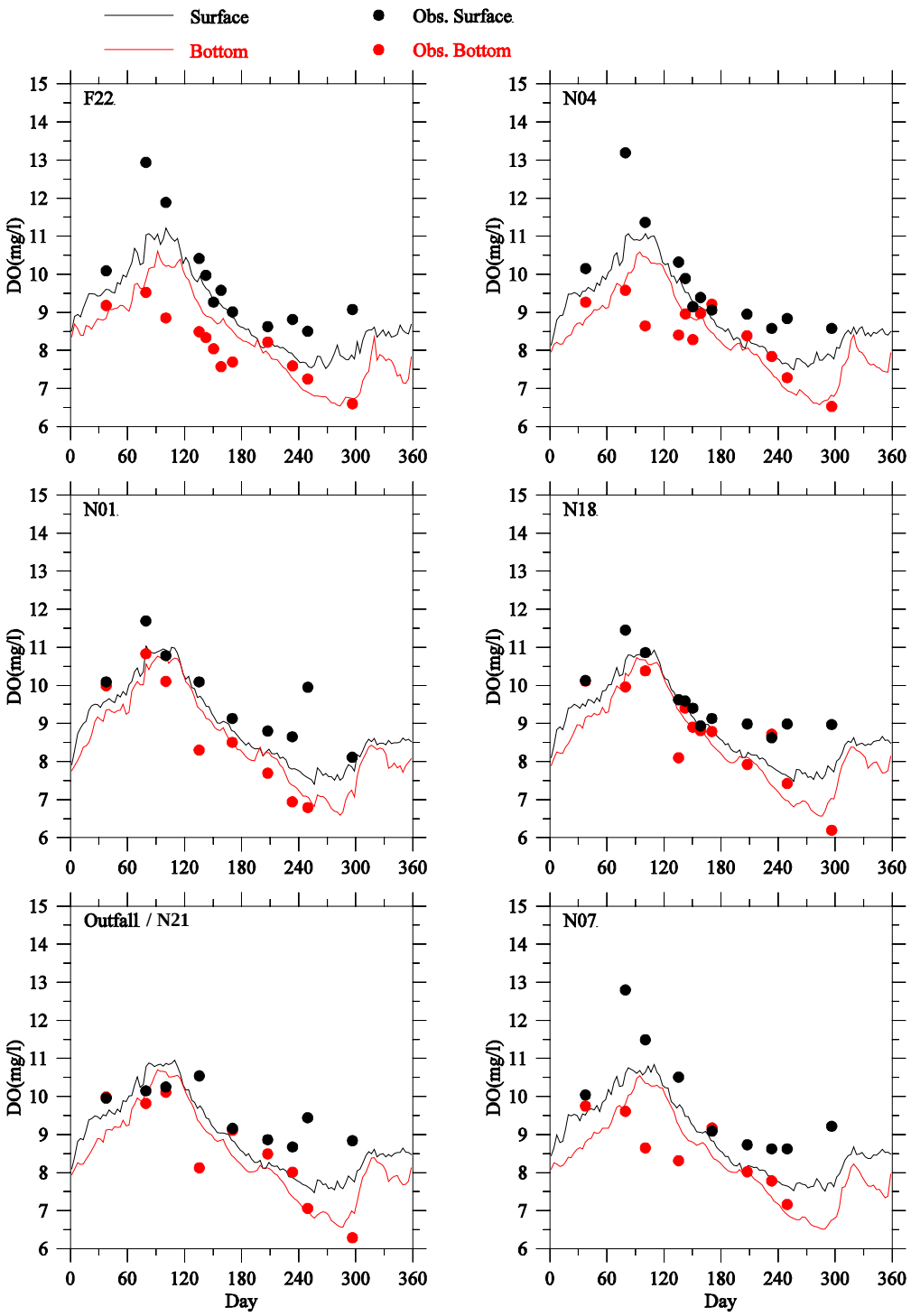

Figure 3.36 DO (mg L^{-1}): observed (dots) and modeled (lines) at northern subset stations in 2012.

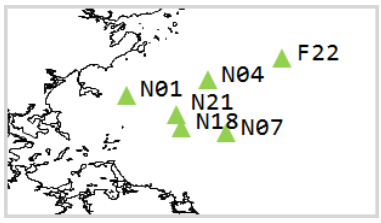

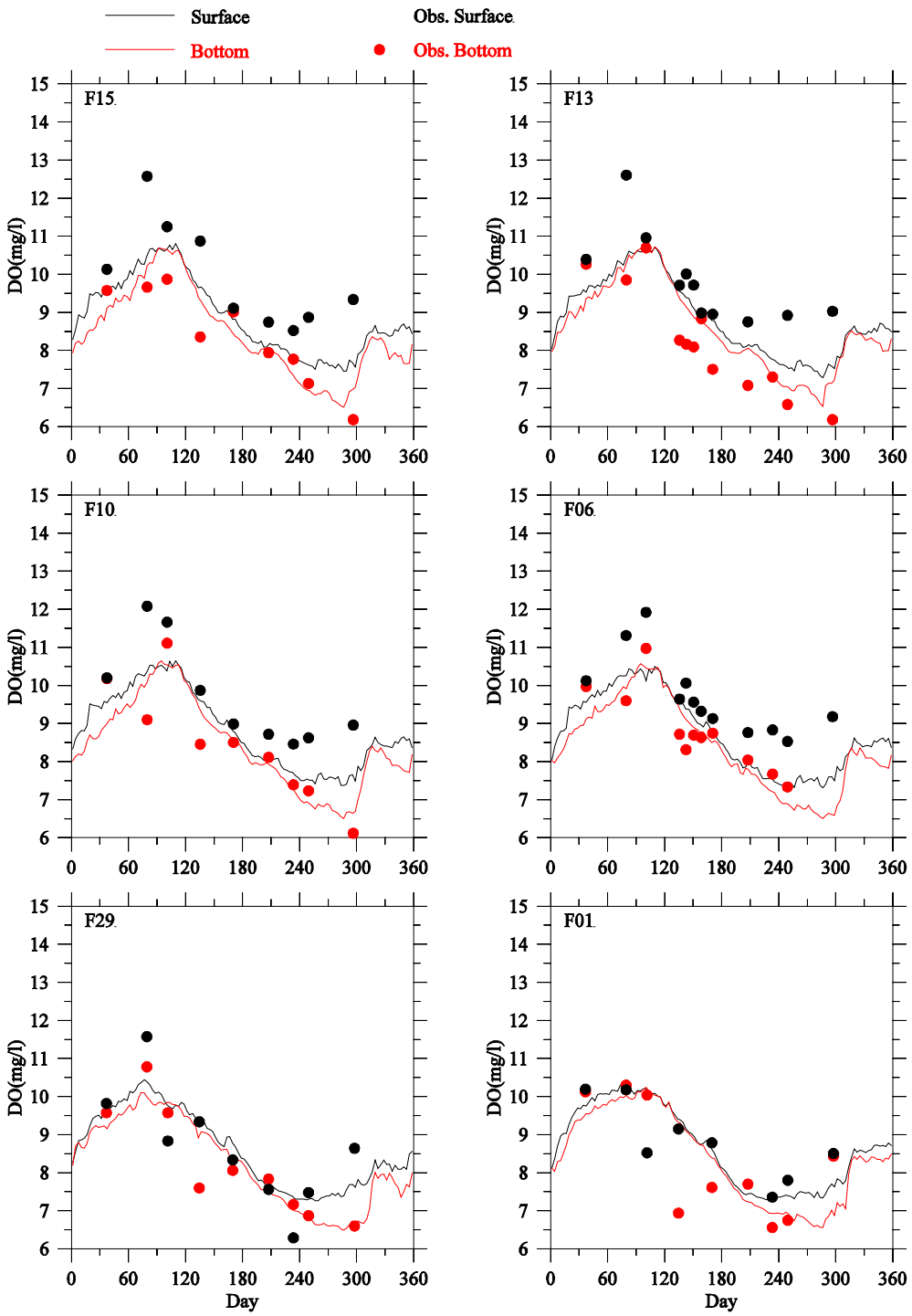

Figure 3.37 DO (mg L^{-1}): observed (dots) and modeled (lines) at southern subset stations in 2012.

.

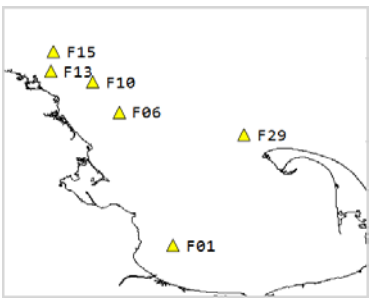

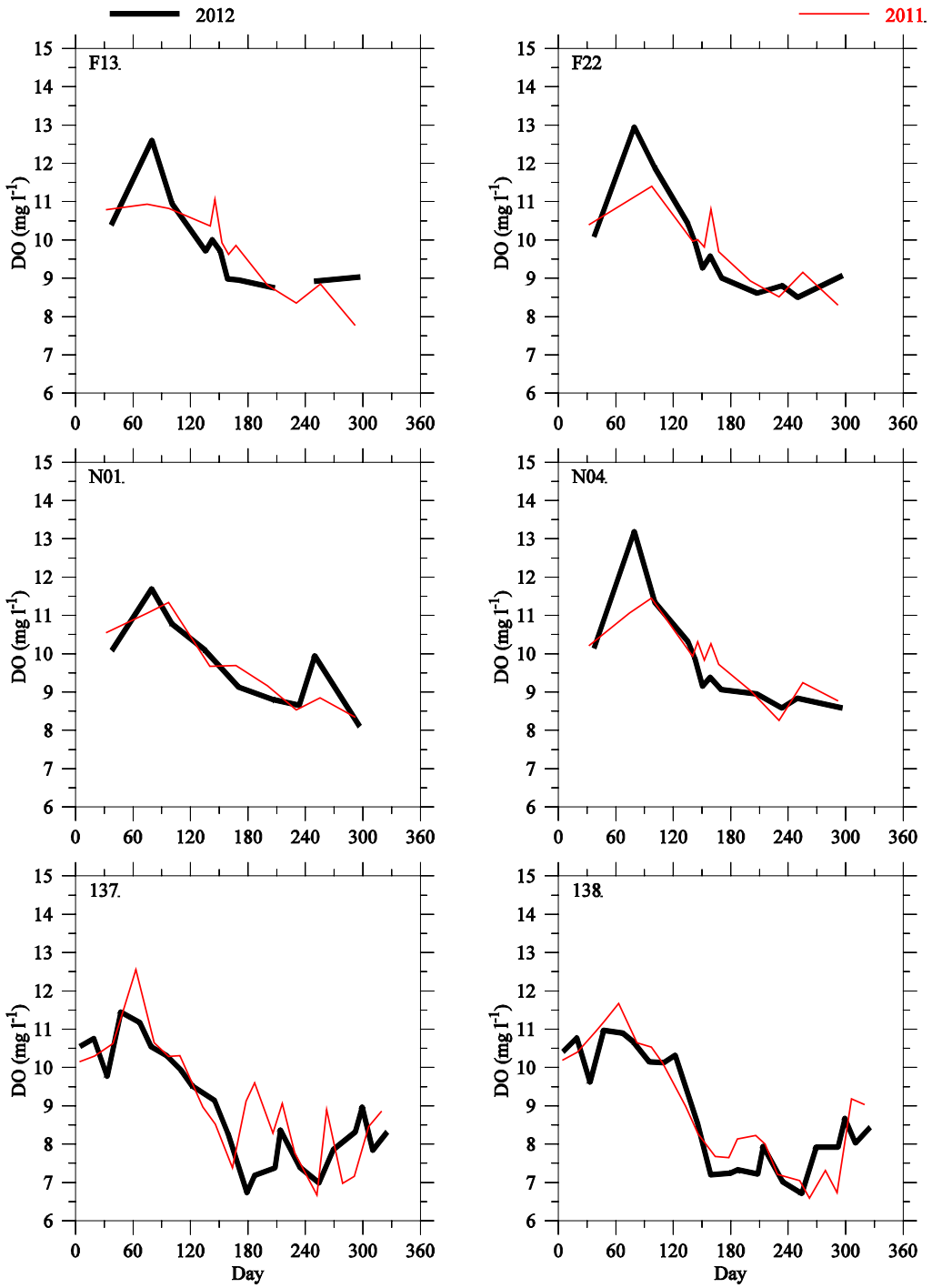

Figure 3.38 Seasonal and interannual variations, observed near-surface DO (mg L^{-1}), select northern subset (F22, N01, N04), southern subset (F13), and harbor (137, 138) stations: 2011 (red) and 2012 (black).

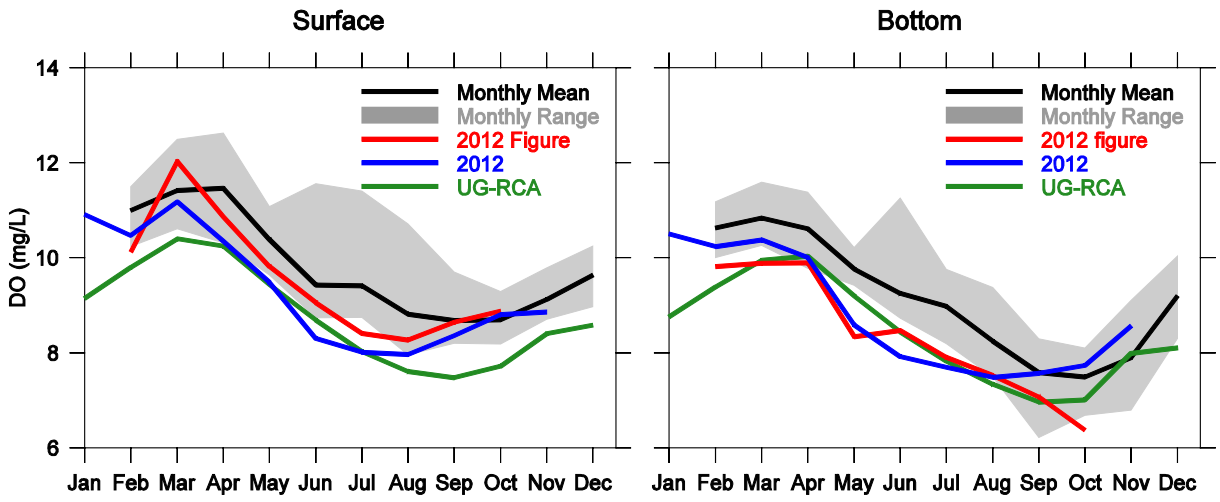

Figure 3.39 Observed inter-annual variability of near-surface and near-bottom monthly-mean DO from 1992-2010, with observations and model results from 2012 superposed.

Near-surface (left) and near-bottom (right). Black line and gray shadow show mean, and minimum/ maximum range of inter-annual variability, of monthly-average observations using all MWRA sampled stations (Figure 3.4**,** all colors**)** during period 1992-2010. Blue line: average across all stations sampled in 2012 (a core subset of the stations sampled 1992-2010, spanning MB, BH, and CCB; green, yellow, blue, and black stations in Figure 3.4), revealing unusually low DO throughout much of 2012 as compared to the historical mean and range (black line and gray shadow). Red and green lines: 2012 observations and model respectively, using all stations (as for blue line) except BH stations.

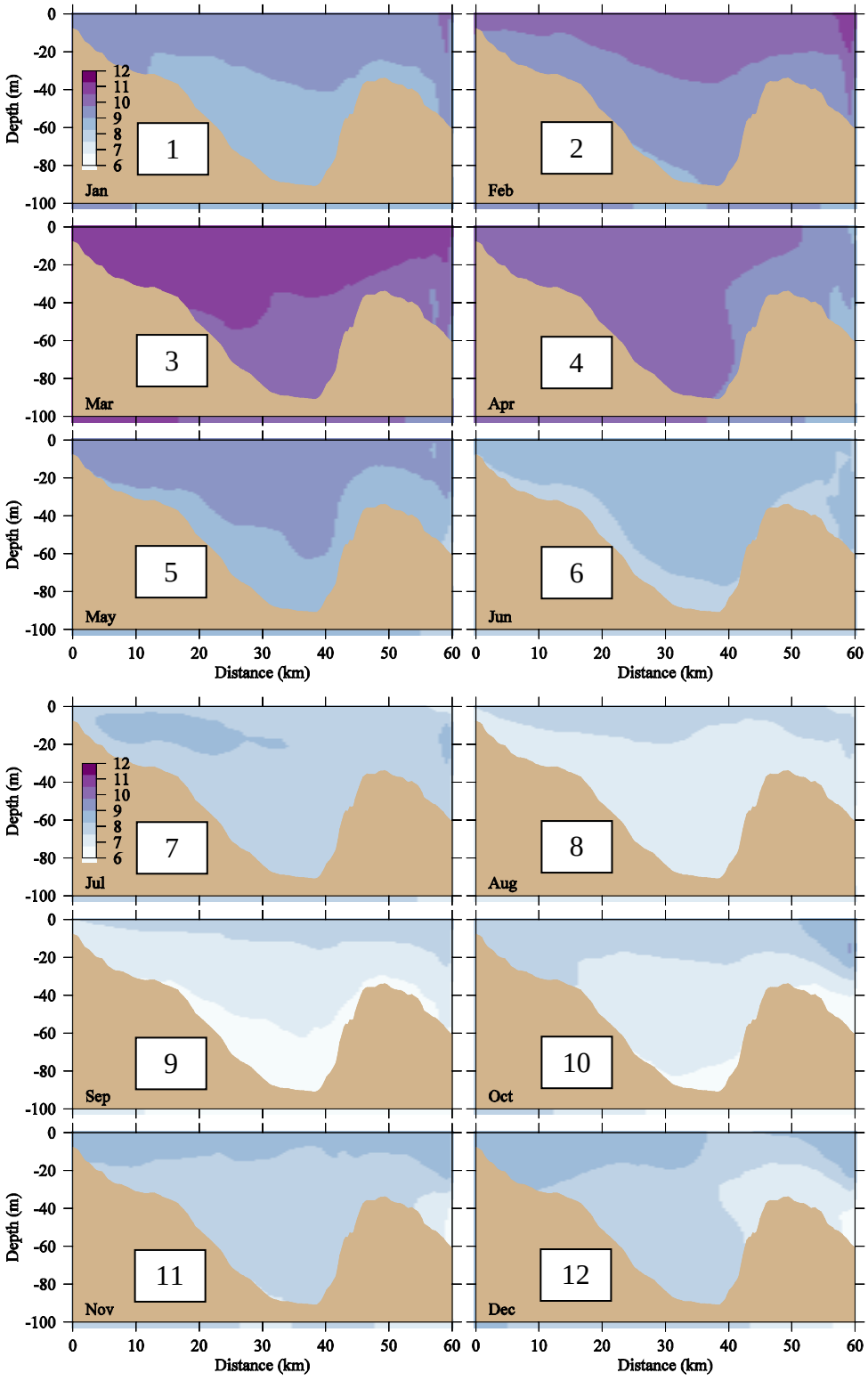

Figure 3.40 Model DO (mg L^{-1}): west-east transect through MWRA outfall, end of each month, 2012.

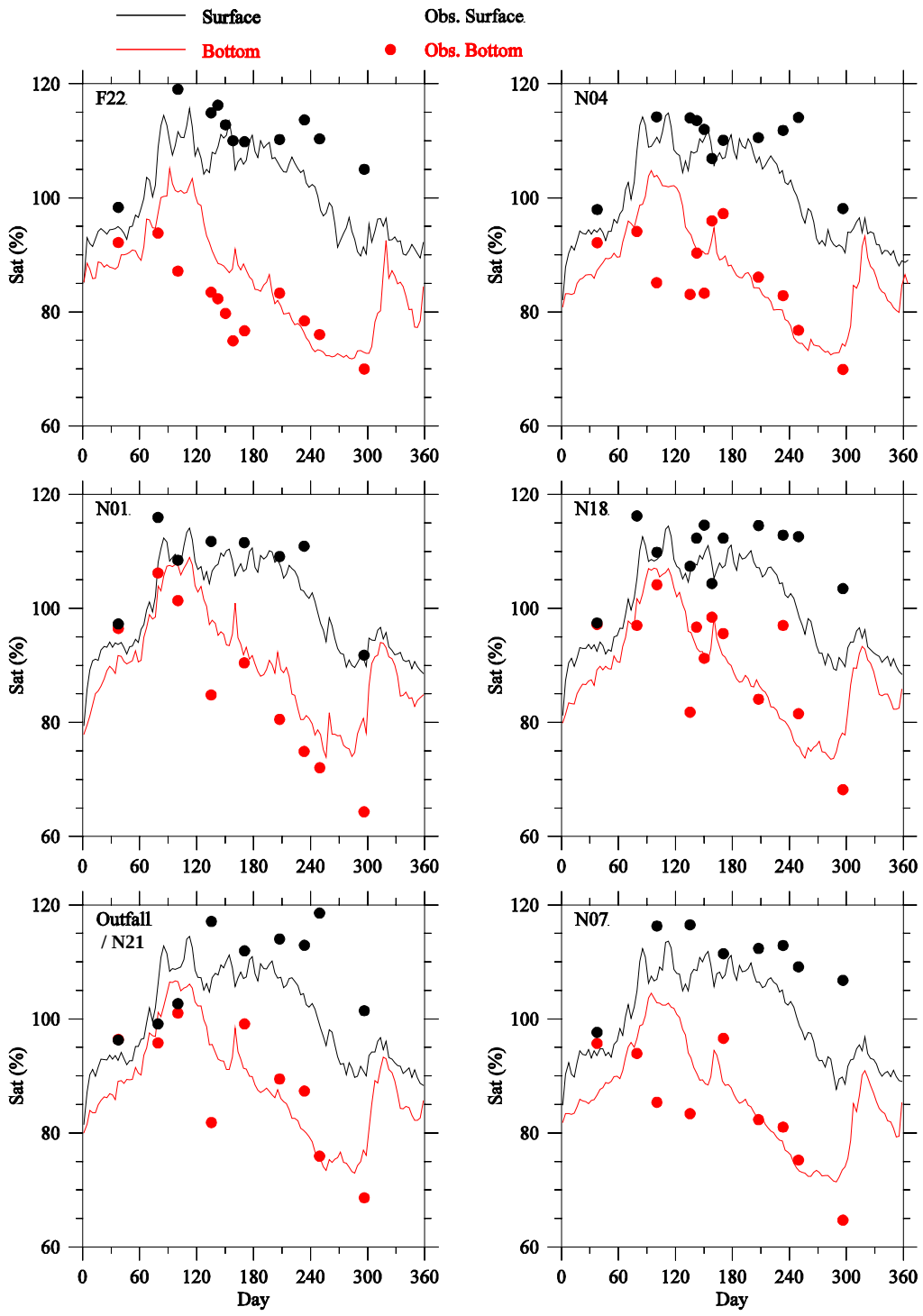

Figure 3.41 DO saturation (%): observed (dots) and modeled (lines) at northern subset stations in 2012.

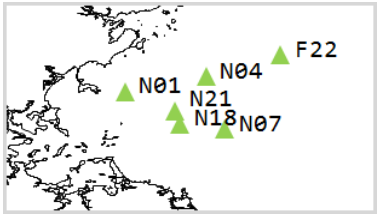

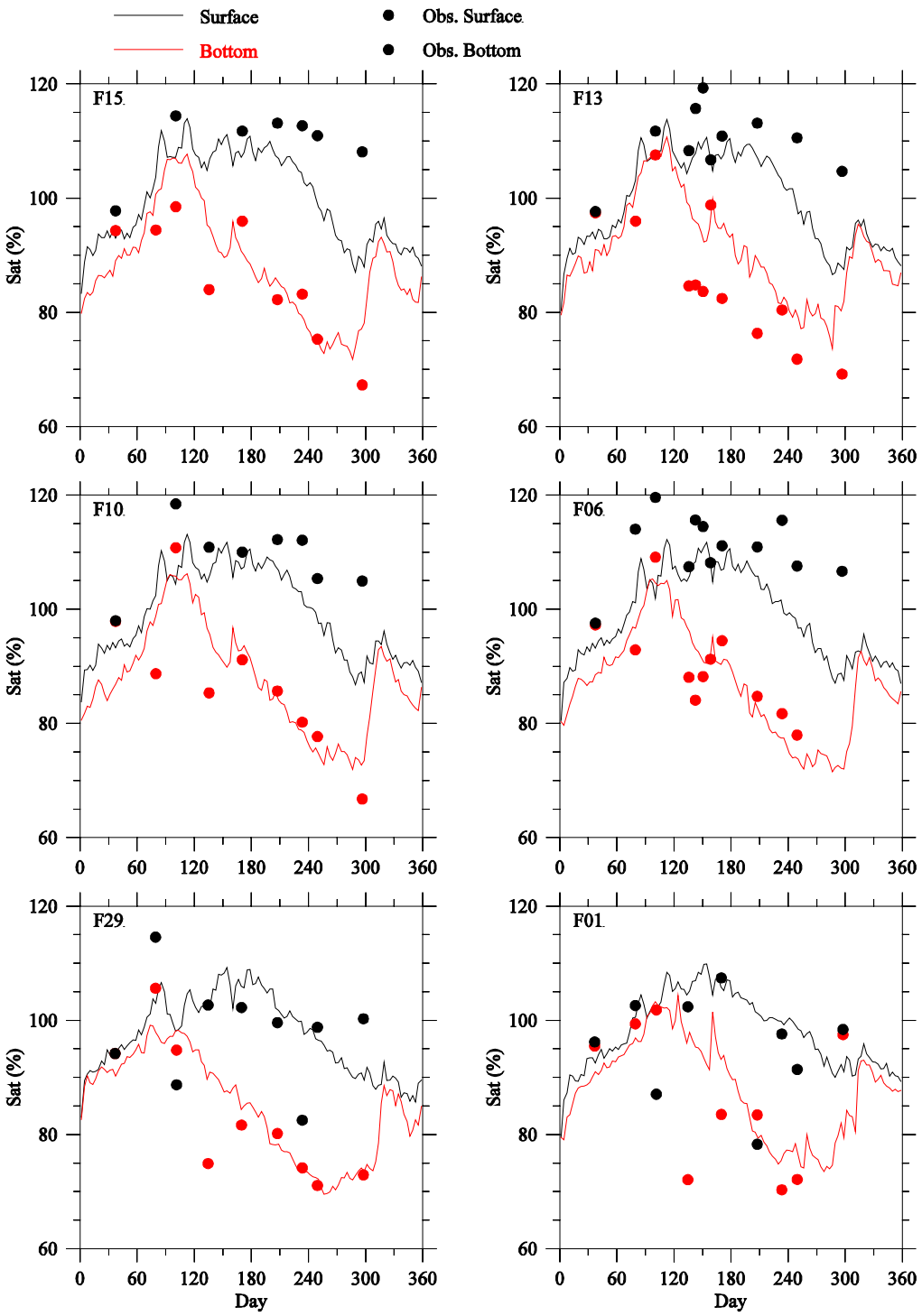

Figure 3.42 DO saturation (%): observed (dots) and modeled (lines) at southern subset stations in 2012.

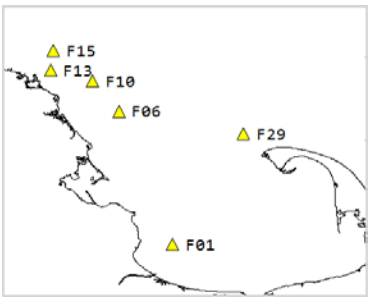

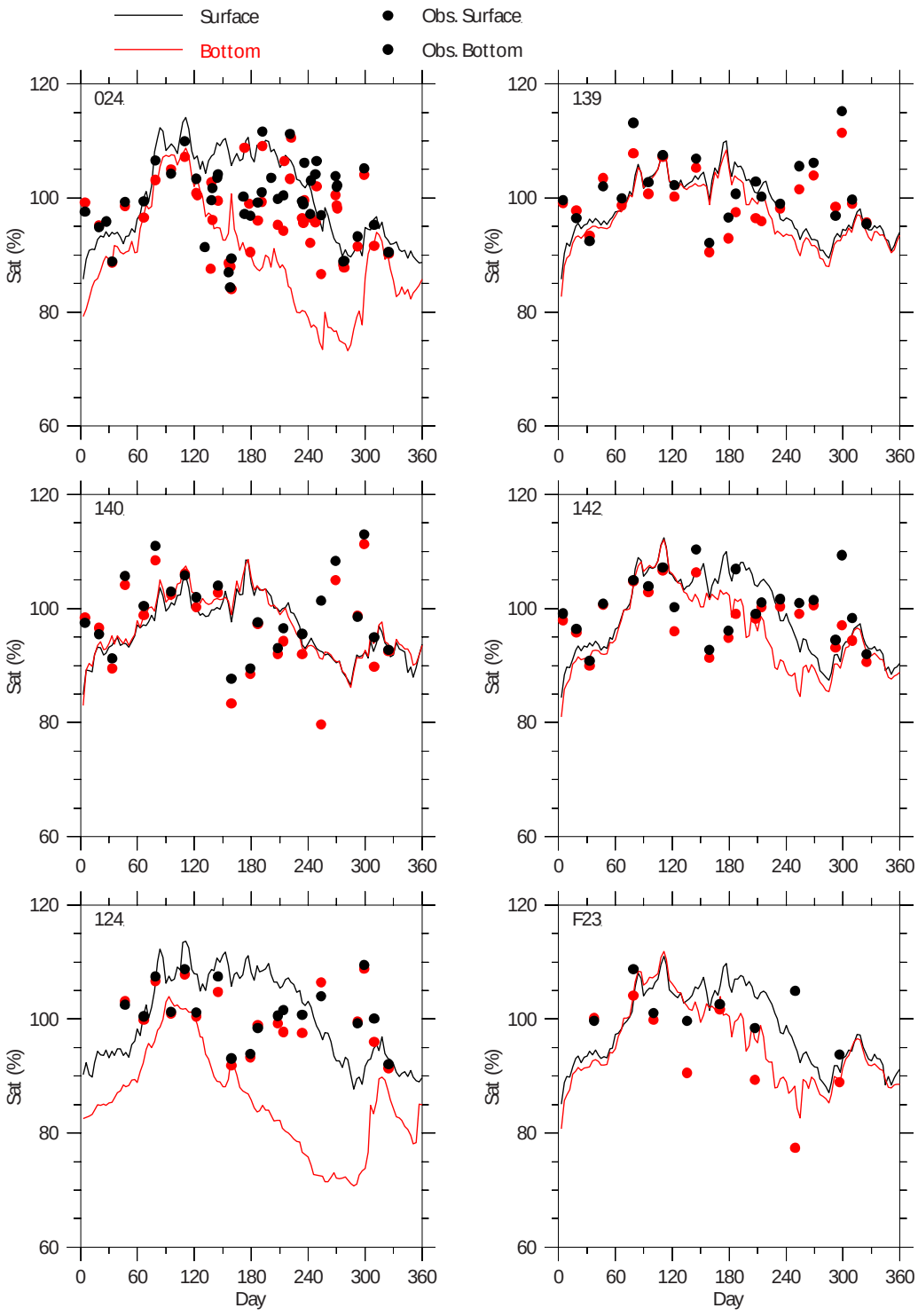

Figure 3.43 DO saturation (%): observed (dots) and modeled (lines) at harbor subset stations in 2012.

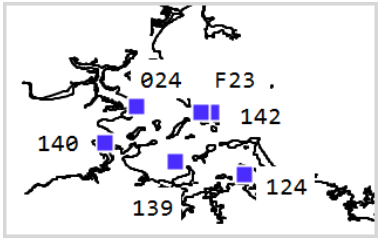

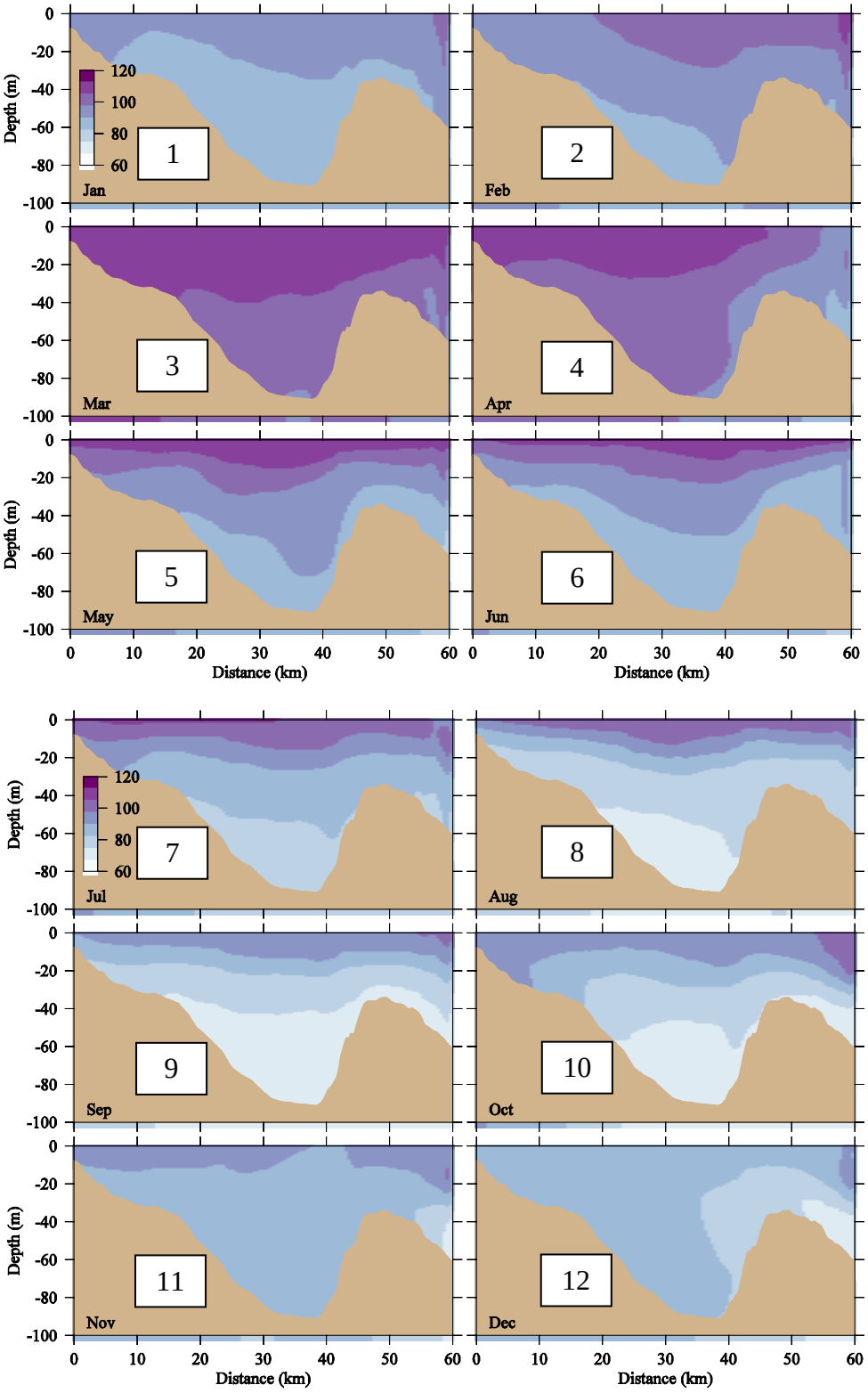

Figure 3.44 Model DO saturation (%): west-east transect through MWRA outfall, end of each month, 2012.

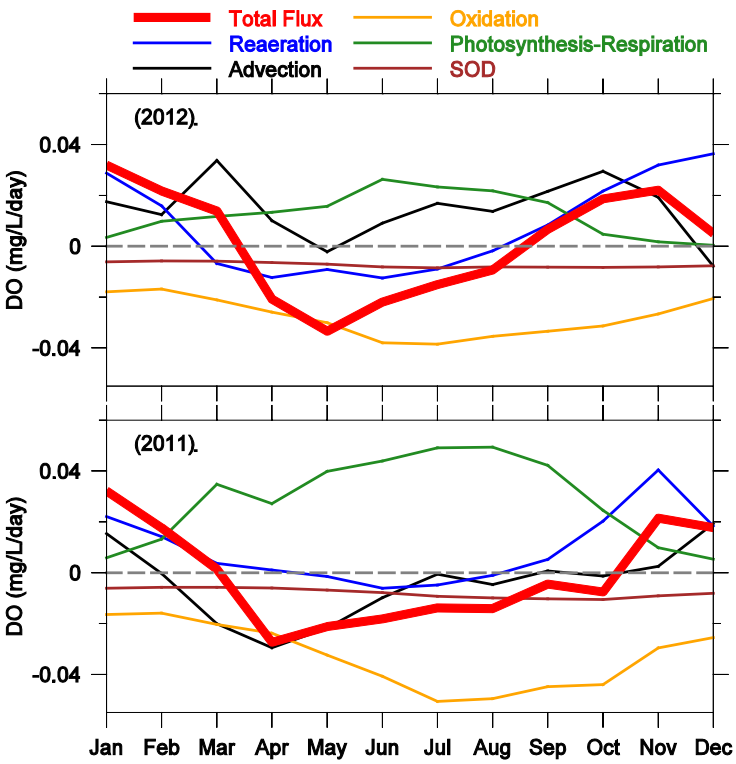

Figure 3.45 Interannual variations of model DO flux terms in vertically averaged 2-D balance (Xue et al., 2014), averaged across the entire BEM domain: 2012 (upper panel) and 2011 (lower panel).

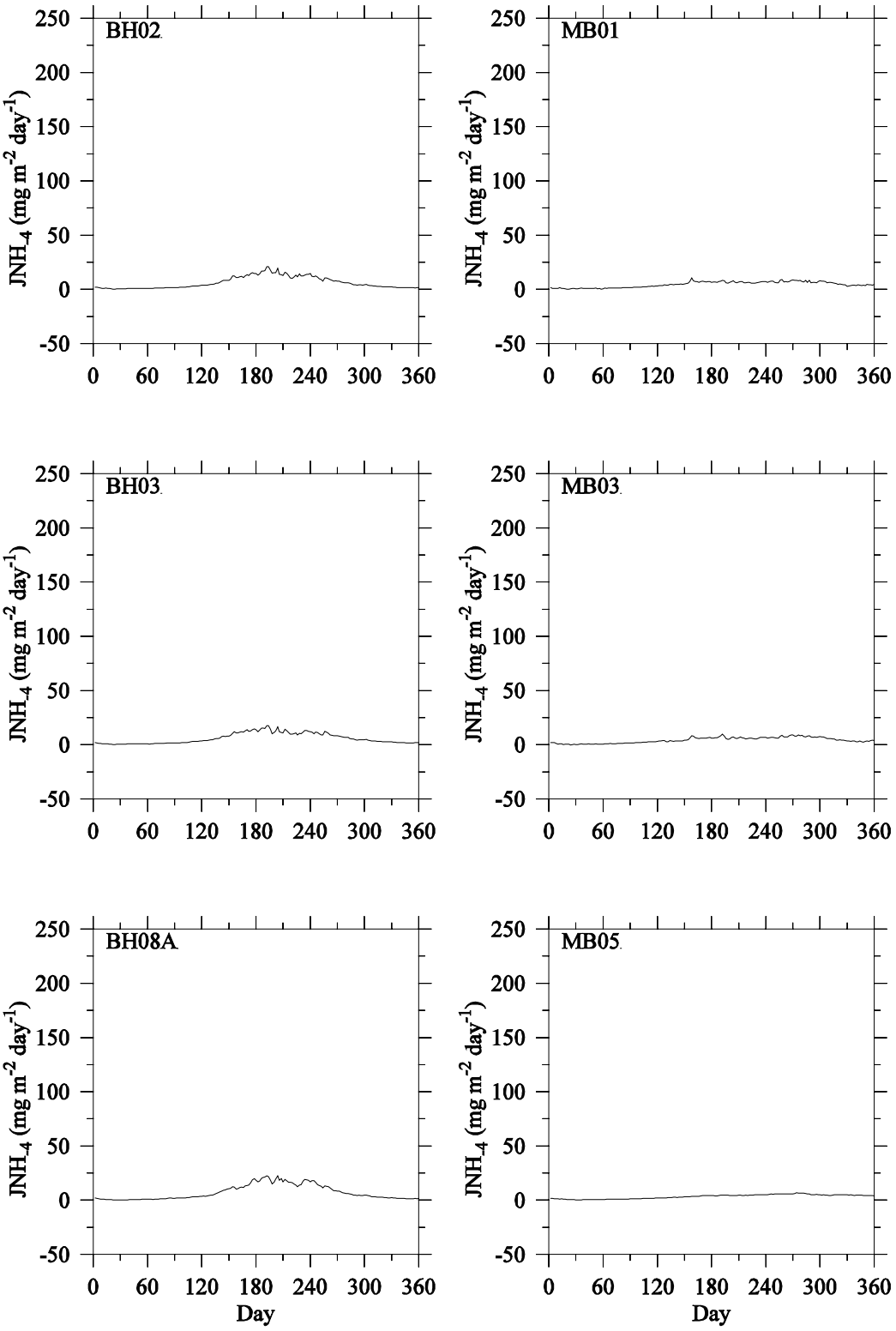

Figure 3.46 Model sediment NH_4^+ flux at select sediment flux study stations in 2012.

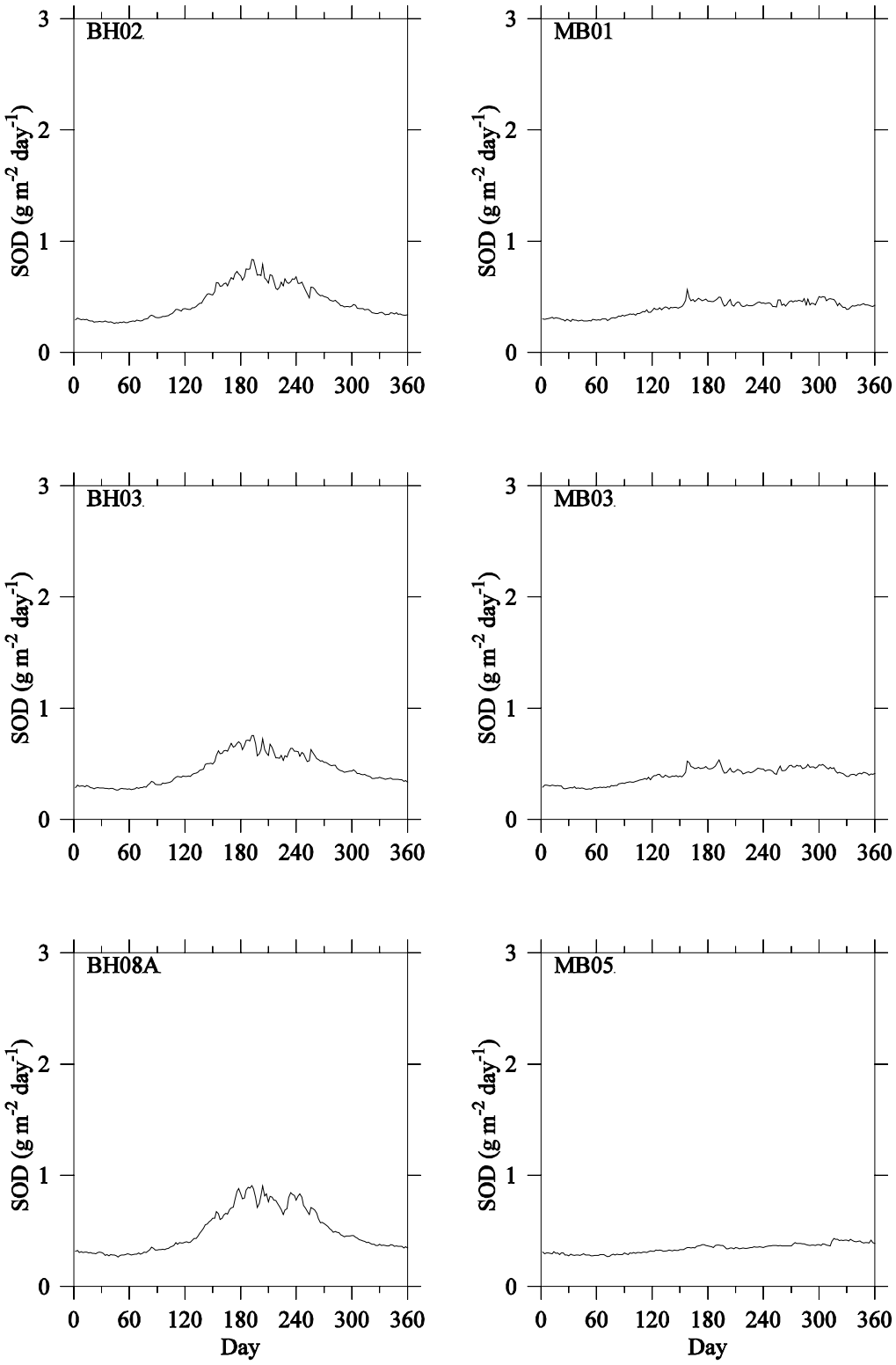

Figure 3.47 Model sediment oxygen demand at select sediment flux study stations in 2012.

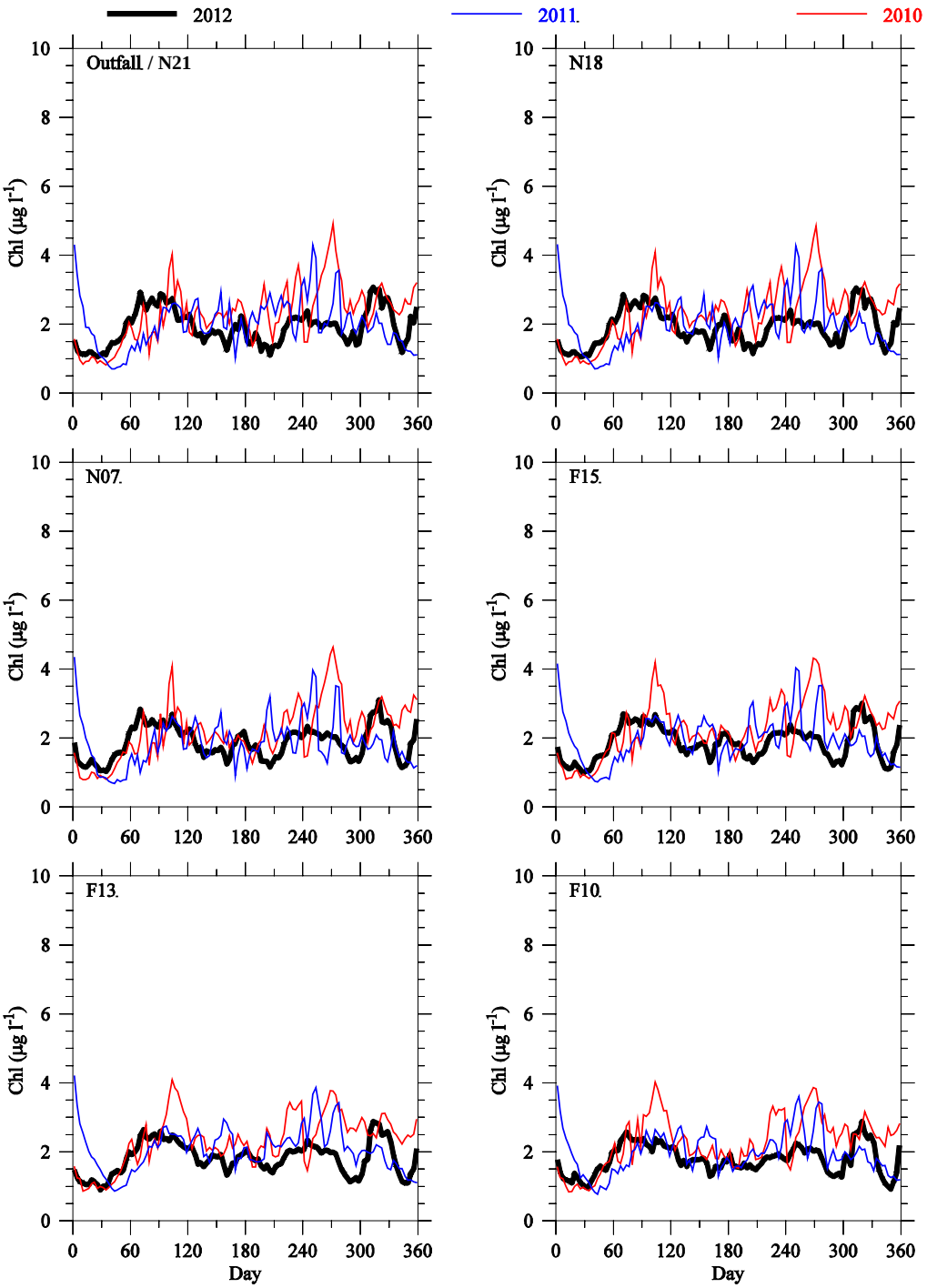

Figure 3.48 Seasonal and interannual variations, model surface chlorophyll, select MB stations: 2010 (red lines), 2011 (blue lines), and 2012 (black lines).

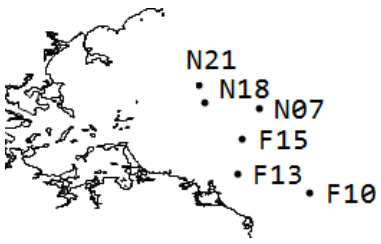

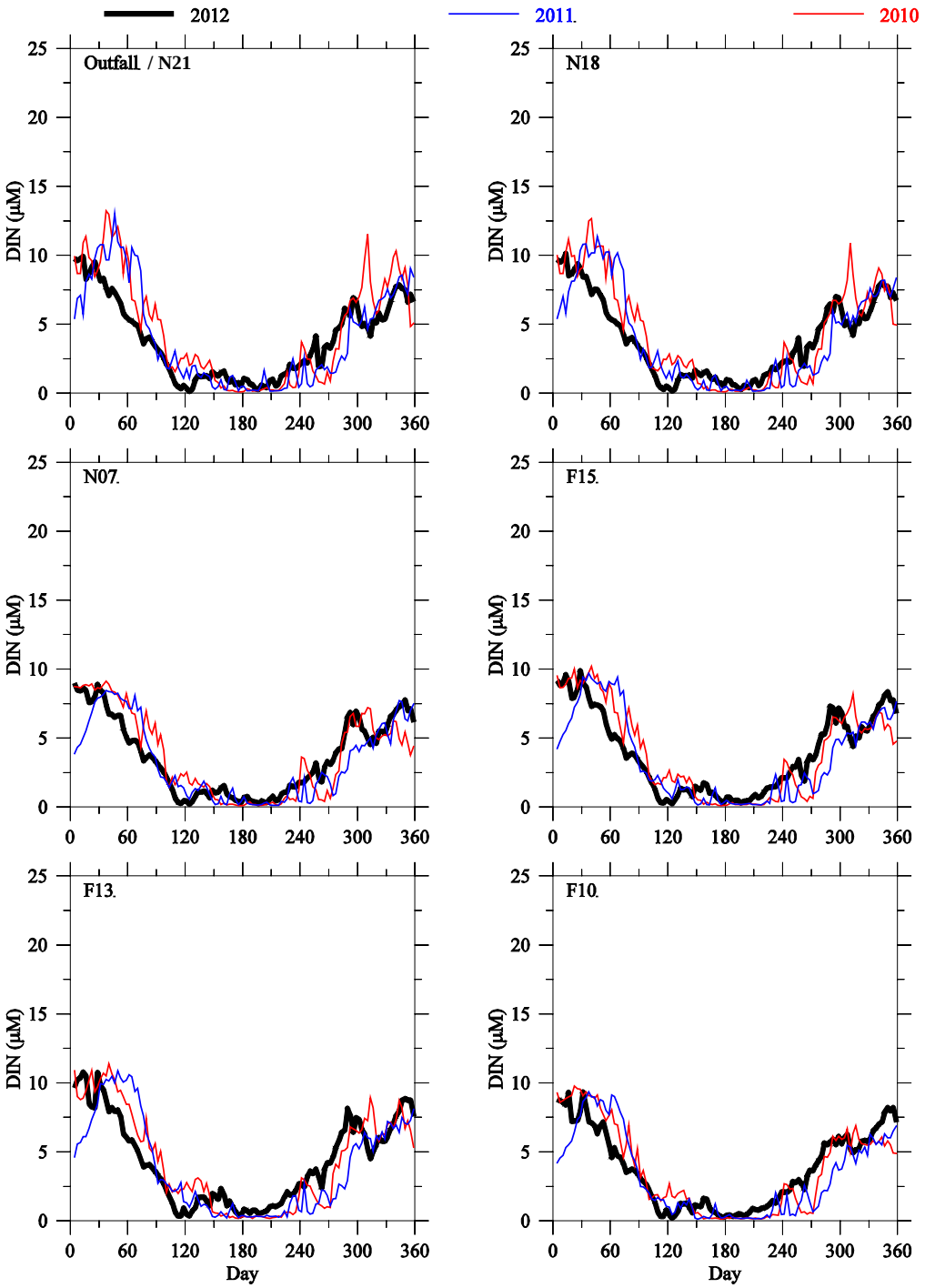

Figure 3.49 Seasonal and interannual variations, model surface DIN at select MB stations: 2010 (red lines), 2011 (blue lines), and 2012 (black lines).

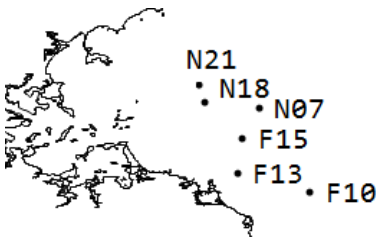

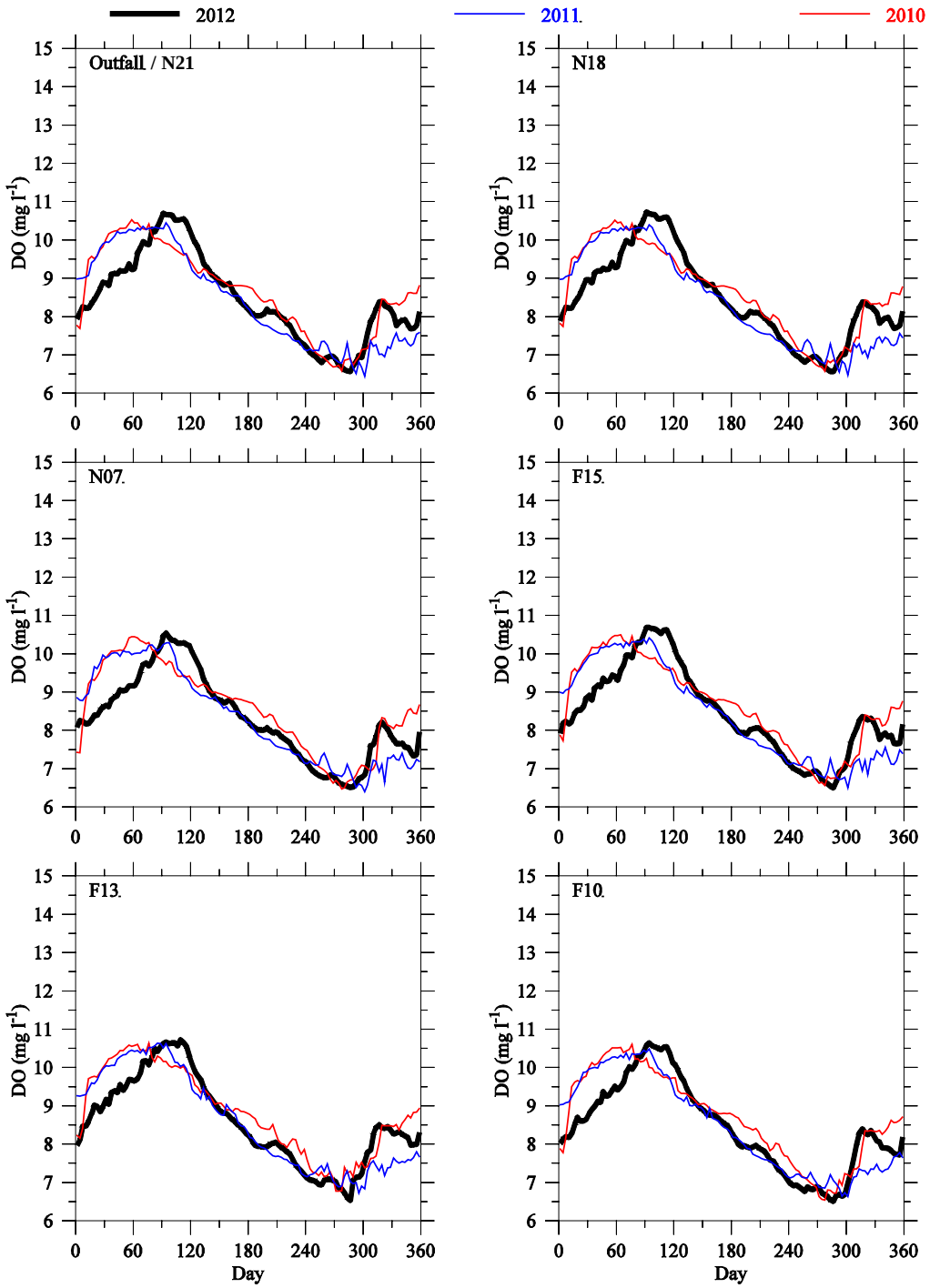

Figure 3.50 Seasonal and interannual variations, model bottom DO (mg L^{-1}) at select MB stations: 2010 (red lines), 2011 (blue lines), and 2012 (black lines).

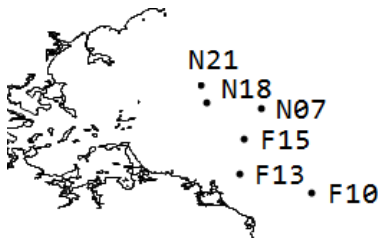

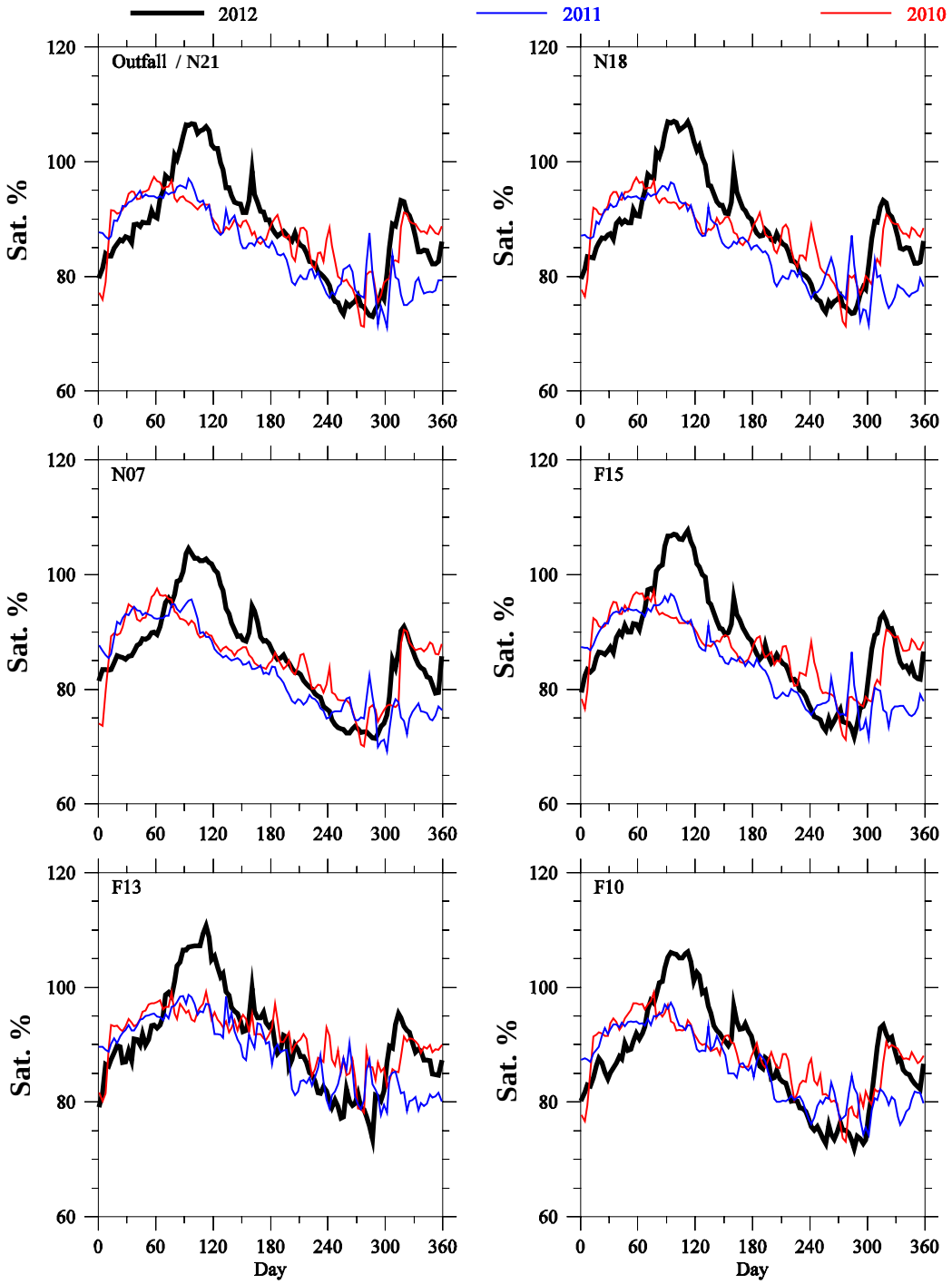

Figure 3.51 Seasonal and interannual variations, model bottom DO saturation (%) at select MB stations: 2010 (red lines), 2011 (blue lines), and 2012 (black lines).

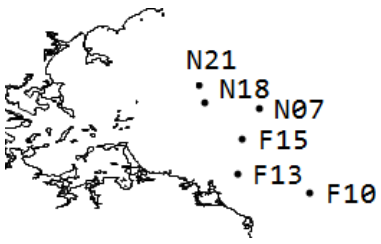

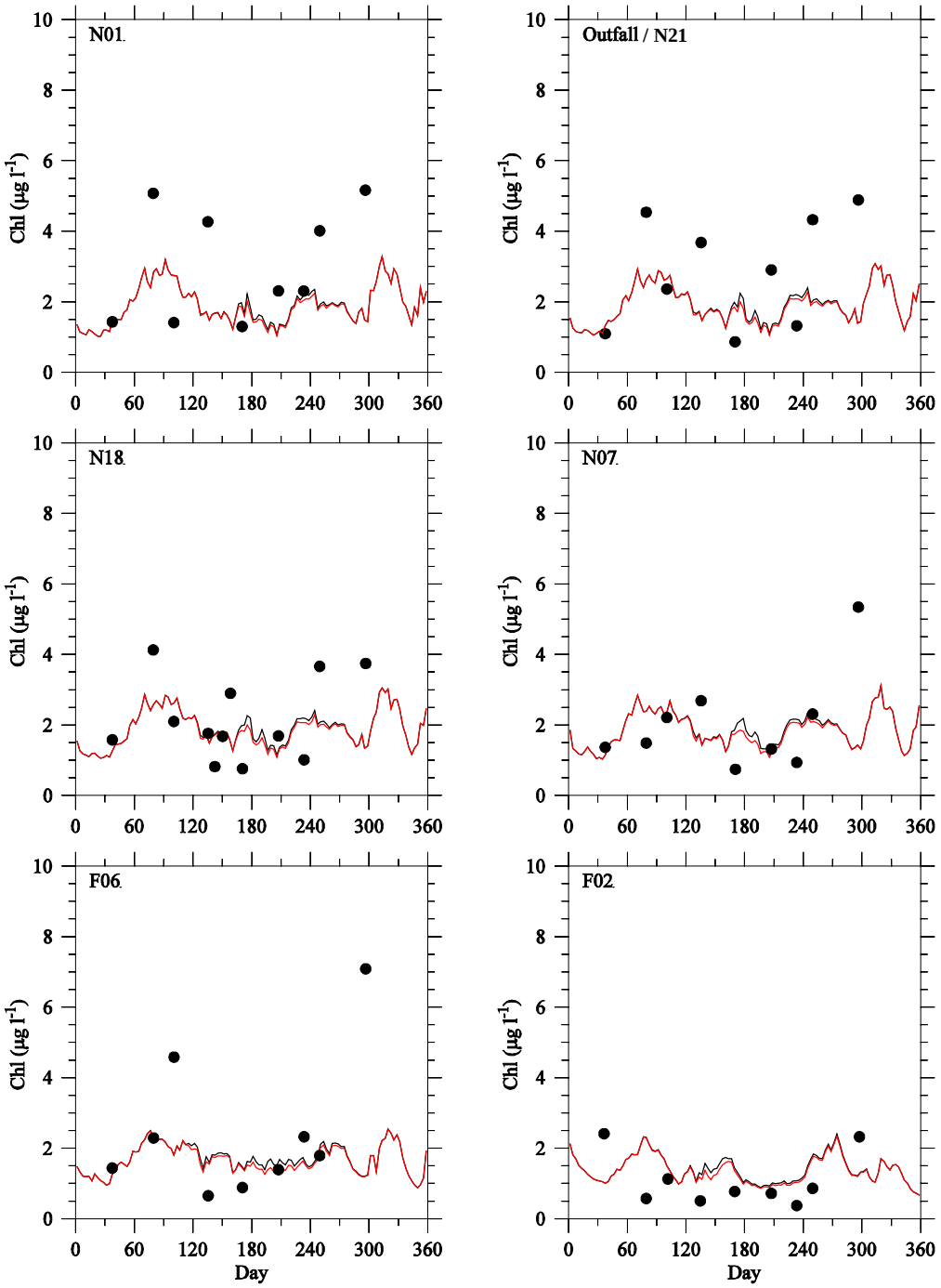

Figure 4.1 Scenario experiment surface chlorophyll: observed (dots), control run (black line), and non-sewage (red line) at select MB stations in 2012.

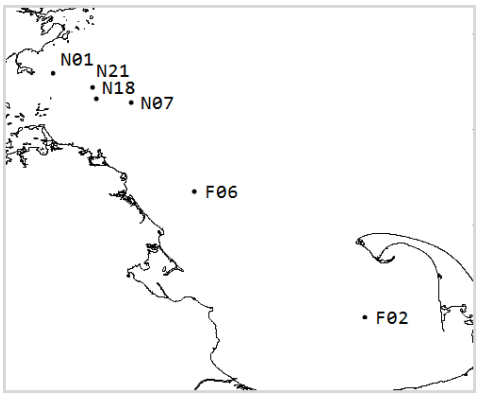

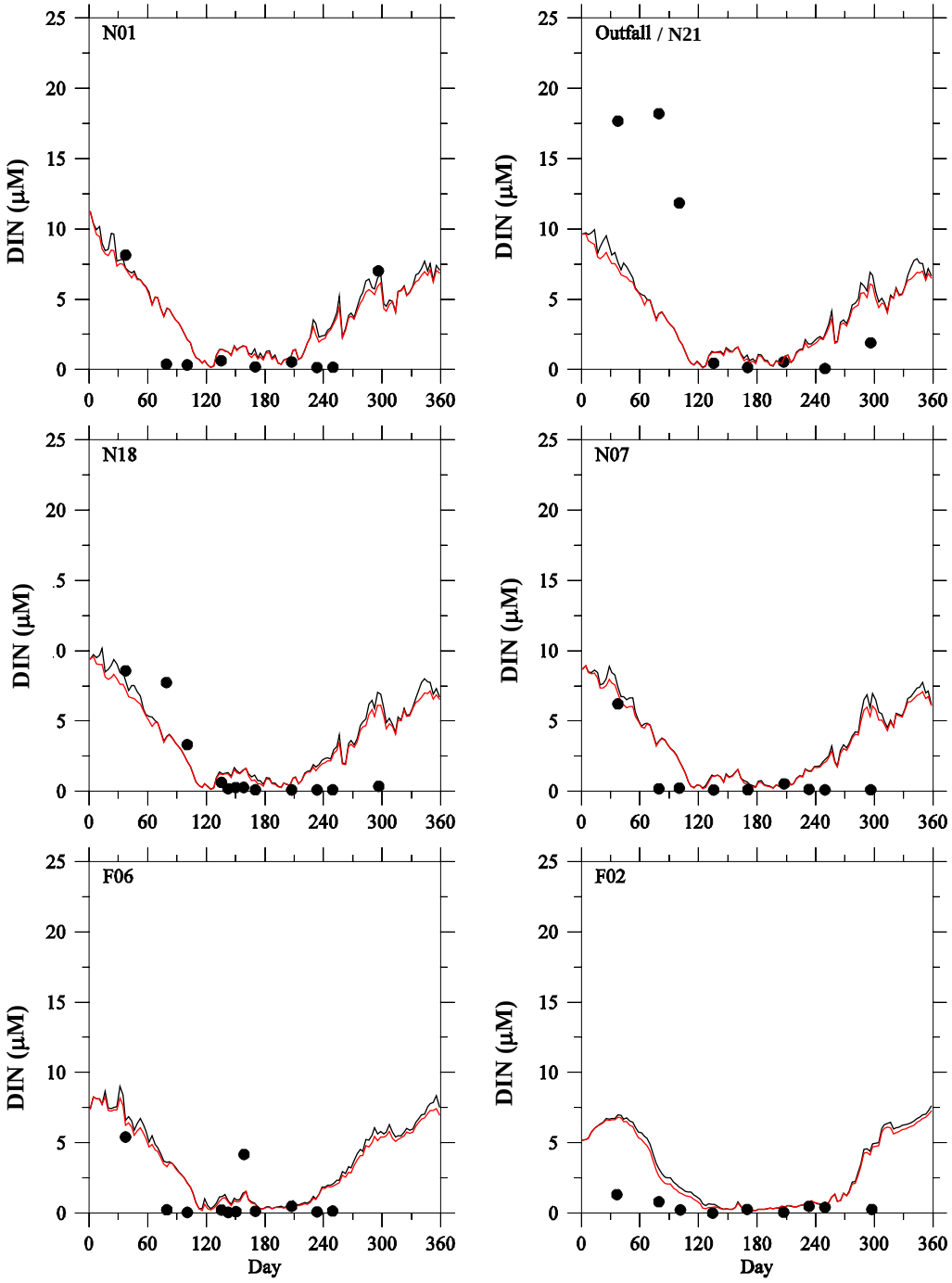

Figure 4.2 Scenario experiment surface DIN: observed (dots), control run (black line), and non-sewage (red line) at select MB stations in 2012.

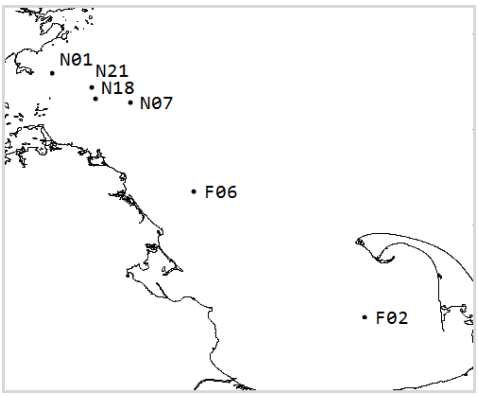

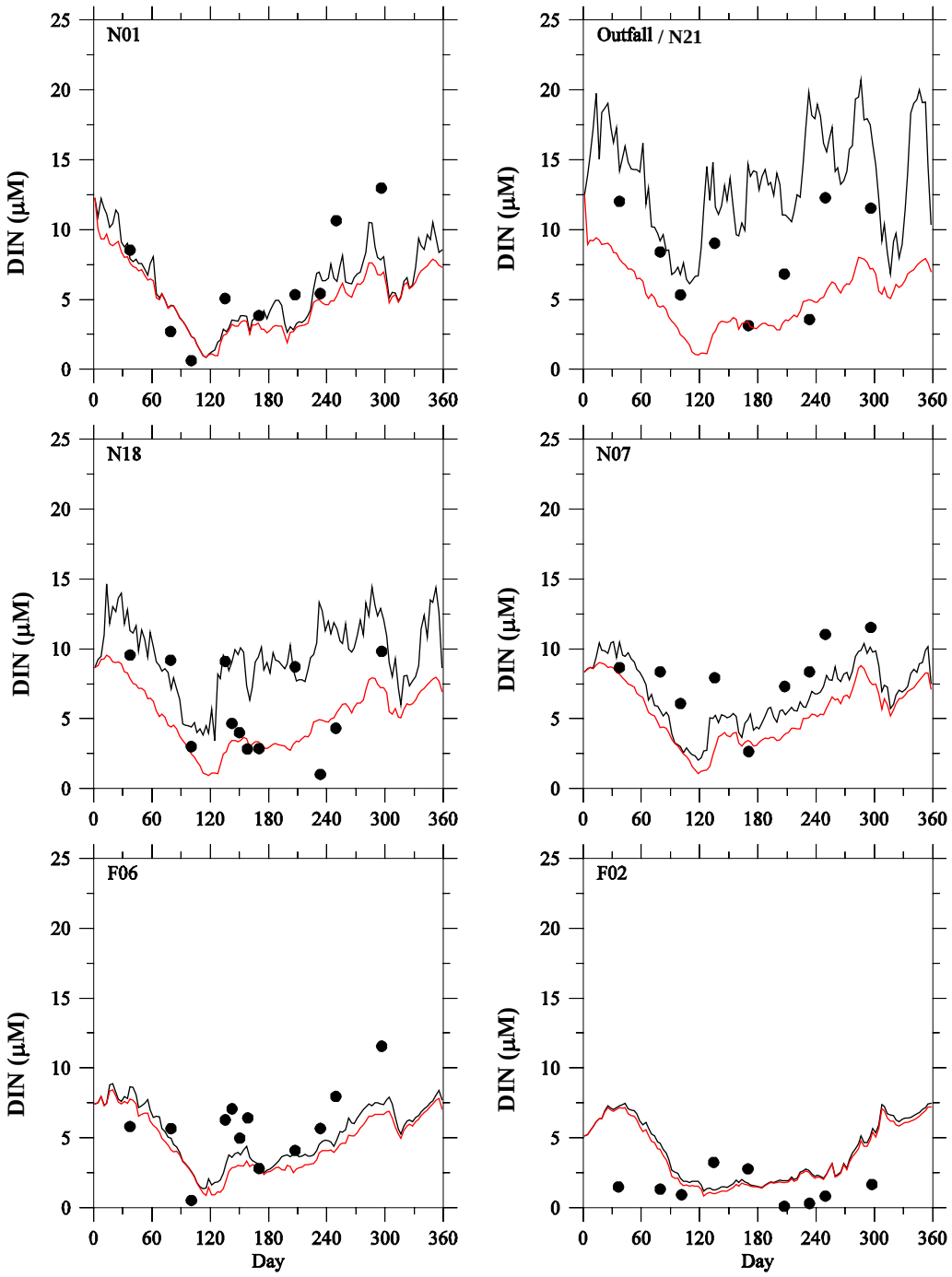

Figure 4.3 Scenario experiment bottom DIN: observed (dots), control run (black line), and non-sewage (red line) at select MB stations in 2012.

.

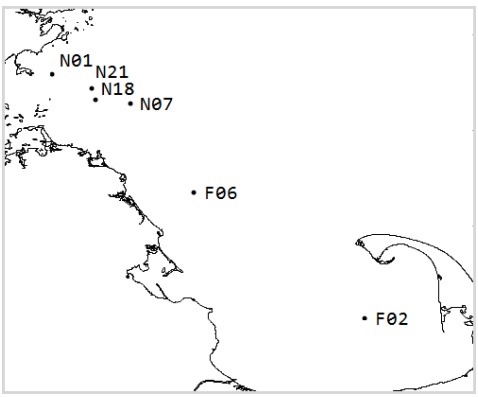

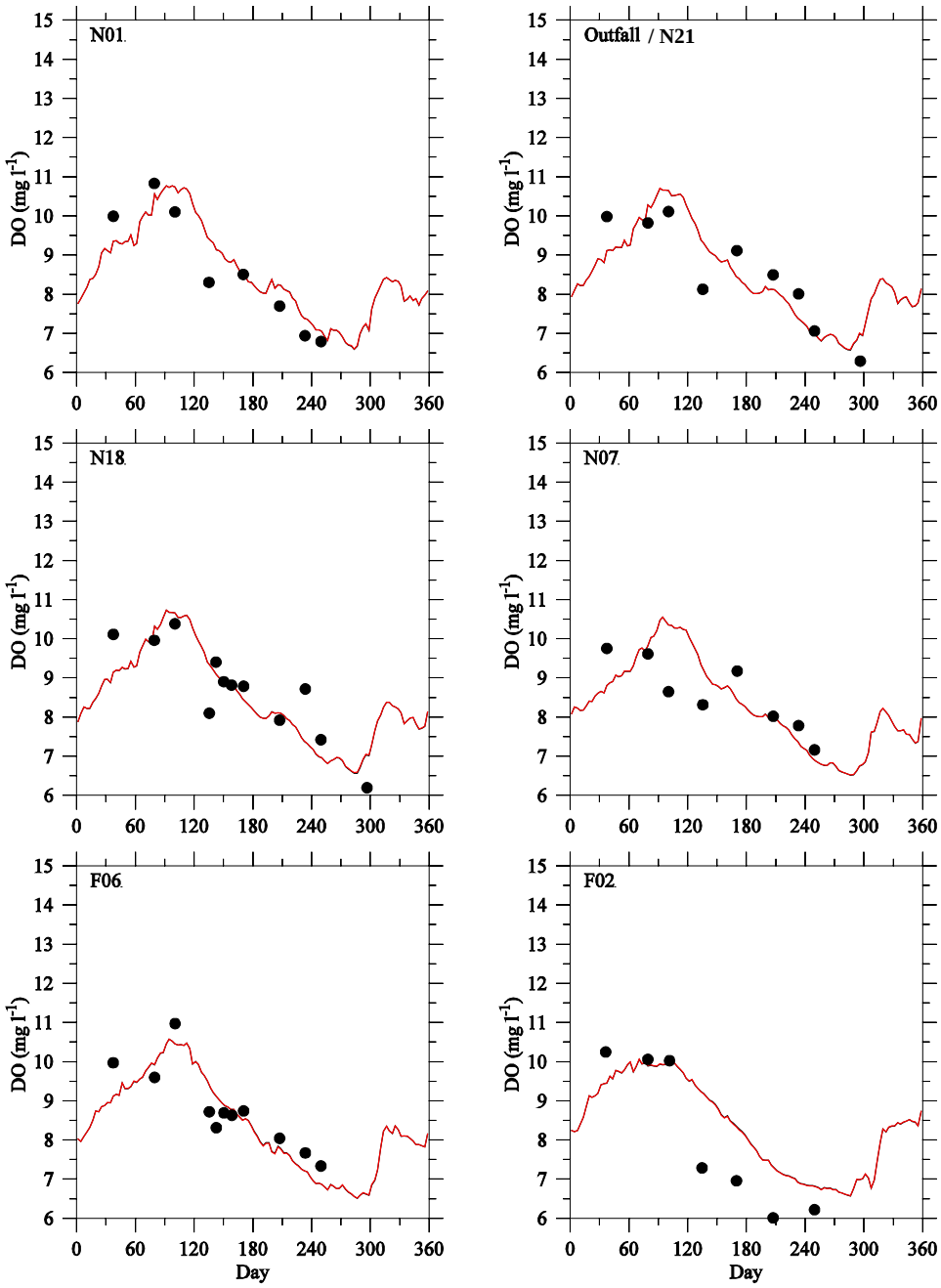

Figure 4.4 Scenario experiment bottom DO (mg L^{-1}): observed (dots), control run (black line), and non-sewage (red line) at select MB stations in 2012.

.

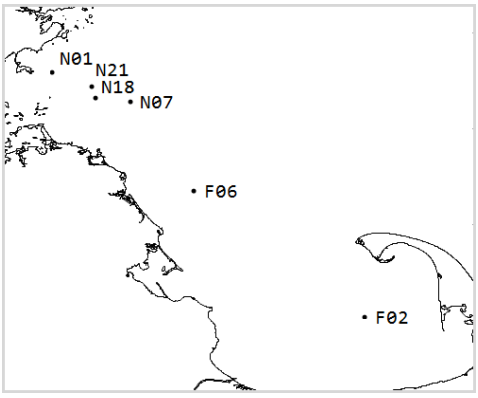

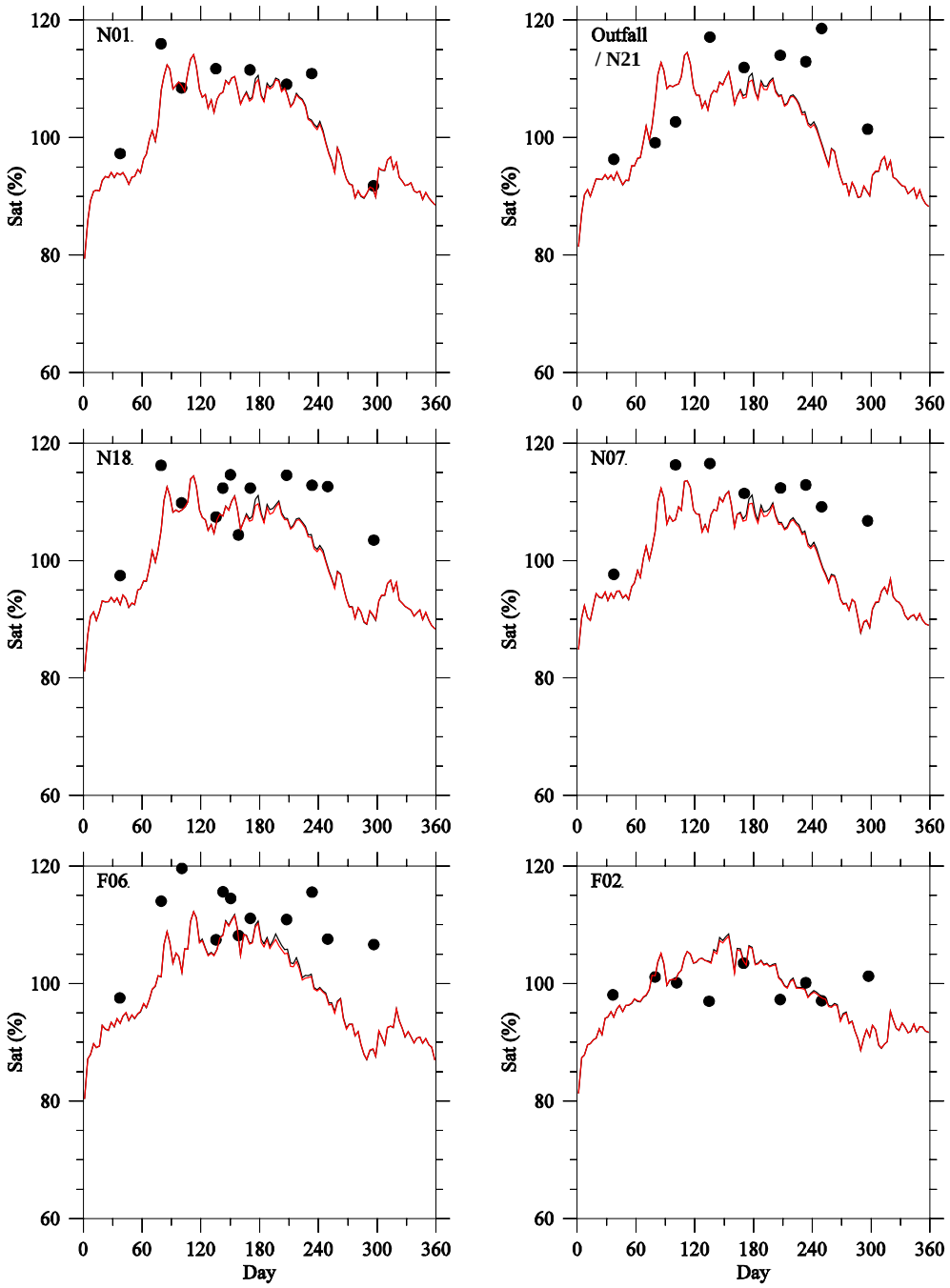

Figure 4.5 Scenario experiment surface DO saturation (%): observed (dots), control run (black line), and non-sewage (red line) at select MB stations in 2012.

.

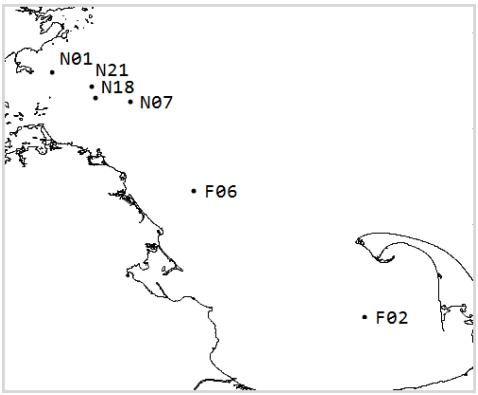

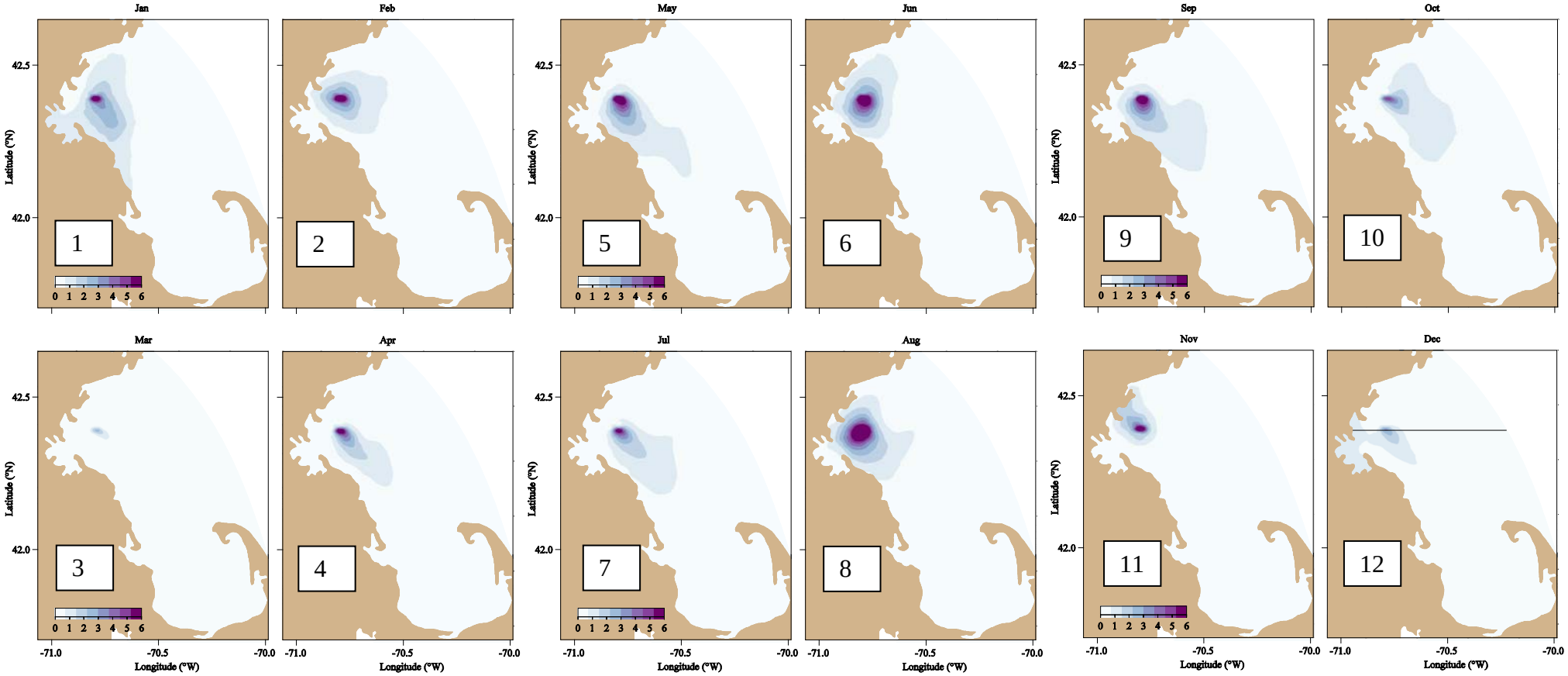

Figure 4.6 Differences in bottom NH_4^+ (μM) between control and non-sewage experiments at end of each month, 2012.

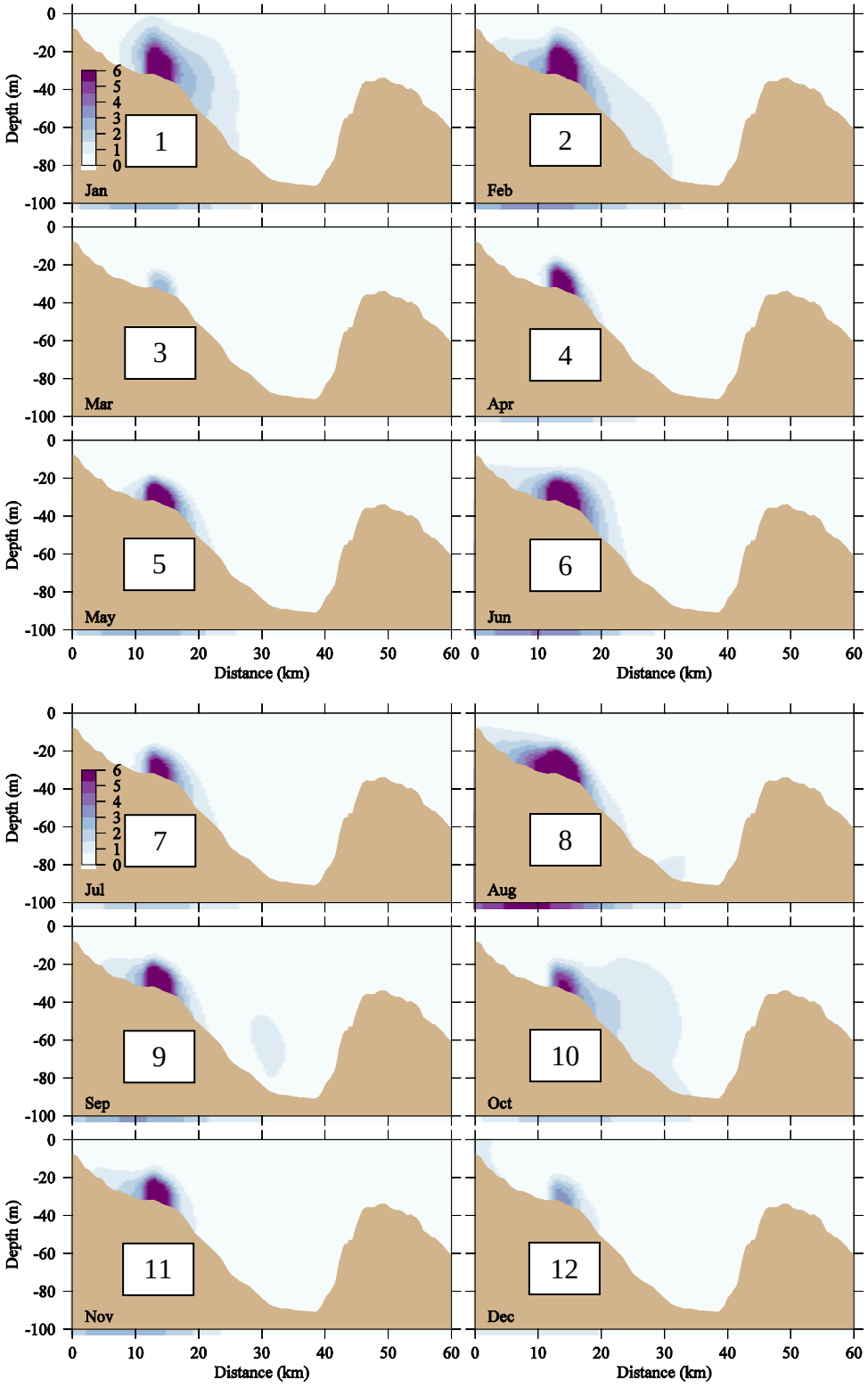

Figure 4.7 Differences in NH_4^+ concentration (μM) between control and non-sewage experiments on west-east transect across MWRA outfall at end of each month, 2012.

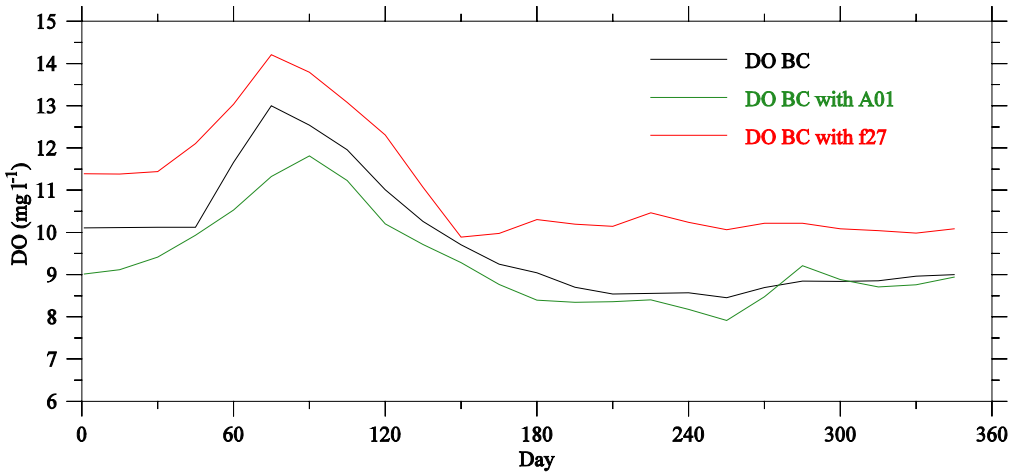

Figure 4.8 DO at open boundary point closest to F27. Black: standard OA mapped observations. Green: modified to use mooring A01 observations. Red: modified to use synthetic F27 record.

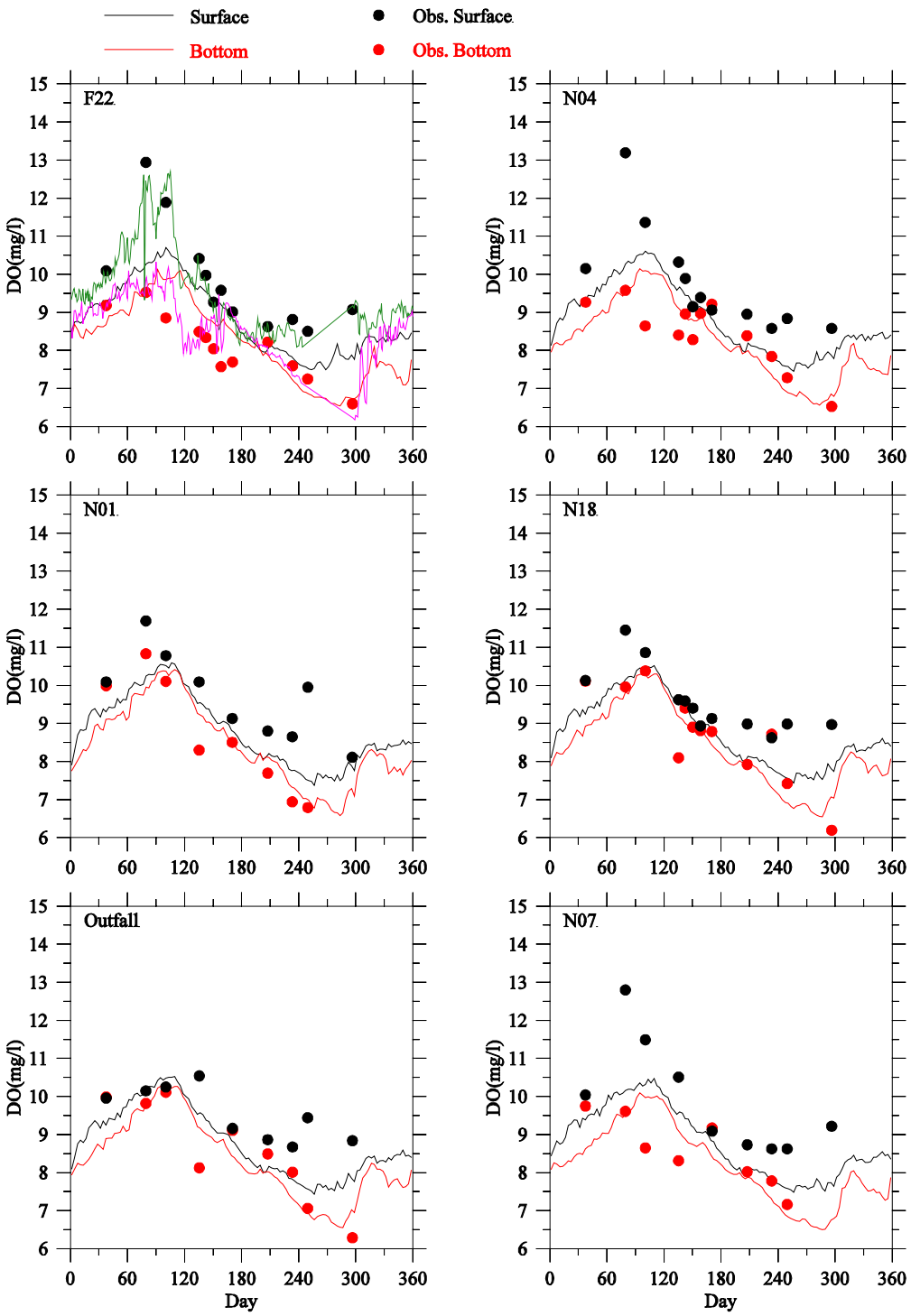

Figure 4.9 Sensitivity experiment A: observed (dots) and modeled DO (mg L^{-1}), northern subset stations, 2012.

Green/pink on F22 frame are mooring A01 surface/bottom observations. Compare to control run (Figure 3.36).

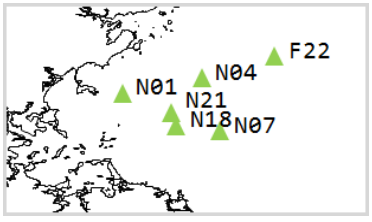

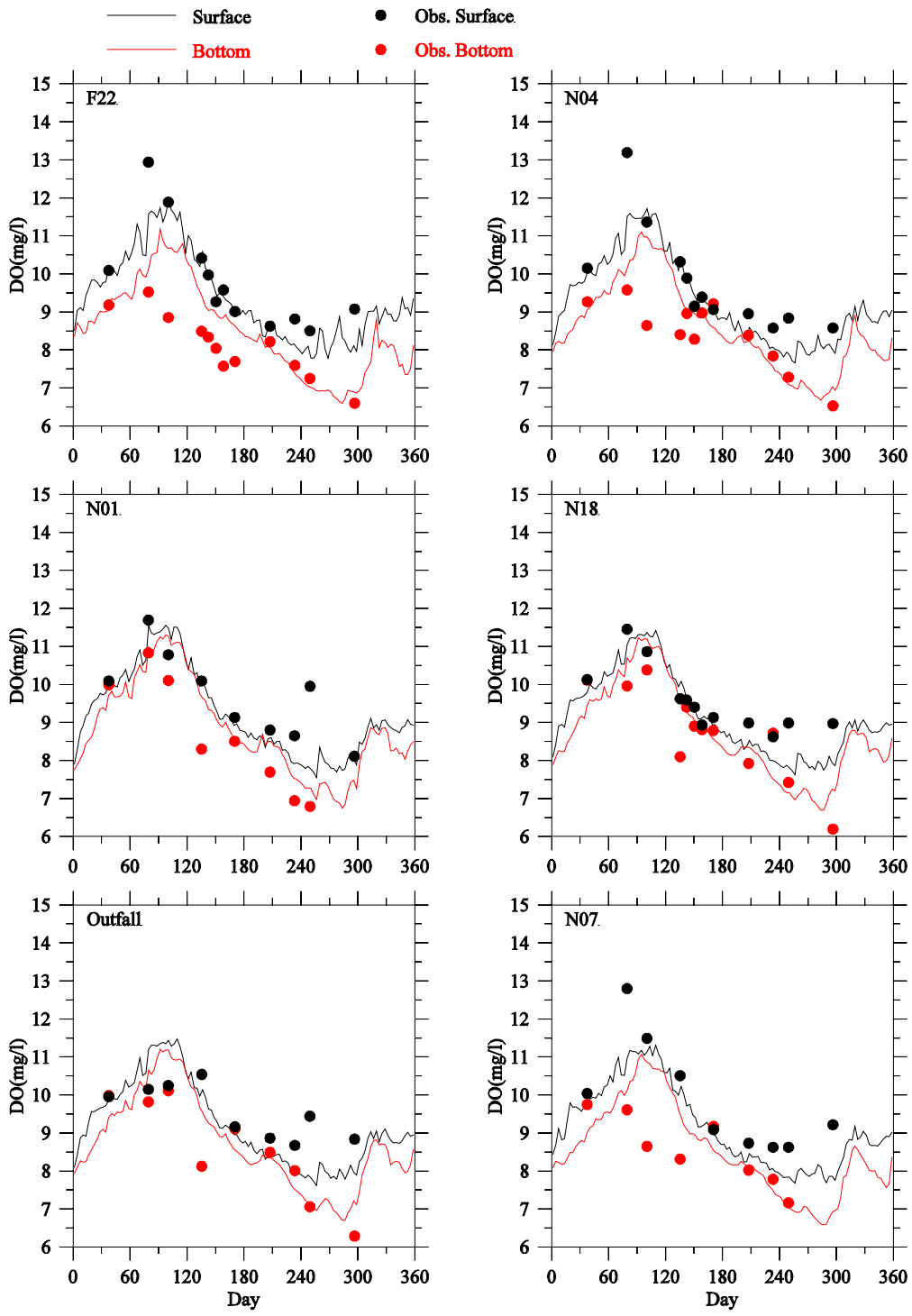

Figure 4.10 Sensitivity experiment B: observed (dots) and modeled DO (mg L^{-1}), northern subset stations, 2012.

Compare to control run (Figure 3.36) and experiment A (Figure 4.9).

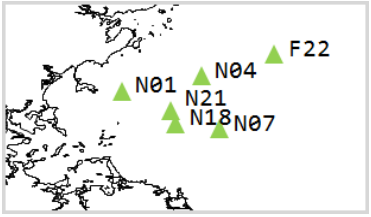

Massachusetts Water Resources Authority
Charlestown Navy Yard
100 First Avenue
Boston, MA 02129
(617) 242-6000
www.mwra.com